UiO-66 metal-organic framework materials as stationary phases in liquid chromatography

Kari Anne Andersen

Thesis for the Master's degree in Chemistry

60 credits

Department of Chemistry

Faculty of Mathematics and Natural Sciences

UNIVERSITY OF OSLO

August / 2020

UiO-66 metal-organic framework materials as stationary phases in liquid chromatography

2020

UiO-66 metal-organic framework materials as stationary phases in liquid chromatography

Kari Anne Andersen

http://www.duo.uio.no/

Trykk: Reprosentralen, Universitetet i Oslo

Abstract

The metal-organic frameworks (MOFs) UiO-66 and UiO-66-NH_2 are composed of zirconium oxide nodes ($Zr_6O_4(OH)_4(CO_2)_{12}$) and benzene-1,4-dicarboxylate (BDC) linkers for UiO-66, and the amino-functionalised linker 2-amino-benzene-1,4-dicarboxylate (ABDC) for UiO-66-NH_2. UiO-66 and UiO-66-NH_2 have large surface areas and a defined pore size and are thus attractive materials for chromatographic separations. The structure of these MOFs also means several retention mechanisms could influence the separation simultaneously, making the retention of functionalised organic molecules on these materials challenging to predict. Hence, the aim of this thesis was to investigate the chromatography of selected compounds on UiO-66 and UiO-66-NH_2 in liquid chromatography (LC), to learn more about the potential applications of these UiO materials.

UiO-66 and UiO-66-NH_2 particles were packed into 100 µm inner diameter (ID) capillaries, and a simple LC-UV system was used for testing. Both materials rapidly (< 30 min) packed into columns of circa 10 cm and provided pressures < 300 bar when used in LC systems. The efficiency (plate height) of the UiO-66- and UiO-66-NH_2-columns were found to be 18 µm and 199 µm, respectively, using uracil as a model analyte. However, phosphate-containing analytes were found to have severe tailing.

With an aqueous mobile phase, the retention of a selection of small hydrophilic molecules was found to increase with decreasing organic component in the mobile phase. The flow rate was also found to affect retention factors, with larger retention factors for lower flow rates. The effect of temperature in the range 25–55°C appeared to follow the expected trend of decreasing retention with increasing temperature for the chosen model substances, benzene, ethylbenzene and butylbenzene.

Pore volume accessibility studies were inconclusive. However, observations made strongly suggest that benzene, ethylbenzene, propylbenzene, butylbenzene, naphthalene and phenanthrene were able to access the pores of UiO-66.

In conclusion, the UiO-66 MOF materials have chromatographic properties different from those of the more common LC separation materials, notably in the ability to retain small polar molecules. However, more research is needed to better understand the retention mechanisms of the materials and to single out application areas for these materials in LC.

Preface

This work was conducted with the Bioanalytical chemistry group at UiO, in collaboration with the Catalysis group. I want to thank my supervisors, Elsa Lundanes, Henriette E. Berg, Steven H. R. Wilson, Sachin Maruti Chavan, Karl Petter Lillerud and Unni Olsbye for their extremely valuable help, advice, guidance and feedback. A special thanks to Elsa and Henriette who were of great help when I got stuck in the writing process while stuck at home.

I also owe great thanks to Marita Claussen and Inge Mikalsen, to the former for lending chemicals, equipment and advice in a pinch, and the latter for invaluable help with the instruments.

The people at the BACh group all have contributed to a good working environment, and I really appreciate having been part of it. Thanks to Ingvild C. Hvinden, Christine Olsen, Jenny Skytte, Jonas Flatval, Harald R. Moe, Alex Websdale and Inga M. Aune for making our shared office more like home and an arena for sharing interesting discussions, questions, answers and chocolate.

A big thanks to Anja M. Aardal, Johannes Botne and Idun Kløvstad who all took time out of their summer holidays to proofread this thesis. I hope you used days when it rained.

Thanks to my friends and family on and off campus who have been there throughout the course of my degree. Finally, thanks to Håkon. It's difficult to imagine what these years would have been like without you.

Kari Anne Andersen
Lørenskog, 06 Aug 2020

Table of contents

Abbreviations 1
1 Introduction 3
1.1 Liquid chromatography 3
1.1.1 Principles of separation 4
1.1.2 Evaluations of chromatographic systems 7
1.1.3 Effect of temperature 15
1.1.4 Detection 17
1.1.5 Miniaturisation of chromatographic systems 18
1.2 Metal-organic frameworks 19
1.2.1 UiO-66 20
1.2.2 UiO-66-NH_2 22
1.2.3 Other UiO-materials 23
1.3 Metal-organic frameworks in chromatography 24
1.3.1 UiO-66 in liquid chromatography 24
1.3.2 UiO-66-NH_2 in chromatography 28
2 Aim of study 31
3 Experimental 32
3.1 Chemicals 32
3.2 Solutions 32
3.3 Materials and equipment 35
3.4 Liquid chromatography system 35
3.5 Packing of columns 37
3.6 Particle imaging and element analysis 40
3.7 Efficiency investigations 40
3.8 Investigation of retention of compounds 40
3.9 Van‘t Hoff experiments 41
3.10 Pore volume accessibility 42
3.11 Treatment of data 42
4 Results and discussion 44
4.1 Packing properties of UiO-66 and UiO-66-NH_2 44
4.2 Column efficiency 50

4.3 Investigation of retention of compounds 56
4.3.1 UiO-66 57
4.3.2 UiO-66-NH_2 63
4.3.3 Suspected adsorption of adenosine phosphates on UiO-66 and UiO-66-NH_2 65
4.4 Van't Hoff experiments 68
4.5 Pore volume accessibility 72
5 Conclusions 80
5.1 Further work 81
References 82
6 Appendix 91
6.1 Supplementary theoretical background 91
6.1.1 Scanning electron microscopy 91
6.1.2 Energy-dispersive X-ray spectroscopy 91
6.1.3 Hypothesis testing 92
6.2 Supplementary information 93
6.2.1 Column efficiency 93
6.2.2 Investigation of retention of compounds 99
6.2.3 Van't Hoff experiments 113
6.2.4 Pore volume accessibility 117
6.3 Extraordinary circumstances due to COVID-19 pandemic 125

Abbreviations

Abbrevation	Definition
ABDC	2-Aminobenzene-1,4-dicarboxylate
ACN	Acetonitrile
ADP	Adenosine diphosphate
AMP	Adenosine monophosphate
ANOVA	Analysis of variance
BDC	Benzene-1,4-dicarboxylate
BPDC	4,4′-Biphenyl-dicarboxylate
cAMP	Cyclic adenosine monophosphate
DCM	Dichloromethane
EDXS	Energy-dispersive X-ray spectroscopy
ESI	Electrospray ionisation
FA	Formic acid
GABA	γ-Aminobutyric acid
GC	Gas chromatography
HILIC	Hydrophilic interaction liquid chromatography
HPLC	High-performance liquid chromatography
ID	Inner diameter
LC	Liquid chromatography
LC-MS	Liquid chromatography coupled to a mass spectrometer
MeOH	Methanol
MOF	Metal-organic framework
MP	Mobile phase
MS	Mass spectrometer
NPLC	Normal-phase adsorption chromatography
OD	Outer diameter
OT	Open tubular
PAH	Polyaromatic hydrocarbons
PGC	Porous graphite carbon
pGMA	Poly(glycidyl methacrylate) monolith
poly(MAA-co-EDMA)	Polymethylarylic acid-co-ethylene dimetharylate monolith
RPLC	Reversed-phase liquid chromatography
SBU	Secondary building unit
SEC	Size-exclusion chromatography

SEM	Scanning electron microscopy
SP	Stationary phase
TMB	3,3’5,5’-Tetramethylbenzidine
TPDC	Terphenyl dicarboxylate
UHPLC	Ultra high-performance liquid chromatography
UiO	University of Oslo
UV	Ultra-violet

1 Introduction

The need for selective and sensitive analysis methods within fields where compounds of interest exist in low concentrations is great. As detection limits are pushed lower and separation power is increased, we learn more about our own biology and the world around us. This knowledge can enable us to treat illnesses at early stages or to halt activities that harm our environment.

An important tool in this endeavour is the mass spectrometer (MS). Even though the MS can be used to both quantify and identify compounds, it is often necessary to separate the components of a sample prior to them entering the MS. For non-volatile compounds, liquid chromatography is commonly used for pre-detection separation.

While much is already achieved, there is still a need for more specialised analysis tools in LC. In fields such as environmental sciences or “omics”-studies, samples are often very complex. This makes creating suitable analysis methods challenging with the toolset that exists today. An expansion of that toolset to give more options for niche applications could help us deepen our understanding of the world even further.

In this thesis, newer separation materials for LC are investigated. These materials are metal-organic framework materials. Before these materials are described, an introduction to present LC separation materials and chromatographic parameters used for characterising LC columns and separations is included.

1.1 Liquid chromatography

Separation prior to detection makes quantification and identification of compounds more reliable, as interferences are less likely to be present. In liquid chromatography, the liquid mobile phase (MP) carries the sample components through the column, where the stationary phase (SP) is located. The various compounds in the sample can be separated based on their different interactions with the SP and the MP. LC is most commonly used for non-volatile compounds, as gas chromatography is preferred when volatile compounds are of interest due to its superior efficiency per analysis time.

High-performance liquid chromatography (HPLC) and ultra high-performance liquid chromatography (UHPLC) are the most used modes of LC today. Historically, HPLC was used when the particle size in packed columns was less than 10 µm. When particles below ca. 3 µm were introduced, the technique was called UHPLC.

There are different kinds of stationary phases in use for LC, and they separate compounds based on different chemical principles of interaction. In addition to the stationary phases discussed in this section and other established SPs, novel SP materials are being explored. An example is metal-organic frameworks, which are discussed in the context of applications in LC in section **1.3**.

1.1.1 Principles of separation

LC separations can be performed according to various chromatographic principles. The kind of separation that occurs within the column is determined by the SP and MP chosen and their chemical or physical properties and interactions with each other.

In adsorption chromatography, the compounds in the sample interact directly with the surface of a solid SP. The interactions can be van der Waals interactions, acid-base interactions, π-π interactions, complexation etc.

In partition chromatography, the SP has liquid characteristics. The compounds in the sample partition between the SP and MP.

Other examples of chromatographic principles are hydrophilic interaction liquid chromatography (HILIC), reversed-phase liquid chromatography (RPLC), and size-exclusion chromatography (SEC).

Reversed-phase liquid chromatography

In RPLC, compounds are separated in order of increasing hydrophobicity. The least hydrophobic compounds elute first, followed by increasingly more hydrophobic compounds. The most common stationary phases used in RPLC are C18 chemically bonded to a silica support, and porous graphite carbon.

C18 and C8 are linear alkyl chains, respectively 18 and 8 carbons long. Both longer and shorter chains are used, but C18 is the most common. The longer the alkyl chain, the more hydrophobic the stationary phase. Totally porous silica particles are most commonly used as supports for the alkyl SPs, and lately solid-core particles have become common. Other materials such as zirconia, titania or organic supports are also available. The mobile phase is in most cases aqueous, where the water is mixed with an organic modifier that is mixable with water in all ratios, with the most common organic modifiers being methanol (MeOH) or acetonitrile (ACN). Acid or buffer is added for pH control, because residual silanol groups, the bond between the silica and the alkyl chains when silica support is used, and compounds in the sample are or may be pH sensitive. For a C18 or C8 stationary phase bound to silica-support to be accessible to the compounds in the sample, at least 5 % organic modifier is used in the mobile phase, unless special phases for aqueous MPs are used. Increasing the amount of organic solvent in the MP increases the elution strength, leading to shorter retention times and lower resolution.

Porous graphite carbon (PGC) is less commonly used in RPLC than C18 on silica-support. PGC particles are fully porous spherical particles of graphite[1]. The particles have been shown to have good mechanical and chemical stability, making them suited for use in HPLC. The graphite surfaces within the pores are flat and crystalline[1,2]. Molecules with larger planar geometries can have more interaction points with the PGC than smaller molecules, leading to larger molecules being more strongly retained. The selectivity of PGC is different from that of alkyl chains supported on silica, as it can also engage in both lone electron pair and dipole interactions. Aqueous mixtures of alcohols with acid or buffer added for pH control are common MPs for PGC.

Hydrophilic interaction liquid chromatography

HILIC provides a selectivity that complements RPLC well with opposite elution order to that of RPLC[3,4]. It is a good option for separation of polar compounds which have little retention in RPLC. In principle, any polar material can be used for HILIC[5]. When combined with an MP with a high percentage of organic solvent mixed with aqueous buffer, the polar material will interact with the water in the MP to form a partly immobilised aqueous layer. This aqueous layer is believed to constitute the SP in HILIC[3,6]. The compounds in the sample partition between the MP and the partly immobilised aqueous layer. The more hydrophilic

compounds interact more strongly with the aqueous layer. Thus, more hydrophilic compounds are more strongly retained[4].

The MP is commonly an organic solvent that is mixable with water such as ACN, acetone or ethanol mixed with aqueous buffer[4,7]. The elution strength of the MP increases with increasing water content. Both MP composition, pH and ionic strength can be tuned to suit the selected HILIC material and sample[7]. Due to water being a strong eluent in HILIC, injected samples should not have a high water content.

While partition between the partly immobilised aqueous layer and the MP is thought to be the main contribution to separation in HILIC, adsorption because of hydrogen bond interaction, electrostatic interactions or hydrophobic interactions can also contribute to the separation[4].

Since the SP is polar and the MP is less polar, HILIC is normal phase partition chromatography.

Normal-phase adsorption chromatography

Chromatography with silica (which has a polar surface) as the SP is also regarded as normal-phase chromatography, but in this case it is adsorption chromatography with a non-aqueous MP and a solid SP. The abbreviation NPLC is used to refer to normal-pahse adsorption chromatography. Compounds are separated according to increasing hydrophilicity, as more hydrophilic compounds interact more strongly with the silica. Hexane modified with dichloromethane (DCM) is a common MP. More polar MPs are stronger eluents when silica is used as a stationary phase.

Size-exclusion chromatography

SEC stands out in that the physical properties of the separation material is the source of the separation. Separation occurs primarily as a function of the size of the molecules present in the sample and to which extent they can enter the porous separation material. The molecules that are too large to enter the pores elute first, while the molecules able to fully permeate the pores elute last. This separation principle requires materials with pores of a well-defined size.

1.1.2 Evaluations of chromatographic systems

There are many ways to describe the performance of a chromatographic system. In this work, emphasis is placed on band broadening, peak shape, and retention factor.

The measured performance of a chromatographic system does not describe that of the column alone, but the whole of the chromatographic system. In the following, the band broadening in the column is first elaborated upon, and then extra-column contributions.

Band broadening and efficiency

Band broadening is understood as the variance (σ_{tot}^2) of the band where the solute elutes, and can be calculated from the variance contribution from each part of the system. The band broadening of the column σ_{column}^2, or σ^2 for short, is related to column efficiency as discussed in the following paragraphs.

The plate number N is the SI unit for column efficiency and is defined as seen in **Equation 1**[8]

$$N = (\frac{V_R}{\sigma})^2 = (\frac{t_R}{\sigma})^2 \qquad \textbf{Equation 1}$$

where V_R is the retention volume, t_R is the retention time of a solute (compound), and σ is the standard deviation of the Gaussian-shaped solute band. The plate number is dimensionless, and hence the measure of the variance must be done in the same dimension as the retention. The band variance can be difficult to measure[5]. For measuring purposes, **Equation 2** is often used

$$N = 5.545(\frac{t_R}{w_{50}})^2 \qquad \textbf{Equation 2}$$

were w_{50} is the peak width at 50% height, measured in time units.

The plate number can be used to describe the efficiency and hence separation power of a chromatographic system. However, plate number increases with column length. In order to

better compare efficiency between columns of different length, plate height H (**Equation 3**) is used.

$$H = \frac{L}{N} \qquad \textbf{Equation 3}$$

Here the column length L is divided by the plate number N.

An injected sample band broadens as it travels through the chromatographic system. In practice, a broader band means that the solute is diluted in a larger volume than if no band broadening occurred, and this gives reduced signal intensity when a concentration-sensitive detector is used.

The band broadening is affected by several processes. In packed column liquid chromatography, these processes are longitudinal diffusion, eddy dispersion, and resistance to mass transport in stationary phase, mobile phase and stagnant mobile phase.

The eddy dispersion, also called eddy diffusion or multipath diffusion, originates from the different paths any molecule from the injected sample might travel. Local varieties in linear velocity give rise to eddy dispersion. Eddy dispersion is proportional to particle size, i.e. smaller particles result in a smaller contribution to the total band broadening from eddy dispersion. Eddy dispersion is greater if the particle size is heterogeneous[5].

Longitudinal diffusion occurs for the same reasons as all diffusion – the system will try to reduce concentration differences within the system. The diffusion in radial direction does not affect the width of the band, but the diffusion in longitudinal direction does. The longitudinal diffusion is dependent on the diffusion coefficient of the solute in the mobile phase and the linear velocity of the mobile phase.

The band broadening caused by what is called resistance to mass transport is caused by the time it takes from a sample molecule to transfer between the stationary phase, the stagnant mobile phase and the mobile phase. The two resistances to mass transfer are inversely proportional to the solute diffusion constant in the medium, and proportional to linear velocity and particle size.

Multiple mathematical models aim to describe the band broadening process. One of the most used is the van Deemter equation (**Equation 4**)[5]. The principal strength of this model is its good fit for most experimental data[9].

$$H = A + \frac{B}{u} + Cu \qquad \textbf{Equation 4}$$

Equation 4 is a minimal notation for the equation, where u is the linear velocity, the A-term describes the contribution from eddy dispersion, B-term describes the contribution from longitudinal diffusion, and C-term describes the contribution from resistance to mass transfer.

Extra-column band broadening

All volumes of a chromatographic system from the point where the sample enters the system that do not contribute to separation are referred to as extra-column volume. Band broadening that happens in extra-column volumes is considered extra-column band broadening[5,10]. There are volumes that contribute to the total band broadening of the system in the injector, connective tubing, unions and detector. The total band broadening (σ_{tot}^2) can be calculated from the variance contribution from each part of the system (**Equation 5**):

$$\sigma_{tot}^2 = \sigma_{column}^2 + \sigma_{injector}^2 + \sigma_{tubing}^2 + \sigma_{unions}^2 + \sigma_{detector}^2 + \sigma_{other}^2 \qquad \textbf{Equation 5}$$

where σ_{column}^2 is the variance contribution from the column, $\sigma_{injector}^2$ that of the injector, σ_{tubing}^2 that of the tubing, σ_{unions}^2 that of the unions, $\sigma_{detector}^2$ that of the detector, and σ_{other}^2 the variance from all other sources.

For traditional HPLC columns with an inner diameter of 4.6 mm, the contribution from extra-column band broadening is small[11]. However, as the inner diameter of the column is reduced, the extra-column band broadening might become an increasingly important contribution to the total band broadening.

Extra-column band broadening can be minimised by using an injector, a detector flow cell (if applicable) and unions that are suited for the dimension of the column, and using as few coupling points and as narrow and short connective tubing as achievable. It is important to ensure that all connections are as snugly fit as possible and that column and tubing ends are square. **Figure 1** illustrates one connection where little extra-column volume is introduced in (a) and (b) where extra-column volume is introduced due to both a capillary not being fully inserted (left) and due to a poorly cut capillary end (right).

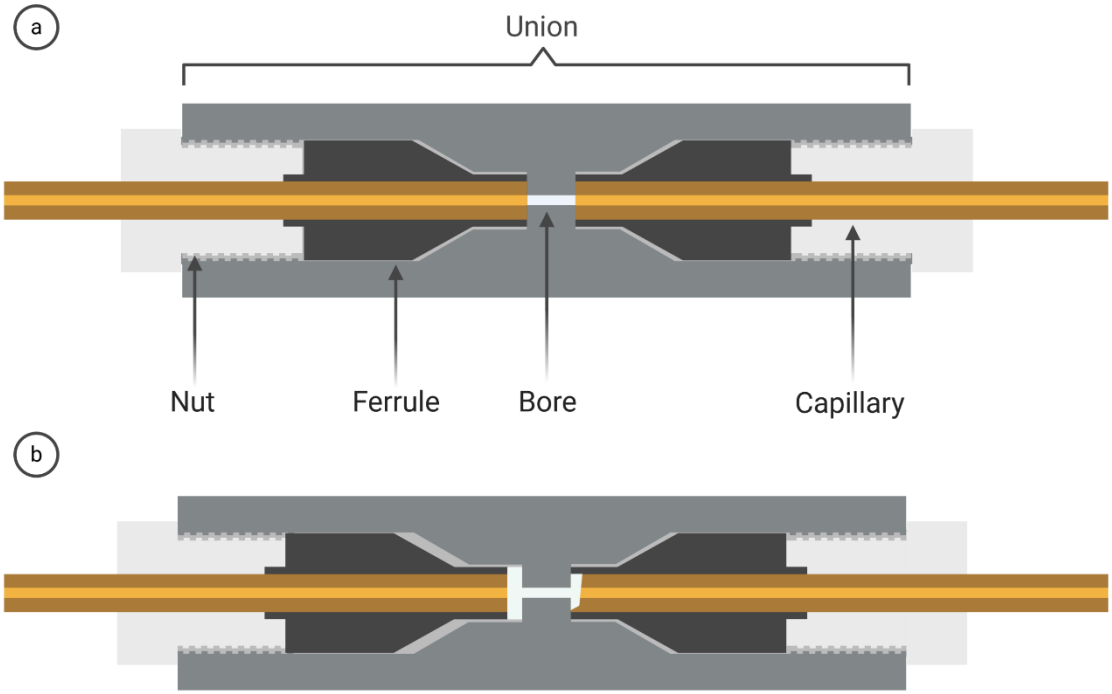

Figure 1 Sketches of a good and a poor coupling. a) Properly connected capillaries where little extra-column volume is present in the union. b) Poorly connected capillaries with capillary not entering the union properly (left) and the effect of a poorly cut capillary end (right). Figure created with BioRender.com.

Peak shape and asymmetry

Chromatographic peaks are often assumed to take the shape of a perfect Gaussian distribution. However, this is not an accurate description of real chromatographic peaks. Most peaks have either tailing, fronting or both to different extents.

Fronting can occur when the column is overloaded, *i.e.* when the injected sample contains high concentrations of compounds that interact with the SP. When large amounts of a solute

interacts with the SP, it can enhance the ability of the SP to interact with the remaining solute in the MP[10]. This leads to a gradual increase in the signal before the apex of the peak followed by a steeper decline.

Tailing can arise from different causes, *e.g.* how well packed a column is. Early eluting peaks that have tailing is commonly a sign of changing packing structure[5]. Additional interactions, for example interactions with residual silanol groups if silica-based particles are used, are also a common cause for tailing.

Asymmetry can be quantified by an asymmetry factor A_s (**Equation 6**)[5], where the distance from the midline (as determined by the apex of the peak) and the tail of the peak (b) and the distance from the midline to the front of the peak (a) at 10 % of total peak height are compared.

$$A_s = \frac{b}{a} \qquad \textbf{Equation 6}$$

The measuring of asymmetry is illustrated in **Figure 2**. Here, the red line illustrates a compound peak which is clearly not shaped like a perfect Gaussian distribution, which is shown in light grey.

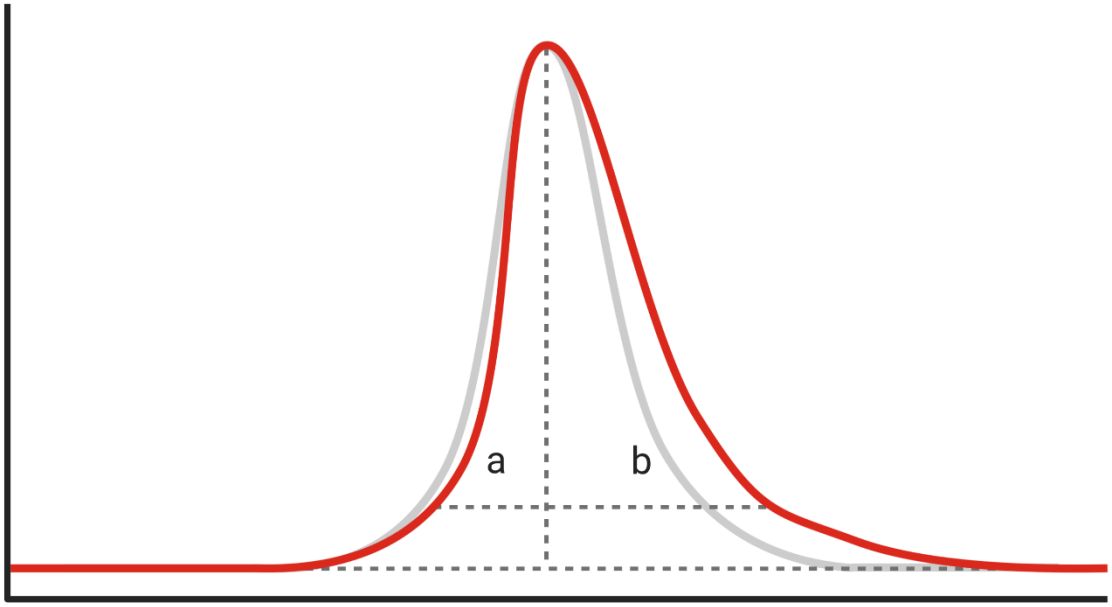

Figure 2 Sketch of the measurement of asymmetry of a solute peak (red). A Gaussian distribution is illustrated in light grey. The measurements of a and b are at 10% of the peak height. Figure created with BioRender.com.

If A_s is greater than 1, tailing is more prominent in the peak, while if A_s is lesser than 1, fronting is more prominent. An A_s value approximately equal to 1 is desired.

Asymmetric peaks make accurate quantification challenging, as determination of peak area becomes more difficult. This is particularly true when there is no baseline separation between peaks. Tailing or fronting peaks also increase the chance that closely eluting peaks elute on the front or tail of a neighbouring peak.

Retention factor

The retention factor k is a measure of how retained a compound is by the stationary phase. The retention factor (**Equation 7**) is defined as the ratio between the adjusted retention volume V'_R (**Equation 8**) and the elution volume V_M[8].

$$k = \frac{V'_R}{V_M}$$ **Equation 7**

The adjusted retention volume is defined as

$$V'_R = V_R - V_M \qquad \textbf{Equation 8}$$

where V_R is the retention volume as defined in IUPAC's guidelines for nomenclature in chromatography[8].

For measuring purposes, **Equation 9** is used:

$$k = \frac{t_R - t_M}{t_M} \qquad \textbf{Equation 9}$$

where t_M is the retention time of an unretained compound, sometimes called the net retention time or migration time, i.e. the time a completely unretained compound takes to elute, and t_R is the retention time, i.e. the time the given compound elutes at.

Determination of retention factor by **Equation 9** demands that the net retention time is well defined. There are several ways of determining the net retention time[12].

A much-used method is injecting a compound known to have no retention in the system, sometimes called an elution time marker. However, this method can give a too high t_M value for many SPs, because it is difficult to find a compound which truly has no retention. Both retention due to interactions between the compound and the SP, and secondary interactions with residual silanol groups, tubing or other parts of the system can give rise to an artificially high elution time. Uracil is a commonly used elution time marker for reversed-phase materials.

Another method for determining elution time is to inject one of the mobile phase components or a mixture of mobile phase components at different ratios than that of the MP. For detectors that are sensitive to changes in the refraction index, a plug of liquid that has a different refraction index from that of the MP will cause a minor disturbance in the baseline, which is an indicator of t_M. This method will yield slightly different elution times for different MP compositions[13–15]. This can be countered by measuring over the entire MP composition range and using the average elution time value. There is also the possibility that the injection of pure

solvents might disturb the SP. However, the method can easily be used for determining t_M for every injection if the sample solvent has a different refraction index than the MP, making it an attractive option.

Unlike for other types of LC columns, it is not recommended to use the MP hold up volume as a t_M marker for SEC columns. This is because the small MP molecules have access to all the pores of the SEC material, and thus will elute last[8].

Resolution

The resolution of chromatographic peaks is a measure of how well separated two closely eluting compounds are. Resolution R_s is defined and measured as described in **Equation 10**

$$R_s = \frac{2(t_2 - t_1)}{w_1 + w_2} \qquad \textbf{Equation 10}$$

where t_1 and t_2 are the retention times of compound 1 and compound 2, where compound 1 elutes before compound 2, and $w_1$and w_2 are the peak widths at baseline for compound 1 and 2, respectively. For baseline separation, R_s needs to be equal to or larger than 1.5.

Backpressure

The backpressure of a chromatographic system is the pressure as measured in front of the column. While the backpressure itself is not an interesting property for chromatography, most LC pumps have a maximum pressure they can tolerate. This puts limitations on the LC systems it is possible to operate.

The backpressure is calculated as shown in **Equation 11**[5]

$$P = \frac{\kappa u \eta L}{d_p^2} \qquad \textbf{Equation 11}$$

where u is the linear velocity, L is the column length, η is the viscosity of the MP, d_p is the particle diameter and κ is a constant. As such, the backpressure is inversely proportional to

the square of the particle diameter, and proportional to the column length, linear velocity and the viscosity of the MP.

1.1.3 Effect of temperature

The temperature at which a separation is performed can be optimised to enhance the separation. Increasing temperature generally lowers the viscosity of fluids (which affects diffusion) and enhances kinetics, hence elevated temperatures often result in reduced band broadening. Temperature can also affect retention.

A useful tool in investigating the effect of temperature on retention is the van't Hoff equation (**Equation 12**)

$$\ln k = \frac{\Delta H^\circ}{RT} - \frac{\Delta S^\circ}{R} + \ln \phi \qquad \textbf{Equation 12}$$

where k is the retention factor, H is the enthalpy, S is the entropy, T is the absolute temperature, R is the gas constant, and ϕ is the phase ratio.

This equation is derived from the two equations for Gibbs free energy (**Equation 13**, **Equation 14**)

$$\Delta G^\circ = \Delta H^\circ - T\Delta S^\circ \qquad \textbf{Equation 13}$$

$$\Delta G^\circ = -RT \ln K \qquad \textbf{Equation 14}$$

where G is Gibbs free energy and K is the equilibrium constant. When used in chromatography, K is substituted by the expression in **Equation 15**

$$K = k\beta = k\frac{V_M}{V_S} \qquad \textbf{Equation 15}$$

where β (**Equation 16**) is called the phase ratio[8], i.e. the ratio between the MP volume V_M and the SP volume V_S. Often, ϕ (**Equation 16**, also called phase ratio) is used instead of β. The two phase ratio expressions are related by

$$\phi = \frac{1}{\beta} = \frac{V_S}{V_M} \qquad \textbf{Equation 16}$$

A van’t Hoff plot where three compounds are being compared is illustrated in **Figure 3**.

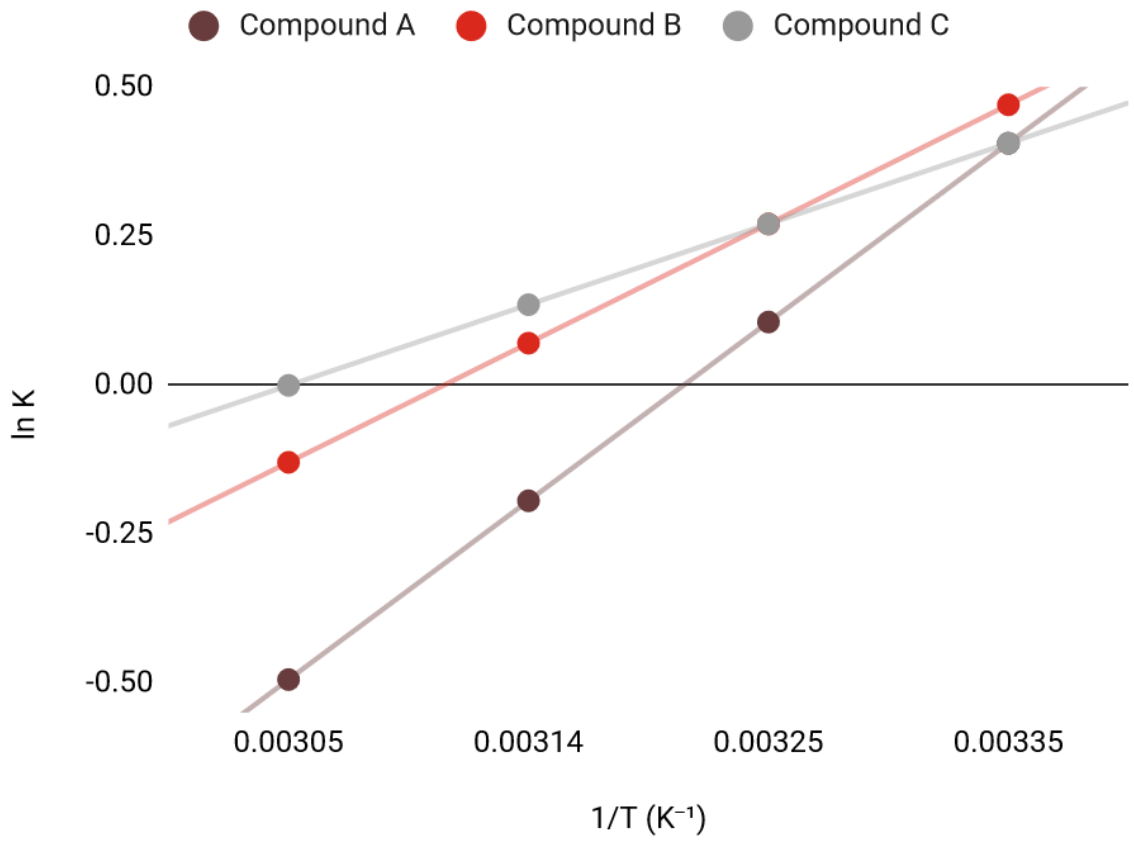

Figure 3 Illustration of van’t Hoff plots for three compounds. The inverse temperature values correspond to 55°C, 45°C, 35°C and 25°C from left to right.

A van’t Hoff plot can be helpful when optimising separation. If two analytes have the same retention factor at one temperature, this might not be the case for all temperatures, as is illustrated in **Figure 3**. Here, the compounds B and C coelute at 35°C, and the compounds A and C coelute at 25°C. These temperatures should be avoided in order to successfully separate the three compounds.

The van’t Hoff plots in **Figure 3** also reveal that the compounds B and C change retention order as the temperature increases.

A positive slope indicates that the transfer of the solute from the MP to the SP is an exothermic process. It follows that increased temperature will push the equilibrium towards the solutes being less present in the SP, and thus reduce the retention times. This can be beneficial because total analysis time can be reduced at increased temperatures.

A linear van't Hoff plot indicates that the retention mechanism is the same throughout the investigated temperature range, and $\Delta H°$ can be determined from the slope. A nonlinear van't Hoff plot indicates that $\Delta H°$ or $\Delta S°$ changes as the temperature changes. Phase ratio can also change with temperature[16], complicating the process of deriving enthalpy and entropy values from van't Hoff plots. If the enthalpy and entropy change over a temperature range, this implies that the nature of the interaction changes as well. In this regard, van't Hoff plots can assist in determining whether the interactions change characteristics with temperature.

1.1.4 Detection

Choice of detection method can provide an additional layer of selectivity depending on the detector used. However, there are many factors that must be taken into account when choosing a suitable detector. Compatibility with the rest of the system (e.g. avoid potential interferences from the mobile phase) and suitability for all compounds of interest at the concentration levels they are present are some of the considerations that must be made.

Ultra-violet (UV) detection will detect all compounds that contain UV chromophores which absorb at the selected wavelength. UV chromophores in organic compounds are typically double or triple bonds, conjugated π-π-systems or functional groups. This enables one detector to be used for several substances at once. Variable wavelength UV detectors provide the opportunity to vary the wavelength of the light used, as the name suggests. Typically, a wavelength where the analytes have high molar absorptivity is chosen. Wavelengths that are also absorbed by solvents in the injection solution or mobile phase, or by coeluting compounds, are avoided.

The UV absorption A for an analyte is described by Beer's law (**Equation 17**):

$$A = \varepsilon b C \qquad \textbf{Equation 17}$$

where ε is the molar absorptivity of the analyte at the selected wavelength, b is the path length of the flow cell, and C is the concentration of the analyte. Thus, the UV detector is a concentration-sensitive detector, where a more concentrated analyte band yields a more

intense detector signal. The detection can also be enhanced by increasing the path length of the flow cell used.

The minimum detectable mass for UV detectors is normally within the 0.1–1 ng range[5]. In comparison, MS detectors have been reported to have a minimum detectable mass in the femtogram to picogram range, while the fully universal refraction index detector is reported to have a minimum detectable mass in the microgram range.

It is necessary to keep in mind that no structural information other than the existence of UV chromophores can be elucidated from UV detection. This is a drawback when compared to for instance MS detectors, which can provide information that enables compound identification such as molecular ion mass and fragmentation patterns. However, the instrumentation of most UV detectors is far less prone to technical malfunction than MS detectors, as no ionisation, vacuum or strong electric fields are required. Increased instrumental robustness compared to MS, in combination with relatively simple operation and lower cost, are considerable advantages. As such UV detection is suited for use where compound identification is not the main goal and the compounds that absorb at the selected wavelength are sufficiently resolved.

1.1.5 Miniaturisation of chromatographic systems

Facing samples of small volumes or low concentrations, miniaturised systems provide several benefits. In miniaturised LC systems, columns with considerably smaller inner diameter than conventional LC columns are used. While conventional LC columns are regularly available in 2.1 mm ID, nano-LC columns have inner diameters in the micrometre scale, with IDs between 10 and 100 µm most common[5].

The most important advantage is the reduced radial dilution of the injected solution, providing more concentrated analyte bands which in turn gives rise to larger amplitude signals on concentration-sensitive detectors. The reduced consumption of solvents used in the mobile phase is also noteworthy. With a smaller inner diameter, a lower flow rate is needed to maintain the optimum linear velocity. This is beneficial both environmentally and financially, and increases compatibility with detectors requiring lower volume input, such as MS using electrospray ionisation (ESI).

However, there are also several challenges associated with miniaturised systems. Large volume injection on narrow columns are time-consuming, so more extensive sample preparation or pre-columns are needed to accommodate samples that would otherwise require larger volumes to be injected. Narrower columns, and accompanying narrow tubing and connections, are also more susceptible to blockages. The performance of miniaturised LC systems is especially vulnerable to extra-column band broadening, as the column volume itself is small. Gaps between tubing or columns in connections can amount to a significant volume when compared to the rest of the system volume and thus contribute to the overall band broadening (**Equation 5**).

1.2 Metal-organic frameworks

MOFs are two- or three-dimensional coordination network structures composed of nodes and organic linkers[17]. The organic linkers coordinate to the nodes to create structures with potential voids. The nodes, also referred to as secondary building units (SBUs), are typically metal ions or metal ion clusters. The linkers need to have functional groups that can successfully ligate the metal nodes, and subsequently often have Lewis base characteristics.

Figure 4 illustrates a simple MOF structure. The metal nodes are symbolized by red squares, and the organic linkers by grey sticks. The MOF illustrated here extends in three dimensions, and the cubic unit cell can repeat multiple times in all directions to create an extensive network.

The topology of the MOF is determined by the coordination numbers of the node and linker. A linker must be able to coordinate to at least two nodes, and a node must be able to coordinate to at least three linkers. The stability of the structure is determined by the strength of the bond between node and linker, and by the coordination number. A higher coordination number means more bonds exist, and thus the stability increases.

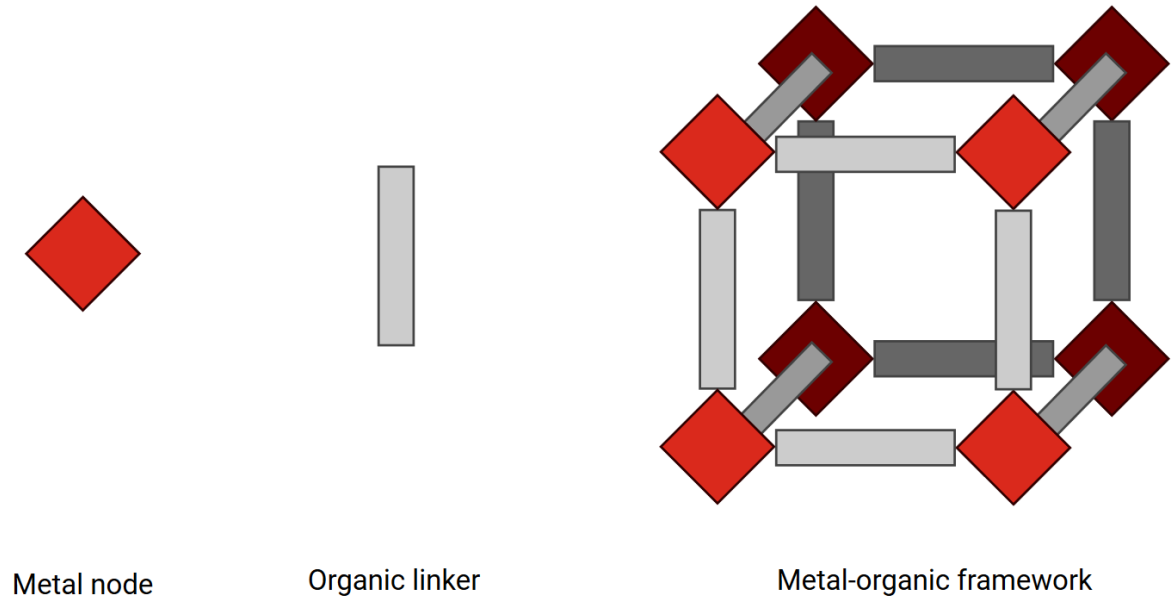

Figure 4 Schematic illustration of a simple MOF.

The first MOFs were reported in 1989[18] and 1990[19] by Hoskins and Robson, but the term metal-organic framework was not suggested until 1995 by Yaghi et al.[20]. Since then, many more MOFs have been created[21–26]. In principle, nodes and linkers can be varied as needed. However, not all combinations of nodes and linkers display the chemical, thermal or mechanical stability required for practical use[27]. Finding high stability nodes is viewed as more challenging than modifying linkers[25]. Per Coulumb's law, cations with high charge density have stronger bonds with ligands – this is also true for MOFs[28]. As long as the functionalities of linkers allow them to ligate the nodes to create the desired network structure, the rest of the linkers can be functionalized to better suit the desired activity. Linkers can be modified after the MOF has been synthesised[29].

MOFs have been a subject of study for over 20 years, and many applications are already proven in lab settings. Examples are catalysis[30–32], gas storage[21,33–35], and adsorption of toxins[36–38] and pollutants[39,40].

1.2.1 UiO-66

UiO-66-BDC, commonly referred to as UiO-66, is a zirconium-based MOF first reported by Cavka et al. at the University of Oslo (UiO) in 2008[25]. The MOF is composed of zirconium oxide nodes with the molecular formula $Zr_6O_4(OH)_4(CO_2)_{12}$ and benzene-1,4-dicarboxylate

linkers. The linker is shown in **Figure 5**. The node has a coordination number of 12, which is high among MOF nodes[25]. The unit cell is face-centred cubic.

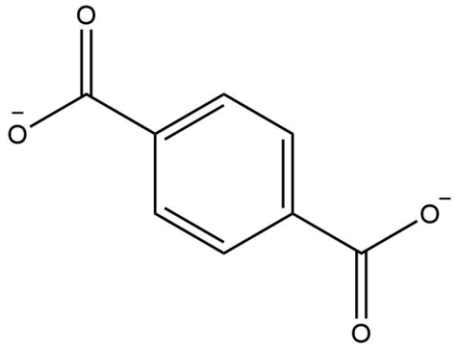

Figure 5 The benzene-1,4-dicarboxylate (BDC) linker of UiO-66.

The structure of UiO-66 gives rise to two kinds of cavities within the structure: tetrahedral and octahedral cavities in a 2+1 ratio. The octahedral cavities have an internal diameter of 12 Å, while the tetrahedral cavities have an internal diameter of 7.5 Å[41]. These cavities have an opening of approximately 6 Å[25].

The structure of UiO-66 can be viewed in **Figure 6**, where the left illustration depicts a "top view" of the crystal structure, while the right illustration gives a side view where the orange and green spheres, respectively, mark the octahedral and tetrahedral cavities.

As indicated in the molecular formula, the nodes of UiO-66 contain four hydroxy groups. These can be removed in a reversible dehydration which occurs at 250–300°C[42].

UiO-66 has a large surface area and pore volume, with a surface area of 1187 m^2/g[25] and a theoretical pore volume of 0.77 cm^3/g[43,44]. This, in combination with the stability of UiO-66[25,41,45,46], makes the MOF a promising candidate for applications both in research and industry. The weakest bond in the structure is the bond between the benzene ring and the carboxylate group that ligates the zirconium cluster[25].

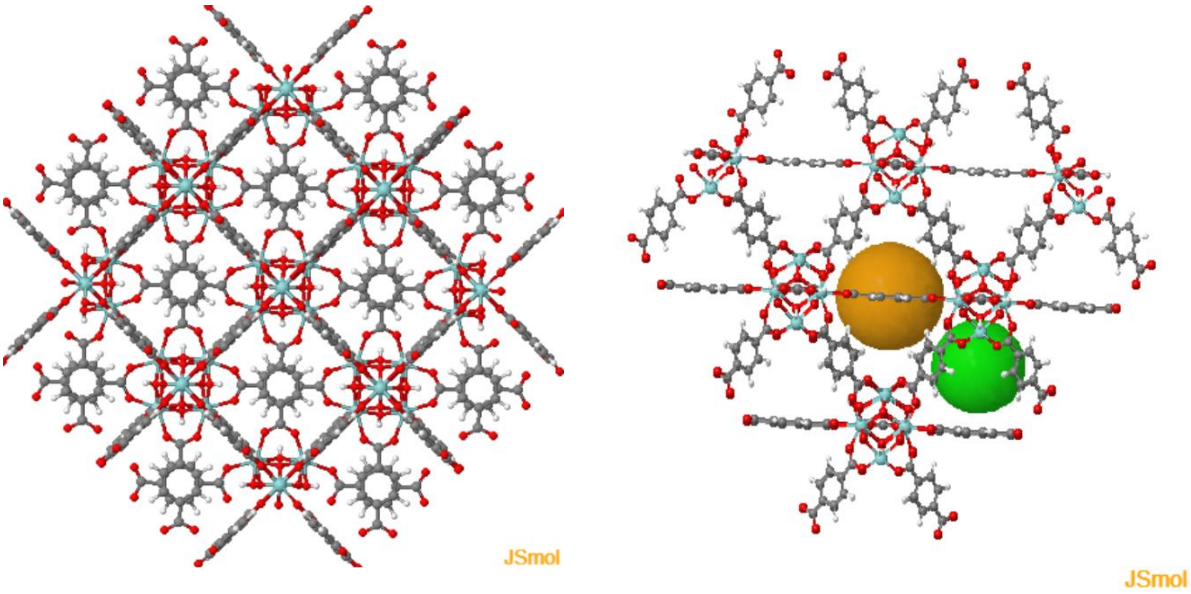

Figure 6 Structure of UiO-66. Figure adapted from Greeves from JSmol, which is hosted by the University of Liverpool[47] under a Creative Commons Attribution-Noncommercial-Share Alike 2.0 license. The orange and green spheres in the right illustration mark the voids in the structure and are not part of the structure itself.

Analogues to UiO-66 have been created, both through functionalising the BDC linkers[48,49] and by using longer linkers to create larger cavities[25].

1.2.2 UiO-66-NH_2

UiO-66-BDC-NH_2, often referred to as NH_2-UiO-66 or UiO-66-NH_2, is a variant of UiO-66 where the BDC linker is replaced by the amino-functionalised linker 2-amino-benzene-1,4-dicarboxylate[48,49]. The linker is shown in **Figure 7**. In this thesis, the MOF UiO-66-BDC-NH_2 will be referred to as UiO-66-NH_2.

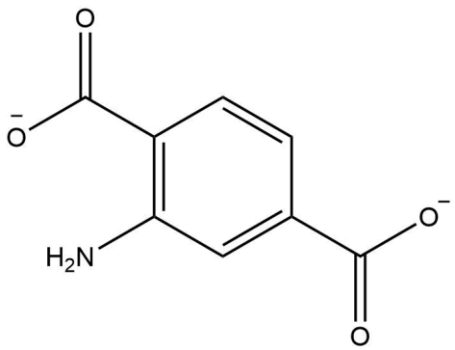

Figure 7 The 2-amino-benzene-1,4-dicarboxylate (ABDC) linker of UiO-66-NH_2.

UiO-66-NH_2 has a pore volume of 0.52 cm^3/g and a surface area of 1266 m^2/g according to the supplier ProfMOF[50]. While the pore volume is smaller than that of UiO-66, the surface area is higher. A 2014 study by Chavan et al.[51] compared a series of MOFs synthesised using 100/0, 50/50, 25/75 and 0/100 ratios of BDC and ABDC. They observed that pore volume and surface area decreased as the ratio of ABDC linker increased, likely due to the amino functionality occupying volume. As such, it is reasonable to assume that the pore opening diameter of UiO-66-NH_2 is narrower than the 6 Å opening diameter of UiO-66[52].

The 2014 study by Chavan et al.[51] found that UiO-66-NH_2 degraded more slowly in acidic environments than UiO-66. They also found that an increased ratio of ABDC linkers correlated with decreasing decomposition temperature.

The amino functionality means that the MOF can be protonated depending on the pH. While the pK_a of UiO-66-NH_2 is not known, a 2020 study by Chang et al.[53] found the point of zero charge to be at pH 5.66. Positive zeta potential was observed at lower pH values.

UiO-66-NH_2 has been proven to be a viable starting point for further functionalisation due to the reactivity of the amino functionality[29,52]. The catalytic properties of the material have also been investigated and proven[54].

1.2.3 Other UiO-materials

The UiO MOF series UiO-66, UiO-67 and UiO-68 all show very good thermal stability and tolerate various solvents well[25,41]. The linkers of UiO-67 and UiO-68 are biphenyl-4,4′-dicarboxylate (BPDC) and p-terphenyl-4,4″-dicarboxylate (TPDC), respectively. The linkers are shown in **Figure 8**. The longer linkers lead to larger pore sizes and surface area per mass, and larger pore openings. For UiO-67 and UiO-68, the pore opening is 8 Å and 10 Å, and the surface area 3000 m^2/g and 4170 m^2/g, respectively[25].

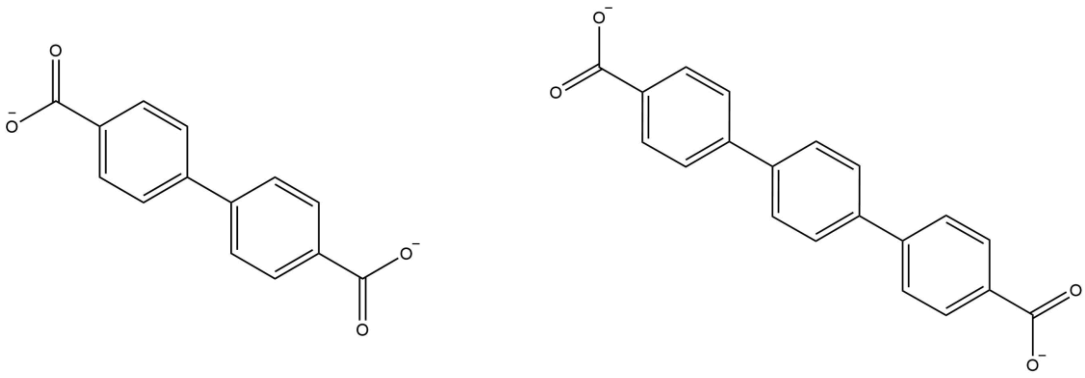

Biphenyl-4,4′-dicarboxylate p-Terphenyl-4,4″-dicarboxylate

Figure 8 The BPDC and TPDC linkers of UiO-67 and UiO-68, respectively.

1.3 Metal-organic frameworks in chromatography

As highly porous material types, with high surface area, MOFs have received attention in separation sciences in recent years. MOFs have been investigated as stationary phases in both gas chromatography[39,55–58] and LC[59–61], and as sorbents in solid phase extraction[62] and solid phase micro extraction[63–65].

In early LC studies of MOFs, MOF particles packed into columns resulted in high backpressures and band broadening[66,67]. The band broadening was hypothesised to be caused in large by uneven particle size and inhomogeneous packing. Addressing these challenges, composite particles have been studied. Both core-shell particles[68–71] and MOF grown on porous silica particle support[67,72] have been shown to yield backpressures compatible with HPLC systems. An alternative use of MOFs as an SP is in monolithic columns. Both MOF synthesised in situ in the column[73] and incorporation of MOF particles into the polymer mixture[61,74] have been reported. Incorporation of MOF particles in organic monolithic columns has resulted in the satisfactory separation of smaller molecules[61,75], a known challenge for traditional organic monolithic columns[76].

1.3.1 UiO-66 in liquid chromatography

As one of the MOFs that tolerate both water and organic solvents used in LC well, UiO-66 has been subject to many studies as an SP in LC[66,68–70,72,75,77,78], and Van der Perre et al.[66]

demonstrated that their observed selectivity in gas chromatography could be transferred to LC. The identified studies performed are summarised in **Table 1**.

The structure of UiO-66 offers several opportunities for interactions with solutes in chromatographic systems. The four hydroxy groups on the Zr-ion cluster node can participate in hydrogen bond interactions[38]; the π-π-system of the linker enables the MOF to participate in π-π-stacking and π-π-interactions[40,56]; the pore window size offers a size exclusion aspect to the material[56]; and the metal ion cluster might also participate in electrostatic interactions[40].

Table 1 Overview of selected previous studies involving UiO-66 in LC. Reference to the described work can be found in the first column. When several MPs are used, the various MPs are separated with a comma. Where information is not given in the published work, N/A is used in the table. L refers to length, DCM refers to dichloromethane, PAH refers to polyaromatic hydrocarbons, TMB refers to 3,3'5,5'-tetramethylbenzidine, UiO-66-poly(MMA-*co*-EDMA) refers to UiO-66-modified polymethylarylic acid-co-ethylene dimetharylate monolith.

Author(s)	**SP type**	**Particle size**	**Column dimensions**	**MP**	**Analytes**
Van der Perre et al.[66]	Neat MOF particles	N/A	2.1 mm ID 100 mm L	ACN/MeOH	Alkanes, small substituted benzenes, dimethylcyclohexanes
Zhao et al.[77]	Neat MOF particles	200 nm	4.6 mm ID 50 mm L	Hexane/DCM, MeOH/water	Small substituted benzenes
Yan et al.[72]	Composite, SiO_2 support	5 µm	2.1 mm ID 100 mm L	Hexane/DCM	Small substituted benzenes, PAHs
Zhang et al.[69]	Composite, SiO_2 support	5 µm	4.6 mm ID 150 mm L	ACN/water	Small substituted benzenes, TMB
Peristyy et al.[68]	Composite, SiO_2 support	5 µm	2.1 mm ID 50 mm L	Hexane	Alkanes, small substituted benzenes, biphenyl, anthracene
Arrua et al.[70]	Composite, SiO_2 support	5 µm, 2.1µm	2.1 mm ID 50 mm L	Hexane, ACN/water	Small substituted benzenes, PAHs
Gao et al.[78]	Composite, SiO_2 support	5 µm	4.6 mm ID 150 m L	CAN/water, ethanol/water, MeOH/water	Small substituted benzenes
Fu et al.[75]	Monolith, UiO-66-poly(MMA-*co*-EDMA)	N/A	4.6 mm ID 70 mm L	ACN/water	Small substituted benzenes, PAHs

Neat UiO-66 particles

By “neat MOF particles”, it is understood that this describes particles composed of only MOF with no support or other particles mixed into the packing slurry.

Van der Perre et al.[66] used neat MOF particles in their study and compared regular UiO-66 to two other varieties of UiO-66. The latter two will not be elaborated upon here. They experienced significant band broadening, which they attributed to variance in particle size and shape, and inhomogeneous packing. However, the authors mention neither size nor shape of the particles they used. The observed selectivity was different from that of traditional normal phase adsorption chromatography and reversed-phase chromatography, and more branched stereoisomers were more strongly retained. This effect was referred to as reverse shape selectivity[79], where molecules that fit more snugly inside the pores of UiO-66 are more strongly retained. In their study, they verified that alcohol groups interact strongly, further strengthening the hypothesis that hydrogen bond interactions contribute to retention.

Zhao et al.[77] used neat UiO-66 particles to separate small substituted benzenes and poly-aromatic hydrocarbons (PAHs) in both normal-phase mode and reversed-phase mode. The elution order was the same for both modes, where reverse shape selectivity was prominent. While they point out that peak symmetry was good, suggesting uniform packing, the efficiency was found to be inferior to typical silica-based C18 columns. The authors attribute this to the variance in particle shape and size. They report the particles to be between 50 nm and 450 nm, with 200 nm being the most common size, but do not comment on particle shape. The study also featured an investigation of the thermodynamics of the separation.

Silica-UiO-66 composite particles

Yan et al.[72] were the first to report UiO-66 synthesised on mesoporous silica particles. The composite particles gave significantly lower backpressures than neat MOF particles. However, few UiO-66-particles were attached to the silica particles. A hexane/DCM MP was used to separate a series of small substituted benzenes, a series of dichlorobenzenes and a series of polyaromatic hydrocarbons. Again the observed selectivity favoured stereoisomers that fit snugly in the UiO-66 pores. The larger PAHs were more strongly retained. It should be noted that there appeared to be inconsistencies within the data published, notably the retention times of the *ortho*-, *meta*- and *para*-isomers of chlorotoluene.

Zhang et al.[69] synthesised UiO-66 on mesoporous silica particles. In the subsequent HPLC use, they successfully separated mono-, di- and trisubstituted benzene compounds as well as 3,3'5,5'-tetramethylbenzidine (TMB). While MPs consistent with those used in RPLC were used, the observed selectivity was not consistent with RPLC. Solutes with size closely matching that of the pores were strongly retained compared to the rest, and different functional groups were observed to result in different retention. Zhang et al. argued that the pore size, π-π-interactions, and hydrophobic interactions, combined with interactions with the residual amino groups on the modified silica support particles, could explain the retention patterns observed.

Peristyy et al.[68] synthesised UiO-66@SiO_2 particles using a method similar to the one used by Zhang et al., and used the material in normal-phase mode with hexane as MP to separate alkanes, small substituted benzenes, biphenyl and anthracene. They reported what they called flow-dependent separation, where the retention factor k changed with varying flow rate. The observed changes were larger for smaller molecules (toluene, ethylbenzene) than for larger (anthracene, cumene, biphenyl), and the authors related the observed effects to SEC. They also reported a significant increase in column volume as suggested by increased t_M with increasing flow rate. They did note that the composite nature of the particles used might result in interactions with residual groups. In a later work by the same group[70], Arrua et al. presented the hypothesis that slow kinetics might be the reason for the flow-dependent selectivity. In this study, they performed separations on UiO-66@SiO_2 particles in both normal-phase mode and reversed-phase mode. They noted that hydrogen bond interactions with the OH-groups in the zirconium cluster of UiO-66 could explain band broadening and retention patterns observed for phenolic compounds.

Gao et al.[78] also synthesised UiO-66@SiO_2 particles and used the material in reversed-phase mode. They separated *ortho*-, *meta*- and *para*-isomers of xylene, testing the separation with both ACN, ethanol and MeOH as the organic modifier in an aqueous MP. MeOH was found to give the most desirable chromatography, as it was reportedly the only MP that successfully separated the *meta*- and *para*-isomers. Reverse-shape selectivity was also observed in this study, with the *ortho*-isomer being the most retained. For comparison, a C18 column was also tested, but this column failed to separate all three isomers.

UiO-66 incorporated in monoliths

Fu et al.[75] demonstrated that UiO-66 incorporated in a polymethylarylic acid-co-ethylene dimetharylate monolith (poly(MAA-*co*-EDMA)) resulted in the successful separation of small substituted benzenes.

In summary, UiO-66 in various formats have been investigated as an SP in LC using MPs common for both NPLC and RPLC. The material exhibits several types of retention mechanisms, with the reversed shape selectivity being an important factor observed in several of the studies[66,72,77,78]*. More recent studies seem to focus more on composite particles, which address the challenges arising from poor particle uniformity for the pure MOF particles. The studies conducted so far have focused primarily on hydrocarbons and hydrocarbons with some polar groups. Hence there is a need for more studies on the suitability of UiO-66 as an LC separation material for various types of compounds. To the best of the author's knowledge, no studies have been published using UiO-66 as an SP in miniaturised LC systems.*

The reader is advised to notice that searches in some of the most well-known search engines (Web of Science, Scopus, Oria, Google Scholar) for the term "UiO-66" AND "chromatography" *have yielded no further results for studies of UiO-66 as an SP for LC as of July 23rd 2020.*

1.3.2 UiO-66-NH_2 in chromatography

While UiO-66-NH_2 has been studied as a sorbent in extractions[65,80,81] and as a component in novel detectors[82], few studies on the material as an SP in LC have been conducted. The identified studies on UiO-66-NH_2 in LC are summarised in **Table 2**. In addition to the studies referred to in the table, a 2020 study by Ning et al.[83] was recently published. However, this study is to the best of the author's knowledge only available in Chinese.

Table 2 Overview of selected previous works involving UiO-66-NH_2 in LC. Reference to the described work can be found in the first column. When more SPs or MP mixes are used, the different ones are separated with a comma. Where information is not given in the published work, N/A is used in the table. L refers to length, OT refers to open tubular capillary column, UiO-66-NH_2-pGMA refers to UiO-66-NH_2-modified poly(glycidyl methacrylate).

Author(s)	SP type	Particle size	Column dimensions	MP	Analytes
Zhao et al.[84]	MOF-particles	N/A	4.6 mm ID 50 mm L	Hexane/DMC, MeOH/water	Small substituted benzenes, PAHs
Chen et al.[85]	MOF-OT Monolith UiO-66-NH2-pGMA	150 nm (neat MOF)	25 µm ID 120 cm L	ACN/water	Small substituted benzenes

Zhao et al. followed their 2014 study of UiO-66 in HPLC[77] with a 2017 study on UiO-66-NH_2 and UiO-67[84]. Neat MOF particles were used. They found that UiO-66 outperformed UiO-66-NH_2 for separation of small substituted benzenes in both normal phase-mode and reversed-phase mode. This was attributed to the amino group reducing the pore volume.

Chen et al.[85] successfully modified a poly(glycidyl methacrylate) (pGMA) open tubular (OT) capillary column with UiO-66-NH_2, creating a UiO-66-NH_2-pGMA column. They also modified a fused silica capillary column with UiO-66-NH_2 particles on the column walls to create a UiO-66-NH_2-OT column, and a pGMA OT column for comparison. The UiO-66-NH_2-pGMA-column showed reversed-phase selectivity for alkylbenzenes. Five different phenols were separated on the UiO-66-NH_2-pGMA-column, while the UiO-66-NH_2 OT column did not provide baseline separation and the pGMA-column could not separate the stereoisomers. The authors pointed to hydrogen bond interactions as the most likely explanation for the retention order observed, where the phenol with the lowest pK_a, the *ortho*-isomer, was most strongly retained. The UiO-66-NH_2-pGMA-column separated anilines successfully. This column was also utilised to perform chromatography of a liquorice extract.

The work by Chen et al.[85] suggests that the amino group might play an important role in hydrogen bond interactions. However, the stronger retention of *ortho*-isomers compared to *meta*- or *para*-isomers was also observed multiple times for UiO-66 as an SP[69,70,72,77]. Hydrogen bond interactions have also been suggested as an interaction contributing to

retention in UiO-66[66,70]. As the zirconium clusters in the nodes of UiO-66 have hydroxy groups[25], hydrogen bonding can also occur in regular UiO-66. Thus UiO-66-NH_2 has two different functionalities that may participate in hydrogen bond interactions.

In summary, very few studies on UiO-66-NH_2 in LC have been published. The studies that have been conducted, suggest that UiO-66-NH_2 in neat form might not be a suitable SP for separation of hydrocarbons. However, the compounds selected for testing are all substituted benzenes or PAHs. Little is known about how small aliphatic molecules or molecules without conjugated π-electrons interact with the MOF. Thus, more studies of UiO-66-NH_2 are needed to conclude about its suitability as an LC separation material.

2 Aim of study

The aim of this thesis was to investigate the chromatography of selected compounds on primarily UiO-66, but also UiO-66-NH_2, and thus to learn more about the potential applications of the UiO materials in LC. The two materials were packed in nano-LC columns of 100 µm ID, and the study was performed with emphasis on small hydrophilic compounds (small neurotransmitters and adenosine phosphates) as solutes in aqueous MPs typically used for RPLC.

The two UiO materials were evaluated based on the packing properties, the effect of mobile phase composition on the chromatography of the selected compounds, the effect of linear velocity on chromatographic efficiency, and the effect of temperature on the chromatography. In addition, an estimate of the maximum molecular size able to access the pores of UiO-66 was also established.

3 Experimental

3.1 Chemicals

Formic acid (98–100%, FA), uracil (>99%), phenanthrene (>97%) and benzene (97%) was purchased from Merck (Darmstadt, Germany). Phenol was provided by Associate Professor Tore Bonge-Hansen, and thus specifications and manufacturer are regrettably unknown. Adenosine monophosphate (AMP) monohydrate (>97%), adenosine diphosphate (ADP) sodium salt (>95%), ethylbenzene (99%), propylbenzene (98%), butylbenzene (>99%), pentylbenzene (99%), heptylbenzene (98%), octylbenzene (99%), nonylbenzene (96%) and decylbenzene (98%) were obtained from Sigma Aldrich (St. Louis, MO, USA). N-nonadecylbenzene (unknown purity) was from Alltech Associates (Columbia, MD, USA). Naphthalene (99+%) was from Alfa Aesar (Haverhill, MA, USA). Chrysene (>95%) was from Fluka AG (Buchs, Switzerland).

Dopamine HCl, serotonin HCl and γ-aminobutyric acid (GABA) were obtained from Sigma Aldrich. 2-(3,4-Dihydroxyphenyl)ethyl-1,1,2,2-d4-amine HCl, serotonin-α,α,β,β-d4 creatinine sulfate complex and 4-aminobutyric-4,4-d2 acid were obtained from CDN Isotopes (Quebec, Canada).

HPLC LC-MS grade acetonitrile and HPLC LC-MS grade methanol for use in mobile phases as well as methanol (99.9%) were purchased from VWR (Radnor, PA, USA). Type 1 water was obtained from a Milli-Q Integral purification system with 0.22 µm filter Q-POD dispenser from Millipore Corp. (Burlington, MA, USA). Nitrogen gas (>99.99%) was purchased from Nippon Gases Norge (Oslo, Norway).

UiO-66-BDC particles with a size distribution of 0.2–0.5 µm and UiO-66-BDC-NH_2 particles with a size distribution of 0.1–0.5 µm were provided by ProfMOF (Kongsberg, Norway).

3.2 Solutions

Solutions were prepared as described in **Table 3**, **Table 4** and the paragraph that follows the tables. As **Table 3** indicates, mass *m* of the compound in question was transferred to a volumetric flask of volume V_1 and diluted to concentration C_1. Volume V_{transf} was transferred

to a volumetric flask of volume V_2 and diluted to the concentration C_{fin}. For chrysene, the solution was made in a one-step dilution.

Table 3 Overview of making of injection solutions of uracil, phenol, ADP, AMP, benzene, toluene, ethylbenzene, propylbenzene, butylbenzene, pentylbenzene, hexylbenzene, heptylbenzene, octylbenzene, nonylbenzene, decylbenzene, nonadecylbenzene, naphthalene, phenanthrene, and chrysene.

Compound	m (mg)	V_1 (mL)	C_1 (mg/mL)	V_{transf} (mL)	V_2 (mL)	C_{fin} (mg/mL)	Solvent
Uracil	5.0	5.00	1.00	1.25	5.00	0.25	T1 water
Phenol	6.1	10.00	0.61	2.05	5.00	0.25	T1 water
ADP sodium salt	5.5	5.00	1.10	1.25	5.00	0.28	T1 water
AMP monohydrate	5.1	5.00	1.02	1.25	5.00	0.26	T1 water
Benzene	97.4	100.00	0.97	2.57	10.00	0.25	MeOH
Toluene	136.5	100.00	1.37	1.83	10.00	0.25	MeOH
Ethylbenzene	99.4	100.00	0.99	2.52	10.00	0.25	MeOH
Propylbenzene	60.5	50.00	1.21	1.03	5.00	0.25	MeOH
Butylbenzene	40.2	50.00	0.80	1.5	5.00	0.24	MeOH
Pentylbenzene	46.2	50.00	0.92	1.35	5.00	0.25	MeOH
Hexylbenzene	53.6	50.00	1.07	1.17	5.00	0.25	MeOH
Heptylbenzene	50.1	50.00	1.00	1.25	5.00	0.25	MeOH
Octylbenzene	62.8	50.00	1.26	1.00	5.00	0.25	MeOH
Nonylbenzene	62.0	50.00	1.24	1.01	5.00	0.25	MeOH
Decylbenzene	76.9	50.00	1.54	0.810	5.00	0.25	MeOH
Nonadecyl-benzene	24.6	25.00	0.98	1.26	5.00	0.25	MeOH
Naphthalene	12.3	5.00	2.46	0.508	5.00	0.25	MeOH
Phenantrene	8.0	5.00	1.60	0.780	5.00	0.25	MeOH
Chrysene	5.2	25.00	-	-	-	0.21	MeOH

Table 4 describes how the injection solutions from already made solutions were made. Solutions used as starting solutions were made as described in **Table 3**. A volume of V_{transf} of the starting solution was transferred to a 5 mL volumetric flask, or an autosampler vial from VWR in the cases where the final volume V_1 was 1 mL. After dilution, the final concentration was C_{fin} in solvent as indicated in the table.

Standard solutions of 2 mg/mL 3', 5'-cyclic adenosine monophosphate (cAMP) solution as made by M.Sc. Ahmad Tsjokajev and stored at -20°C. The thawed standard solution was diluted as described in **Table 4**.

Table 4 Overview of making of solutions of toluene, ethylbenzene and butylbenzene, benzene, naphthalene and phenanthrene, toluene, ethylbenzene, butylbenzene, benzene, naphthalene, and phenanthrene.

Compound	C_1 (mg/mL)	V_{transf} (mL)	V_1 (mL)	C_{fin} (mg/mL)	Solvent
cAMP	2.00	0.630	5.00	0.25	T1 water
AMP	1.10	1.25	5.00	0.28	T1 water
ADP	1.10	1.25		0.28	
cAMP	2.00	0.630		0.25	
Toluene	1.37	0.920	5.00	0.25	75% MeOH 25% T1 water
Ethylbenzene	0.99	1.26		0.25	
Butylbenzene	0.80	1.56		0.25	
Benzene	0.97	1.28	5.00	0.25	52% MeOH 48% T1 water
Naphthalene	2.46	0.510		0.25	
Phenanthrene	1.60	0.830		0.27	
Toluene	0.25	0.500	1.00	0.12	50% MeOH 50% T1 water
Ethylbenzene	0.25	0.500	1.00	0.13	50% MeOH 50% T1 water
Butylbenzene	0.24	0.500	1.00	0.12	50% MeOH 50% T1 water
Benzene	0.25	0.500	1.00	0.13	50% MeOH 50% T1 water
Naphthalene	0.25	0.500	1.00	0.12	50% MeOH 50% T1 water
Phenanthrene	0.25	0.500	1.00	0.12	50% MeOH 50% T1 water

Standard solutions of 1 mg/mL GABA and 4-aminobutyric-4,4-d2 acid, dopamine and 2-(3,4-dihydroxyphenyl)ethyl-1,1,2,2-d4-amine HCl, and serotonin and serotonin-α,α,β,β-d4 creatinine sulfate complex prepared by Dr. Elin Johnsen[86] were used as starting materials. These standard solutions were originally prepared by Johnsen for MS detection in 2015, and have been stored in a -80°C freezer in 1.5 mL Eppendorf Safe-Lock Tubes (Eppendorf, Hamburg, Germany). The volume of the solutions varied slightly and was only approximately determined by the help of the measurement indicators on the tubes themselves. Dilution was

done in the Eppendorf tubes; the serotonin solution, the volume of which was approximately 0.3 mL when thawed, was diluted with 1.2 mL T1 water to a final concentration of approximately 0.2 mg/mL; the dopamine solution, the volume of which was approximately 0.5 mL when thawed, was diluted with 1.0 mL T1 water to a final concentration of approximately 0.3 mg/mL; and the GABA solution, the volume of which was approximately 0.5 mL, was diluted with 1.0 mL T1 water to a final concentration of approximately 0.3 mg/mL.

Mobile phases were made from HPLC-MS grade ACN or MeOH, T1 water and FA. All MPs were mixed v/v.

3.3 Materials and equipment

All weighings were done on an AT 2000 model analytical balance from Mettler Toledo (Columbus, OH, USA).

All MPs were sonicated using a Branson 5510 ultrasonic bath from Marshall Scientific (Hampton, NH, USA) for minimum 15 minutes prior to use.

Fused silica tubing was purchased from Polymicro Technologies (Phoenix, AZ, USA). Fused silica tubing with 20 µm ID was used for tubing, and 100 µm ID was used for columns. All fused silica tubing had an outer diameter (OD) of 360 µm.

3.4 Liquid chromatography system

Three different LC setups were used during this study.

In the first LC setup, an Easy-nLC pump from Proxeon (Odense, Denmark, currently Thermo Fischer Scientific) was used. In the other two, a Nano Aquity Ultra Performance LC pump from Waters (Milford, MA, USA) was used. In all setups the pump was attached to a two-position four-port valve injector with a 50 nL loop from VICI (Huston, TX, USA). ZU1C (250 µm bore) and ZU1XC (150 µm bore) unions used to connect the appropriate tubing in the LC setup were also purchased from VICI.

For the two first setups (I and II), the column was directly attached to the injector. The outlet frit end of the column was attached to a 20 µm ID 360 µm OD fused silica capillary of 25 cm

length which was attached to the detector. The detector was a VWD-3400RS variable wavelength UV detector from Dionex (Sunnyvale, CA, USA) equipped with a 30 nL flow cell with a 10 mm path length. Injections were initiated by sending an analogue signal through a Dionex UCI-50 Universal Chromatography Interface, which linked the detector to a PC with the chromatography software Chromeleon™ 7.1.0.898 Chromatography Data System from Thermo Fischer Scientific (Waltham, MA, USA). A sketch of setup I and II is shown in **Figure 9**.

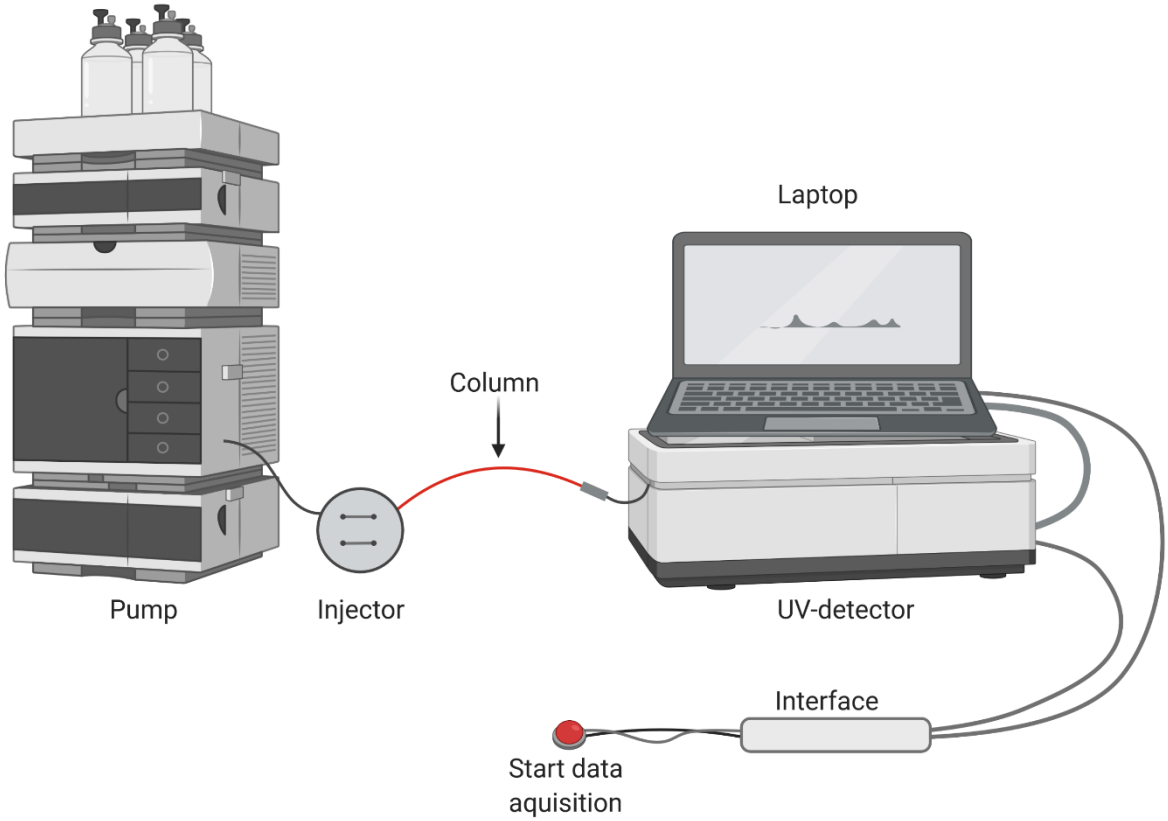

Figure 9 Sketch of LC setup I and II. Figure created with BioRender.com.

For LC setup III, 65.2 cm 20 µm ID 360 µm OD fused silica tubing connected the injector and the column, which was housed inside a Mistral 880 column oven from Spark Holland (Emmen, The Netherlands). A 72.1 cm long piece of 20 µm ID 360 µm OD fused silica tubing connected the frit end of the column to a 20 µm ID 360 µm OD fused silica capillary of 21.5 cm length which was attached to the detector. A sketch of LC setup III is shown in **Figure 10**.

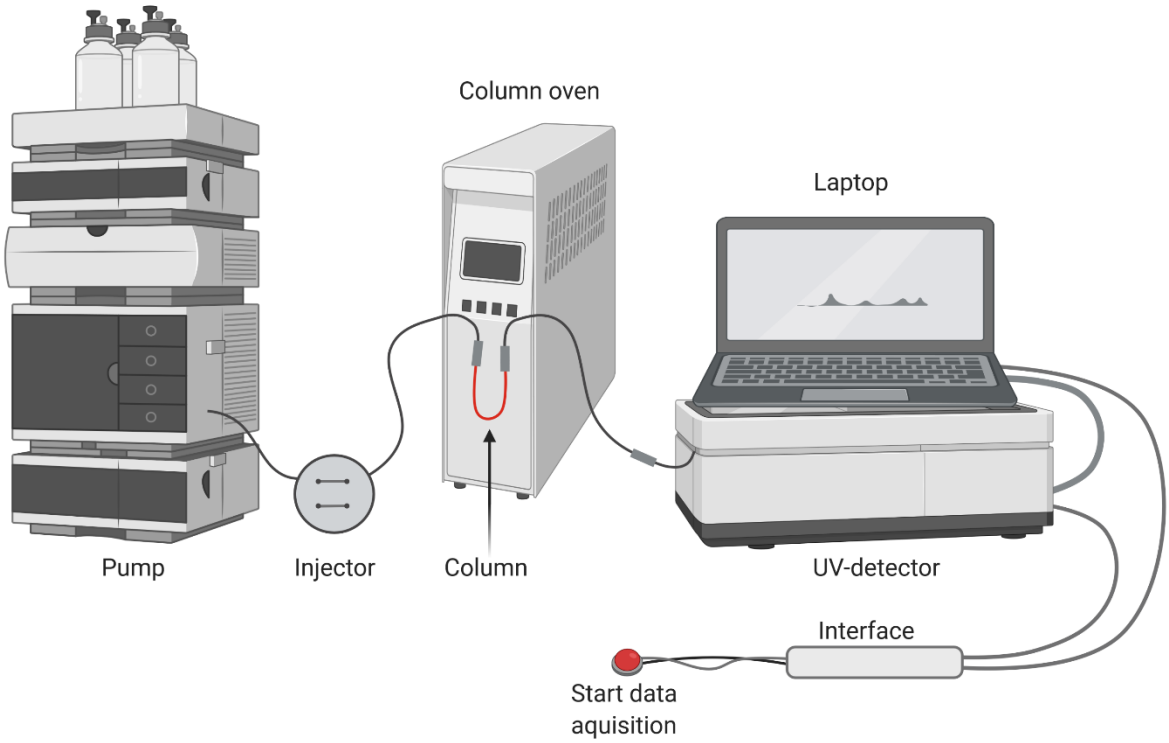

Figure 10 Sketch of LC setup III. Figure created with BioRender.com.

The extra-column volume ($\boldsymbol{V_{extra-column}}$) in both LC setup II and III for the different columns are shown in **Table 5**. The column volume ($\boldsymbol{V_{column}}$) is also shown, both in nm^3 and in relative volume ($\boldsymbol{V_{\%,\ column}}$).

Table 5 Overview of volume of packed column and extra-column volume for the different columns in the different LC systems. The column numbering is as in **Table 6** in section **4.1**.

Column	SP	LC setup	$\boldsymbol{V_{column}}$ (nm^3)	$\boldsymbol{V_{extra-column}}$ (nm^3)	$\boldsymbol{V_{\%,\ column}}$
a	UiO-66	II	0.67	0.32	68%
b	UiO-66	II	0.51	0.80	39%
b	UiO-66	III	0.51	1.23	29%
d	UiO-66-NH_2	II	0.55	1.41	28%

3.5 Packing of columns

The method for preparation of columns was based on the method described by Berg et al[87].

Columns were made from 100 µm ID, 360 µm OD fused silica tubing. The frits of the columns were prepared using Frit Kit from Next Advance (Averill Park, NY, USA) which

contained Kasil 1, Kasil 1624 and formamide. Both Kasil 1 and Kasil 1624 are 29/71 potassium silicates/water w/w, where Kasil 1624 has a SiO_2/K_2O w/w ratio of 1.65. Frits were made by mixing 6 µL Kasil 1624 and 2 µL formamide in an Eppendorf tube. Pieces of fused silica tubing of approximately 20–40 cm length were dipped into the mixture for a few seconds, and the mixture was pulled into the tubing by capillary forces. The pieces of tubing were then dried in a GC-17A oven from Shimadzu (Kyoto, Japan) overnight or over the weekend. The frit ends were cut to leave a 1–2 mm frit. Columns were flushed through with MeOH before packing.

The slurry was prepared in glass vials with a 3x3 mm magnetic stirring bead, both from VWR. The vial was filled with 30 mg MOF particles, and 1 mL MeOH was added. The vial was sonicated in an ATM40-0.7LC model ultrasonic bath from ATU Ultrasonidos (Valencia, Spain) for 15 minutes, creating a slurry. The vial was then transferred to the packing station, where packing was performed with a mobile and airtight packing module as seen in Figure 11. The top part of the module featured an entry point for capillary tubing to be secured with a ferrule and a nut. During packing the module was placed on a Topolino model magnetic stirrer from IKA (Staufen, Germany).

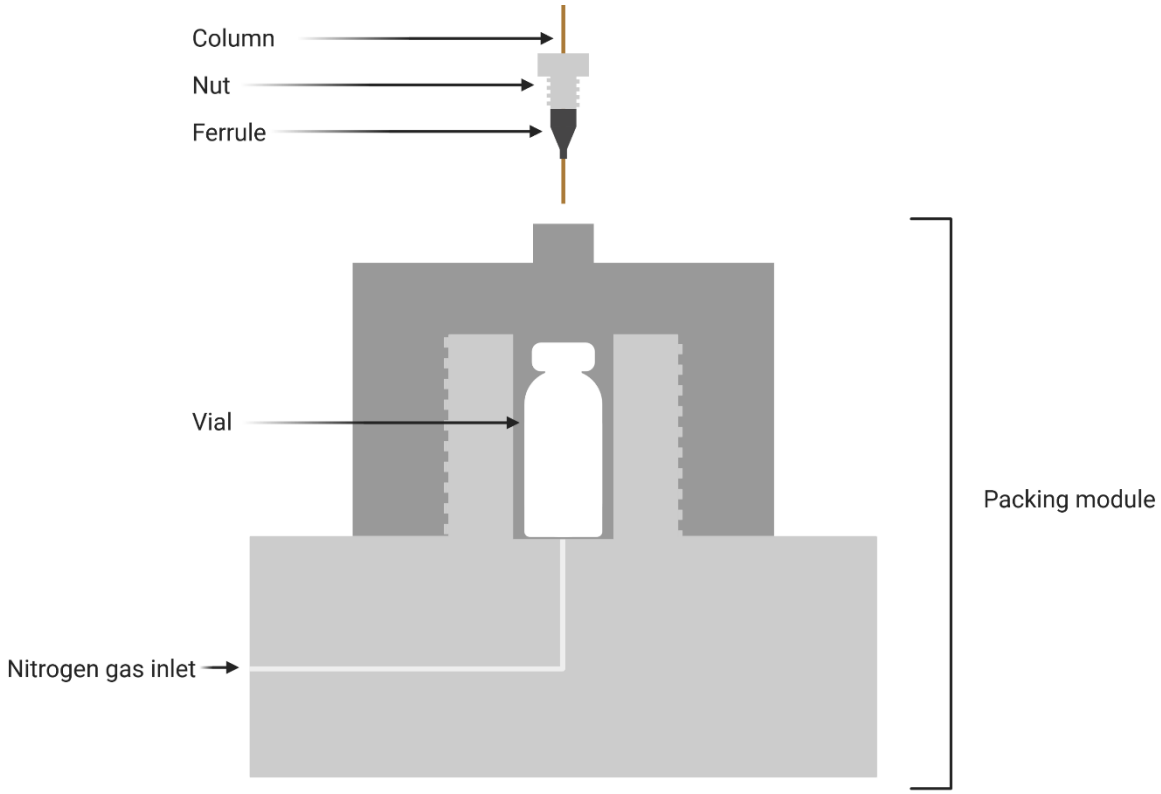

Figure 11 Sketch of the packing module. Figure adapted from Berg et al.[87]

Determination of packing speed was done by measuring packed length with a 20 cm ruler and noting the time passed from the beginning of the packing process as measured with the stopwatch feature of a Samsung Galaxy S8 smartphone (Seoul, South Korea).

Visual inspection of the column packing and column ends was performed with a light microscope manufactured by Motic (Xiamen, China) with eyepiece lenses of W10X/30 power and an objective lens of 4X power.

3.6 Particle imaging and element analysis

For particle imaging and elemental analysis of both UiO-66 and UiO-66-NH_2, an SU8230 ultra-high resolution cold-field emission scanning electron microscope from Hitachi (Tokyo, Japan) was used. The scanning electron microscope (SEM) was equipped with an Energy Dispersive X-ray Spectrometer (Quantax EDS) from Bruker (Billerica, MA, USA). The SEM imaging and elemental analysis by energy dispersive x-ray spectroscopy (EDXS) were performed by Prof. Karl Petter Lillerud.

3.7 Efficiency investigations

Three injection solutions of uracil and phenol were used for this part of the study. The first solution was uracil in T1 water, the second phenol in T1 water, and the third was uracil and phenol in T1 water. All solutes were present in 0.25 mg/mL concentration.

LC setup was as shown in **Figure 9**. Initially, setup I as described in section **3.4** was used. Subsequently, setup II was used. A 100 µm ID 50 mm L capillary column was used in setup I. A 100 mm ID 52 mm L capillary column was used in setup II. Both columns were packed with UiO-66 MOF particles. UV detection was performed at 270 nm.

The following description is for both setups: MP reservoir A contained 0.1% FA v/v. MP reservoir B contained 90% ACN/0.1% FA v/v. The pump was set to deliver 15% MP B, which equals to 13.5% ACN v/v in the MP delivered.

The uracil solution and the phenol solution were injected once to establish retention time for the compounds. The solution with uracil and phenol was then injected three times or more, if deemed necessary.

3.8 Investigation of retention of compounds

Aqueous solutions of AMP, ADP, cAMP, GABA, serotonin, and dopamine were used. There were four AMP, ADP and cAMP solutions, one of each solute at 0.26 mg/mL, 0.28 mg/mL and 0.25 mg/mL respectively, one containing all at 0.28 mg/mL, 0.28 mg/mL and 0.25 mg/mL respectively. The GABA, serotonin and dopamine solutions were 0.3 mg/mL, 0.2 mg/mL and 0.3 mg/mL respectively.

LC setup II (**Figure 9**) as described in section **3.4** was used, but with various columns. UV detection was performed at 270 nm.

MP reservoir A contained 0.1% FA v/v. MP reservoir B contained 90% ACN/0.1% FA v/v. A flow rate of 0.55 µL/min was used.

One UiO-66-column of 100 µm ID, 52 mm L, one UiO-66-column of 100 µm ID, 95 mm L and one UiO-66-NH_2-column of 100 mm ID, 71 mm L were used.

With the <115 mm long UiO-66-column, MP compositions of 1%, 2%, 5%, 10% and 15% B were investigated, corresponding to 0.9%, 1.8%, 4.5%, 9.0%, and 13.5% ACN v/v, respectively.

With the 52 mm long UiO-66-column, MP compositions of 0%, 15% and 30% B were investigated, corresponding to 0%, 13.5% and 27.0% ACN, respectively.

On the UiO-66-NH_2-column, MP compositions of 0%, 15% and 30% B were investigated,corresponding to 0%, 13.5% and 27.0% ACN, respectively.

All solutions were injected three times or more for all MP compositions on all columns, with the following exceptions: the solution containing AMP, ADP and cAMP was injected twice at 5% B, once at 10% B, and not on the <115 mm long column at 15% B; the AMP solution was injected twice at 0% B and 15% B on the 52 mm long UiO-66-column; the ADP solution was injected twice at 0% B and 15% B on the 52 mm long UiO-66-column; the cAMP solution was injected twice at 0% B and 15% B on the 52 mm long UiO-66-column; the solution containing AMP, ADP and cAMP was not injected on the UiO-66-NH_2-column.

The 0.25 mg/mL uracil solution was also injected three times or more for all MP compositions on all columns.

3.9 Van‘t Hoff experiments

Eight different solutions were used in this investigation. Four were solutions containing toluene, ethylbenzene and butylbenzene, one where all solutes were present at 0.25 mg/mL concentration, and one for each solute individually at 0.12 mg/mL, 0.13 mg/mL and 0.12 mg/mL respectively. Four were solutions containing benzene, naphthalene and phenanthrene,

one where all solutes were present at 0.25 mg/mL, 0.25 mg/mL and 0.27 mg/mL concentration respectively, and one for each solute individually at 0.13 mg/mL, 0.12 mg/mL and 0.12 mg/mL concentration respectively.

LC setup III (**Figure 10**) was used with a 100 µm ID, 95 mm L column packed with UiO-66. UV detection was performed at 255 nm.

MP was 75% MeOH/0.1% FA v/v, pre-mixed.

All alkylbenzene solutions were injected minimum three times for all temperatures. The PAH solutions were only injected three times for one temperature. The naphthalene solution and the phenanthrene solution were only injected once.

In addition, T1 water and ACN were injected three times for all temperatures to determine t_M.

3.10Pore volume accessibility

In this investigation, 15 different solutions were used. Eleven were solutions of the alkylbenzenes toluene, ethylbenzene, propylbenzene, butylbenzene, penylbenzene, hexylbenzene, heptylbenzene, octylbenzene, nonylbenzene, decylbenzen, and nonadecylbenzen, all solutes present at 0.25 mg/mL except for butylbenzene, which was at a 0.24 mg/mL concentration. Four were solutions of benzene, naphthalene, phenanthrene and chrysene, the former three at 0.25 mg/mL concentration, the latter at 0.21 mg/mL concentration.

LC setup II (**Figure 9**) was used with a 100 µm ID, 95 mm L column packed with UiO-66. UV detection was performed at 255 nm.

MP was 100% MeOH.

Each solution was injected three times or more if deemed necessary. T1 water and ACN were also injected tree times to establish t_M.

3.11Treatment of data

Retention times, peak width and peak area were determined using the Chromeleon™ 7.1.0.898 Chromatography Data System. Length of the packed column was measured after the

column was detached. Plate numbers (**Equation 2**), plate height (**Equation 3**), and retention factors (**Equation 9**) were calculated in Google Sheets (Google, Mountain View, CA, USA). Averages, standard deviations, and replicate counts were found using the inbuilt AVERAGEIFS, COUNTIFS, STDEV and FILTER functions in Google Sheets.

Where applicable, data sets were compared using F-tests followed by Student's t-test where two sets were to be compared, and one-way analysis of variance (ANOVA) where more data sets were to be compared.

4 Results and discussion

The focus of the present study was to provide a better understanding of UiO-66 and UiO-66-NH_2 as stationary phases for LC. More emphasis was placed on UiO-66 than UiO-66-NH_2. The packing properties of the MOF particles and the efficiencies of the packed columns were to be investigated. The chromatography of a selection of small polar biomolecules on both materials was to be studied, as well as the effect of temperature on the chromatography. In addition to this, an estimate of how large molecules could access the pores of the materials was to be established.

Due to the COVID-19 pandemic, the investigations conducted had to be cut back in scope. The reader is referred to section **6.3** in the appendix for more information.

In the following, the packing properties of the UiO-66 and UiO-66-NH_2 particles are presented, followed by the column efficiency study of UiO-66. Then the chromatography of a selection of small neurotransmitters and adenosine phosphates on UiO-66 and UiO-66-NH_2 as well as the chromatography of alkylbenzenes on UiO-66 is presented, followed by investigations of the effect of temperature on chromatography on UiO-66 and investigations of pore volume accessibility for UiO-66.

In section **6.2** in the appendix, supplementary information and chromatograms to illustrate typical chromatogram appearance can be found.

4.1 Packing properties of UiO-66 and UiO-66-NH_2

In this section, a comparison of the packing speed of UiO-66 and UiO-66-NH_2 is presented, loss of packed particles during the packing procedure is commented on, and the particle size used is discussed.

Packing properties of SP particles are important for the chromatographic performance of the system, as well as for practical and economic reasons. For these reasons, information about the column packing procedure of UiO-66 and UiO-66-NH_2 was recorded.

For capillary columns, in-house packing has been found to be a cheap and well-performing option for silica-based C18 particles[87]. For the work presented in this thesis, narrow columns of 100 µm ID were chosen because of the advantages of narrow column inner diameter in

terms of avoiding radial dilution, reduced mobile phase consumption and the lower packing material requirement. The already established packing method[87] and available equipment were also important factors when deciding to pack fused silica capillary columns in-house.

The packing method used was largely as described by Berg et al.[87], using MeOH as the solvent for the slurry. Optimisation of the packing procedure for the particles used was not attempted, as this was not in line with the aim of the present study. One attempt was made to pack without using a magnetic stirring bar, but the packing stagnated at 3 cm packed length, and the stirring bar was used for all subsequent column packings.

When packing, the final column length was kept between 5 and 10 cm long, because longer columns would mean longer retention times. As all injections were manual, long retention times were undesirable seeing as they would greatly limit the number of injections possible.

The slurries used for packing consisted of ca. 30 mg of MOF particles in 1 mL of MeOH. One slurry was sufficient to pack a minimum of four columns.

Comparison of packing speed

The columns packed with UiO-66 particles were observed to pack more quickly than UiO-66-NH_2 particles. Therefore, packing speed was measured to quantify the packing speed of UiO-66 and UiO-66-NH_2 during a routine packing. Two columns were packed with each MOF material, as there were only four fused silica tubing pieces available with good frit remaining from the last batch made.

In **Figure 12**, the packed lengths of the four columns are plotted as a function of time. The gas pressure used for packing was 240 bar. UiO-66 particles packed to a length of 15 centimetres approximately twice as quickly as UiO-66-NH_2. A ruler and the stopwatch on a smartphone were used as measuring tools. This relative primitive measuring equipment was effective, but there is uncertainty associated with the measurements. The series from the packing of column *b* in **Figure 12** is sparser than the other measurement series because of the manual nature of the measuring and the consequential need of the operator to establish a routine for measuring.

While fast packing was a desired feature due to the short time needed to pack the columns, it should be noted that rapid packing has been associated with poorer efficiencies[88,89], as the particles have less time to rearrange into a more densely packed formation.

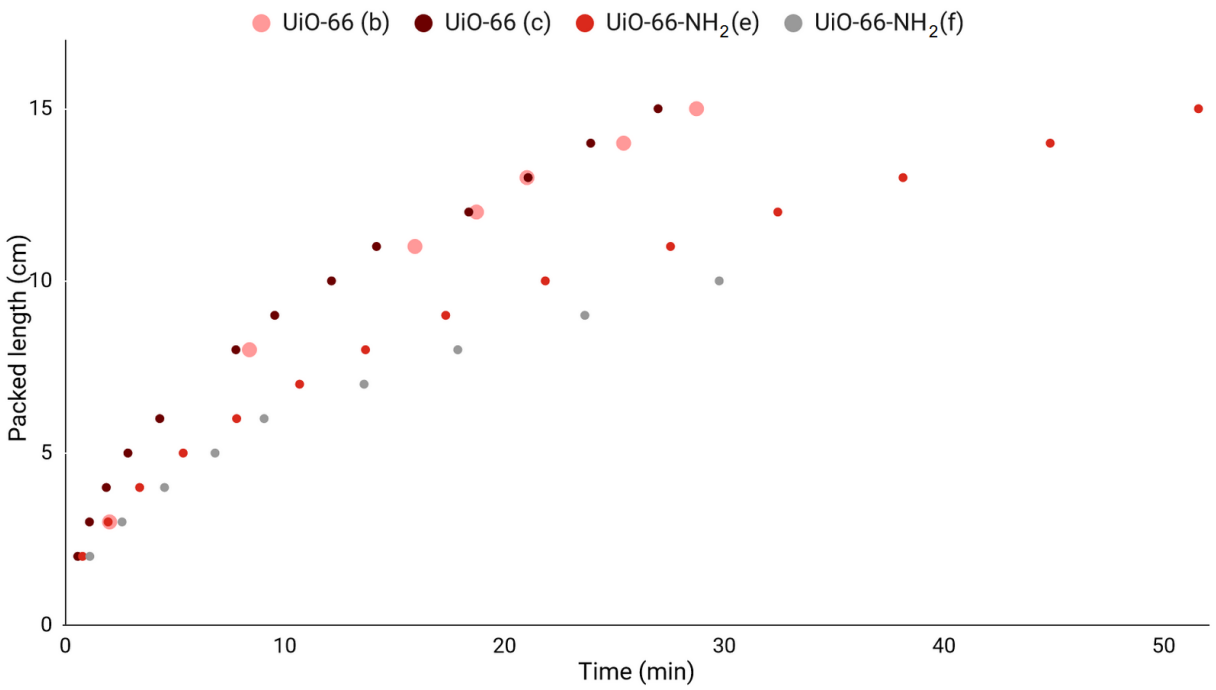

Figure 12 Packed length plotted as a function of time. Particles of UiO-66 and UiO-66-NH_2 were used as packing material in 100 µm ID capillary columns, using 240 bar nitrogen gas to pack. The numbering of the columns is as in **Table 6**.

When comparing packed length remaining after the release of pressure, the UiO-66-NH_2-columns retained more of their packed length. Because of this, the packing of the last UiO-66-NH_2-column (column *f* in the figure) was stopped once it reached 10 cm length. When the pressure was released from the packing system, the packing process was partially reversed. Some of the packed material was observed to "unpack" from the column bed and slip towards the opening of the column due to the rapid pressure drop. Some of the packed material might even leave the column entirely. A slow release of pressure can reduce this effect. For UiO-66, the effect was prominent, even with a slow pressure release – while UiO-66 particles packed quickly, they also "unpacked" easily. Therefore, it was necessary to pack longer than the desired length, as a loss of several centimetres was common. This can be seen in **Table 6**.

Table 6 Packing length during the various stages of a column in the making and in use. N/A signifies 'not applicable', as these columns were never used for LC.

Column	SP	Packed length before pressure release (cm)	Length of tightly packed particles after pressure release (cm)	Packed length after use in LC system (cm)
a	UiO-66	17.0	11.5	8.5
b	UiO-66	15.0	6.5	9.5
c	UiO-66	15.0	8.6	9.7
d	UiO-66-NH_2	10.0	8.0	7.1
e	UiO-66-NH_2	15.0	15.0	N/A
f	UiO-66-NH_2	10.0	10.0	N/A

After the release of pressure and subsequent "unpacking" of the particles, gaps in the stationary phase were present. The length of tightly packed particles as described in **Table 6** was measured from the frit to the first gap in the packed stationary phase, and should not be considered the total packed length. The true packed length could not be measured before the column had been exposed to pressure again to "repack" the column. This is thought to be due to the particles shifting to be less tightly packed as the pressure is released at the end of the packing process. In this work, the "repacking" was done by attaching the column to the LC system and leaving it for several hours for both "repacking" and conditioning. The total packed length was measured after the column had been used in an LC system, and can be viewed in the last column of **Table 6**. The decrease in packed length from the initial pressure release to after repacking is thought to be due to the particles being packed more tightly after the repacking. In order to perform an accurate measuring, the column had to be detached from the LC system, because the column outlet is inside a stainless steel union. At this point, the columns had all been attached to the LC system for several days minimum. While it is possible that particles could "unpack" from the column when the pressure drops upon reduction of flow rate or upon loosening of the nut at the connection point, this is thought to not be very likely, as the deliberate attempt to remove the particles from the column after several days attached to the LC system was unsuccessful. This attempt is described in greater detail at the end of this subsection.

UiO-66-NH_2 packed more slowly but did not suffer from pronounced loss of packed material upon release of pressure the same way UiO-66 did. This made it easier to control the packed length of the UiO-66-NH_2-columns. Because little additional length had to be packed before

the release of pressure for the UiO-66-NH_2-columns, the packing time for the same final length might not be so different between UiO-66 and UiO-66-NH_2.

Particle size of UiO-66 and UiO-66-NH_2

According to the supplier, the UiO-66-particles have a size distribution of 0.2–0.5 µm, while the UiO-66-NH_2-particles have a size distribution of 0.1–0.5 µm. This is an order of magnitude smaller than what is typically observed in UHPLC, HPLC and miniaturised LC systems. Conventional HPLC particles are typically 3–5 µm[5] and UHPLC particles are typically 1.5–2 µm[90], while particles for miniaturised LC typically range 1.5–3 µm[91]. However, when particle size is reduced but linear velocity remains the same, system backpressure is significantly increased[90]. However, the backpressures found in the present study were below 300 bar for 5–10 cm long columns packed with MOF particles, and higher backpressures were deemed to be due to clogged columns. These are remarkably low backpressures when the particle size is considered. For reference, the reduction in size from 1.7 to 1.1 µm in UHPLC is expected to result in backpressures five times higher at optimal flow rate[90], and the smallest core-shell particles require pumps that can withstand up to 1000 bar[5]. The MOF particles used in this study had a diameter of less than half the diameter of the smallest in the example. In other studies where UiO-66 was used as an SP in LC in the form of neat MOF particles, the authors noted the high backpressure[66]. Why remarkably low backpressures for UiO-66 and UiO-66-NH_2-columns were observed in the present study is unknown.

SEM images (**Figure 13** and **Figure 14**) were taken of particles of both MOF types after use in LC columns. As the images are too low-contrast and locally blurred, determination of particle size from the images was deemed to not be possible. For SEM images to be used for particle size determination, measures should be taken to disperse the particles prior to application to the imaging plate[92]. This is done to prevent agglomerates, which enables imaging software or operator to accurately determine particle outlines. However, due to reasons described in the following paragraph, this was not an option for the particles which had already been used in columns. Instead, columns were cut with a fused silica capillary cutter and the particles were dispensed onto the imaging plate by tapping the column against the carbon tape.

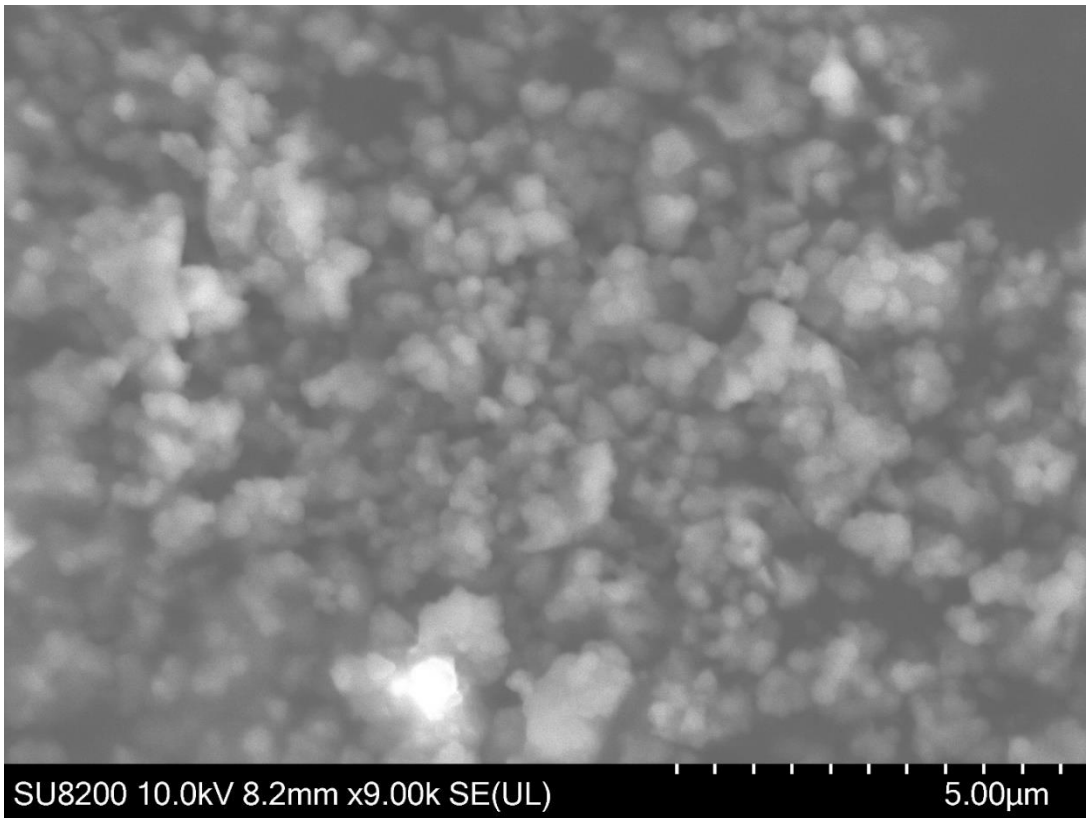

Figure 13 SEM image of UiO-66 particles after use in chromatography. Imaging performed by Prof. Karl Petter Lillerud. The ruler in the bottom right corner marks 5 µm in total.

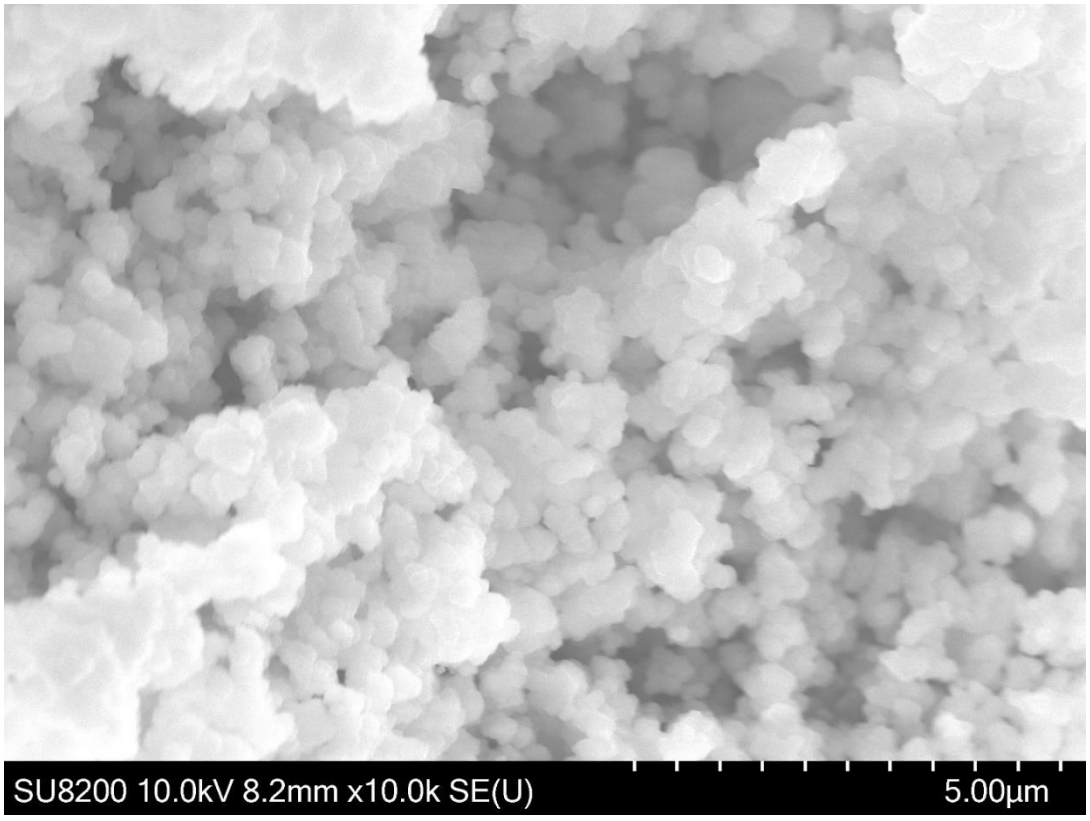

Figure 14 SEM image of UiO-66-NH_2 particles after use in chromatography. Imaging performed by Prof. Karl Petter Lillerud. The ruler in the bottom right corner marks 5 µm in total.

As part of the preparation for SEM imaging and x-ray fluorescence analysis of the particles discussed in section 4.3, unpacking the particles from the column was attempted for UiO-66-column *a* and UiO-66-NH_2-column *d* (as numbered in **Table 6**). Both the packing station (140 bar nitrogen gas) and the NanoAquity pump (maximum pressure exerted during this attempt was 250 bar) were used in this attempt. Both methods proved ineffective: the UiO-66-particles remained in place in the column, while a small portion of the UiO-66-NH_2 particles was removed from the column by the LC pump. However, the goal of this procedure was not to investigate how well the packed columns were at withstanding backflushing. Thus quantitative data describing the inefficiency of the attempt at removing the particles were not gathered, and the observation was not pursued further. Nevertheless, the observations made indicated that UiO-66 and UiO-66-NH_2-columns could withstand backflushing in an LC system after being exposed to a pressure of >100 bar for several days.

In summary, the UiO-66-particles packed more rapidly than the UiO-66-NH_2-particles. It was necessary to pack the UiO-66-columns nearly twice as long as the intended length. This was not the case for the UiO-66-NH_2-columns. The size of the MOF particles used is considerably smaller than what is common in HPLC, UHPLC and miniaturised systems, yet the backpressures for the MOF columns in the present study were remarkably low.

4.2 Column efficiency

The efficiency of one of the packed UiO-66-columns was investigated to find the optimal flow rate. Uracil and phenol were chosen as model substances to create a van Deemter curve, as they had already been used for comparison of UiO-66 and C18 on silica particles by Ago Mrša during his Bachelor's project[93]. Mrša showed that uracil and phenol were well separated with 13.5% ACN in the MP at a 0.55 µL/min flow rate, which corresponds to a linear velocity of 0.117 cm/s.

The separation of uracil and phenol on the column used in the efficiency studies conducted in this thesis is demonstrated in **Figure 36** (section **6.2.1** in the appendix), where uracil has a t_R of ~3.8 min and phenol has a t_R of ~5.2 min.

Flow rates of 0.40–0.70 µL/min at 0.05 µL/min increments were investigated. The corresponding linear velocities can be found in **Table 10** (section **6.2.1** in the appendix). Due to experiments unrelated to this thesis, the column regrettably had to be detached between the different data collection times. The data collection times and which flow rates where investigated at which time are described in **Table 7**.

Table 7 Overview over when which data points were collected for the efficiency investigation. Where flow rates are given in intervals, the interval was investigated with increments of 0.05µL/min.

Timepoint	Flow rates investigated	Replicates per flow rate	Data deemed reliable
1	0.55–0.70 µL/min	3	Yes
2	0.40 µL/min, 0.45 µL/min	3	Yes
3	0.40–0.50 µL/min	3	No

The data collected at timepoint 1 followed an expected plate height vs. flow rate trend, but did not cover sufficient flow rate range to determine the ideal flow rate. Because of this, data from more flow rates were collected at timepoint 2.

The data collected at timepoint 2 did not follow any expected trends, with plate height for phenol lower at 0.40 µL/min than at 0.45 µL/min. The changes in plate heights for phenol were much higher than the plate heights for uracil, as were the changes in retention time. Due to the inproportional changes in plate height and retention time, and as data for 0.50 µL/min had not been collected yet, more data was collected at timepoint 3.

The data collected at timepoint 3 was suspected of differing significantly from the previously collected data, as baseline separation of uracil and phenol was not obtained and the system backpressure was abnormally low (about half of the pressure observed for 0.40 and 0.45 µL/min during the collection of the second data set). The lack of baseline separation is shown in **Figure 37** (section **6.2.1** in the appendix). Two-sided unpaired t-tests were performed to determine whether the retention times for uracil and phenol collected at timepoints 2 and 3 were from the same population for flow rates 0.40 and 0.45 µL/min. The calculations are shown in **Table 11** in section **936.2.1** in the appendix. The P-values were evaluated at a confidence level of 0.05. The t-tests indicated that the data collected at timepoint 3 differed significantly from the data collected at timepoint 2 for both uracil and phenol at both flow rates. Because of this, the data collected for 0.50 µL/min at timepoint 3 were also discarded.

The partial van Deemter plot in **Figure 15** was constructed from the data collected in series 1 and 2. The lowest observed plate height for uracil was 18 µm at 0.55 µL/min, corresponding to a linear velocity of 0.117 cm/s. This flow rate was used for the rest of this study. Average backpressures for the different flow rates are displayed in **Figure 16**. For the column used in this part of the study (column a in **Table 6**), backpressure under 90 bar was the norm at a 0.55 µL/min flow rate. In other words, during the work related to this thesis, no challenges due to high backpressure were encountered.

The observed efficiencies for UiO-66 in this study were 18 µm and 43 µm for uracil and phenol, respectively, at 0.55 µL/min. It should be noted that well-packed conventional HPLC columns with C18 of silica support are commonly expected to have plate heights of 5–10 µm[5]. This is considerably lower than for the UiO-66-column. In the previous work by Mrša, the highest plate number found for a UiO-66-column was 22 000 plates/m for phenol. The corresponding plate number found in the current study for phenol was 23 000 plates/m, which is very similar to Mrša's find. The highest plate number found for uracil in this study was 55 000 plates/m. For comparison, Mrša found a plate number of 96 000 plates/m for ethylbenzene on a C18-column using the same LC setup, which is considerably higher.

The column efficiencies reported in previous studies of UiO-66 as an SP in LC are found in **Table 8**. It should be noted that the highest reported efficiencies in previous studies have been for composite particles on silica support, which were chosen by the respective authors improve upon the packing properties compared to neat MOF particles. As this study found a maximum plate number of 55 000 plates/m, the efficiency found was comparable to the highest efficiencies found by others.

Table 8 Efficiencies reported in previous studies using UiO-66 as an SP in LC.

Study	SP type	Analytes	N/L (plates/m)
Yan et al.[72]	Composite, SiO_2 support	Ethylbenzene *p*-Chlorotoluene *p*-Dichlorobenzene Styrene	8 780 9 060 9 990 5 130
Arrua et al.[70]	Composite, SiO_2 support	Biphenyl Ethylbenzene Styrene *m*-Xylene Phenyl acetylene Naphthalene	23 050 23 860 32 440 25 760 20 800 24 020
Zhao et al.[77]	Neat MOF particles	m-Xylene	2 154
Peristyy et al.[68]	Composite, SiO_2 support	N/A	58 100

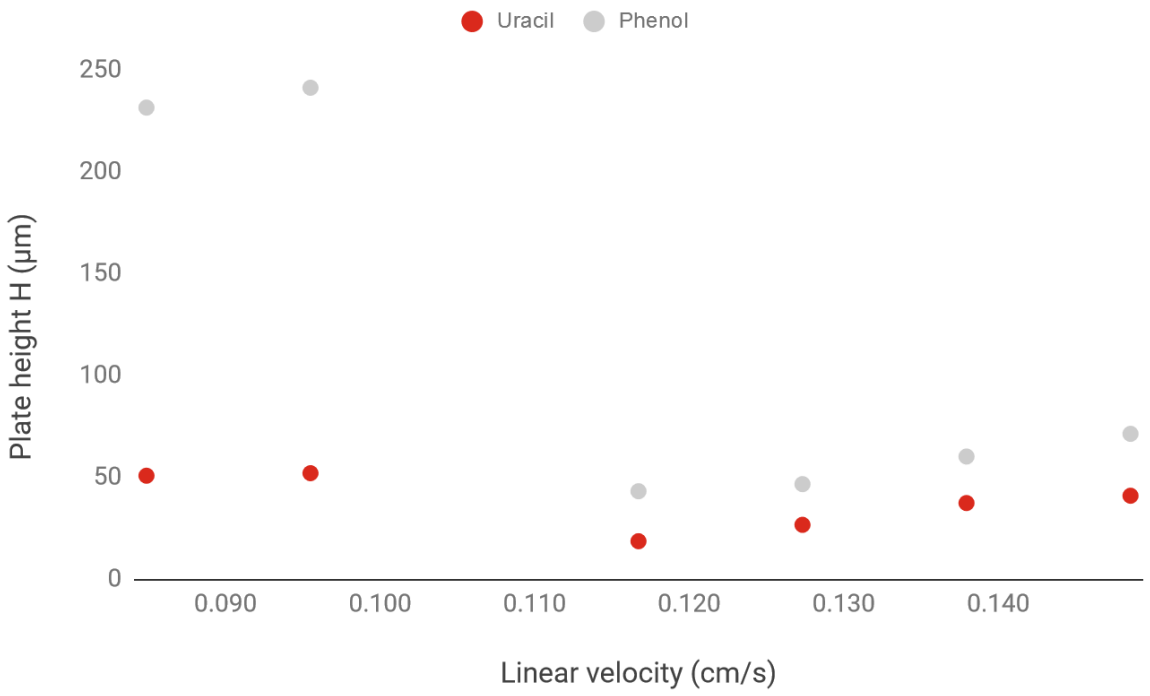

Figure 15 Van Deemter plot for UiO-66-column (100 µm ID x 52 mm) in LC setup II for uracil and phenol (0.25 mg/mL each). The mobile phase was ACN/0.1% formic acid (13.5/86.5, v/v). The injection volume was 50 nL and UV detection was performed at 270 nm. Points are the average from n=3 injections for all flow rates.

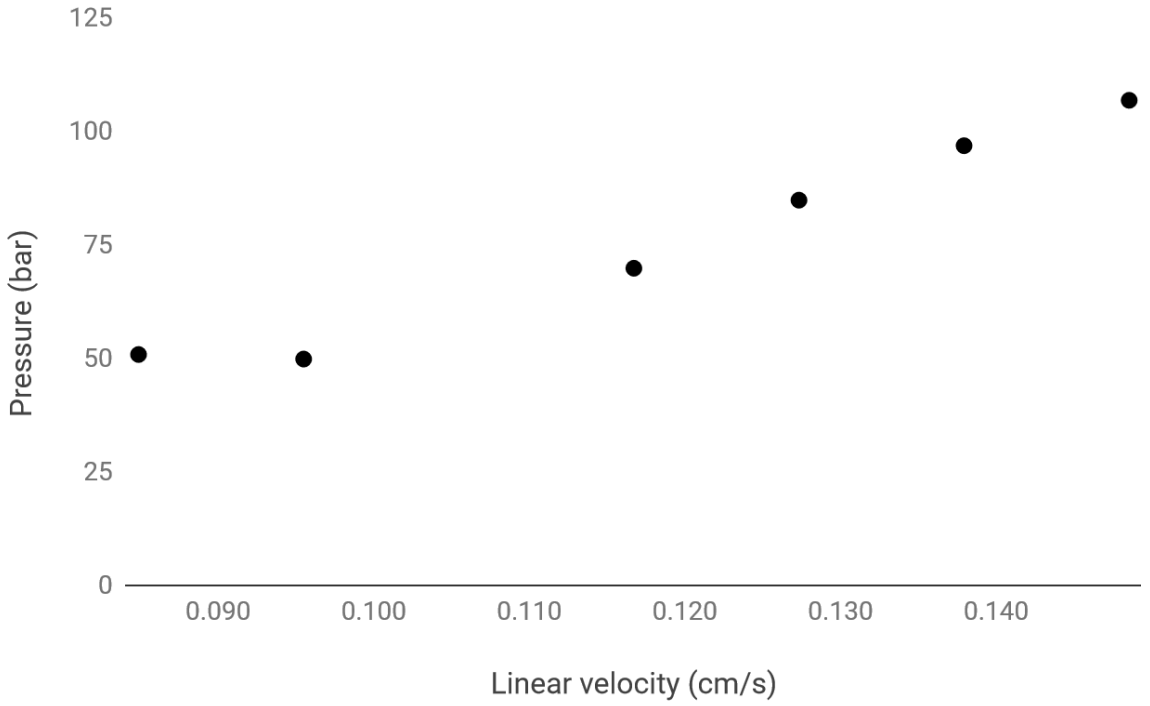

Figure 16 Average backpressure observed at linear velocities corresponding to flow rates 0.40, 0.45, 0.55, 0.60, 0.65 and 0.70 µL/min. Chromatographic conditions as described in **Figure 15**.

According to the van Deemter equation (**Equation 4**), smaller particle size should result in a smaller contribution from the A and C terms, as both the eddy dispersion (A term) and the resistance to mass transport is proportional with particle diameter. With the size of the UiO-66 used in this study being an order of magnitude smaller than particles generally used in packed LC columns, these contributions are expected to be greatly reduced. However, the benefits of these expected reductions in band broadening did not result in very low plate heights. This could be due to inhomogenous packing, which is known to cause greater Eddy dispersion[89].

Extra-column band broadening will also contribute to the measured plate height. LC setup II had quite large volumes of tubing compared to the maximum volume of the packed column. For this column, the volume contributing to separation was calculated to be only 39% of the total volume of the LC setup where band broadening might occur, as is shown in **Table 5** in section **3.4**. This illustrates a substantial room for improvement in the LC-UV test system.

Peristyy et al.[68] reported what they name flow-dependent separation on UiO-66 in a 2016 study, where the retention factor k decreased with increasing flow rates. This was discovered while attempting to establish a van Deemter curve for the material. During the work associated with this thesis, the same phenomenon was observed. When uracil was used as a t_M marker, the retention factor of phenol changed as the linear velocity changed, as demonstrated in **Figure 17**. The retention factor was greater at lower linear velocities, and there was little variation in retention factor at linear velocities higher than 0.115 cm/s (corresponding to a 0.55 µL/min flow rate).

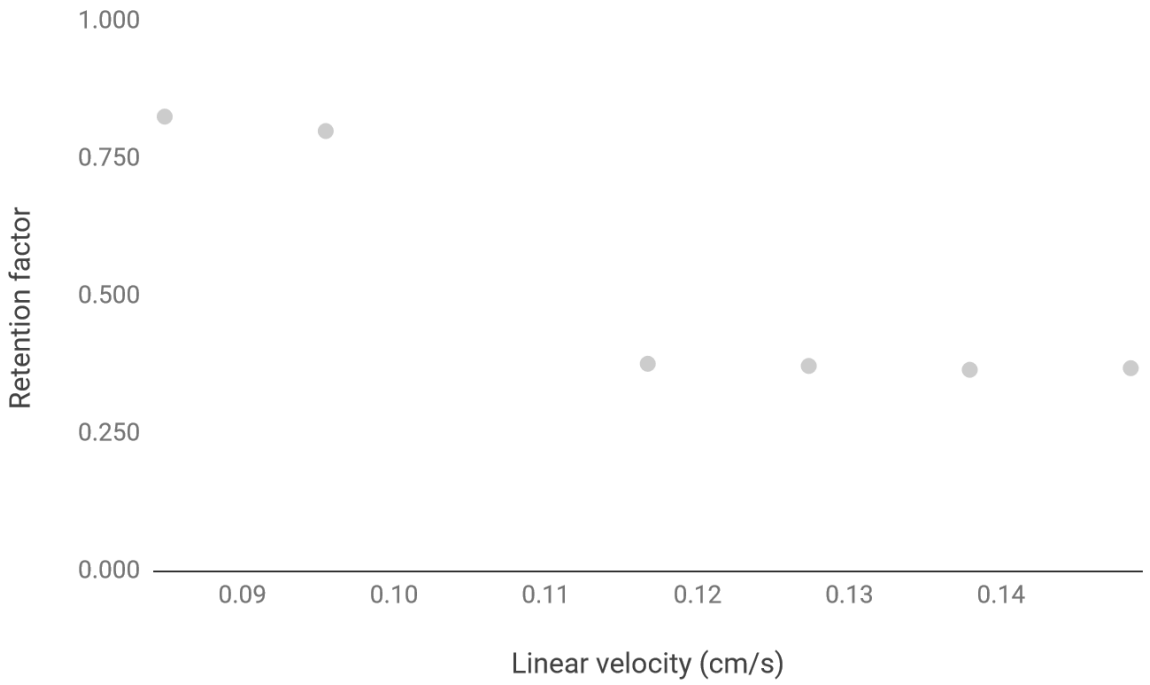

Figure 17 Retention factor of phenol at linear velocities corresponding to flow rates 0.40, 0.45, 0.55, 0.60, 0.65 and 0.70 µL/min. Chromatographic conditions were as described in **Figure 15**.

The linear velocities for which the retention factor of phenol was the highest were also the linear velocities for which the plate height for phenol was the highest.

The use of uracil as a t_M marker for the calculation of k for phenol might not yield the true retention factor, as uracil was observed to display behaviour not associated with a suited t_M marker at other times in the study. This is further discussed in **4.3**. However, no minor baseline disturbance, which could be used to establish t_M, was observed when performing the chromatography that was the basis of the investigation of the effect of linear velocity on efficiency for UiO-66, and thus the only option available given the time-frame of this study was to use uracil as a t_M marker.

The fact that k for phenol varied over the investigated linear velocities, calls into question whether the van Deemter curve for UiO-66 can be used as a tool for optimising system efficiency. Traditionally, k is constant throughout the linear velocities covered by the van Deemter plot. When Peristyy et al. made this observation, they concluded that a van Deemter plot could not be constructed[68]. Nevertheless, the changing of k with linear velocity suggests

linear velocity used should be carefully considered when using UiO-66 as an SP, both in terms of column efficiency *and* in terms of selectivity.

In summary, the lowest plate numbers for the UiO-66-column were observed at a linear velocity of 0.117 cm/s, corresponding to a flow rate of 0.55 µL/min. Based on this observation, 0.55 µL/min was used as the flow rate for all other investigations in this study. The k value for phenol changed with changing linear velocity, suggesting linear velocity must be chosen with care when using UiO-66 as an SP. While the plate heights found for UiO-66 were high when compared to plate heights found for C18 on silica support in similar LC systems, the selectivity of UiO-66 might still make it an interesting SP, as investigated in the following sections.

4.3 Investigation of retention of compounds

Most of the compounds tested for retention of UiO-66 and UiO-66-NH_2 so far have been either substituted benzenes or PAHs. However, little attention has been given to molecules with several polar functionalities. Small molecules in biological samples often have several polar functionalities, and these can have little to no retention on common reversed-phase materials[94]. The retention of small polar molecules known to be present in biological samples on MOF materials was therefore of interest.

For this part of the study, a series of adenosine phosphates (**Figure 18**, first row) and neurotransmitters (Figure 18, second row) were chosen based on size, availability and the risk associated with handling them. Uracil (Figure 18, third row) was initially used as a hypothesised t_M marker, because of its common use in this manner on reversed-phase materials. In addition, some alkylbenzenes were investigated. The chromatography of some of these compounds on UiO-66-materials has been studied by others[66,68–70,72,77].

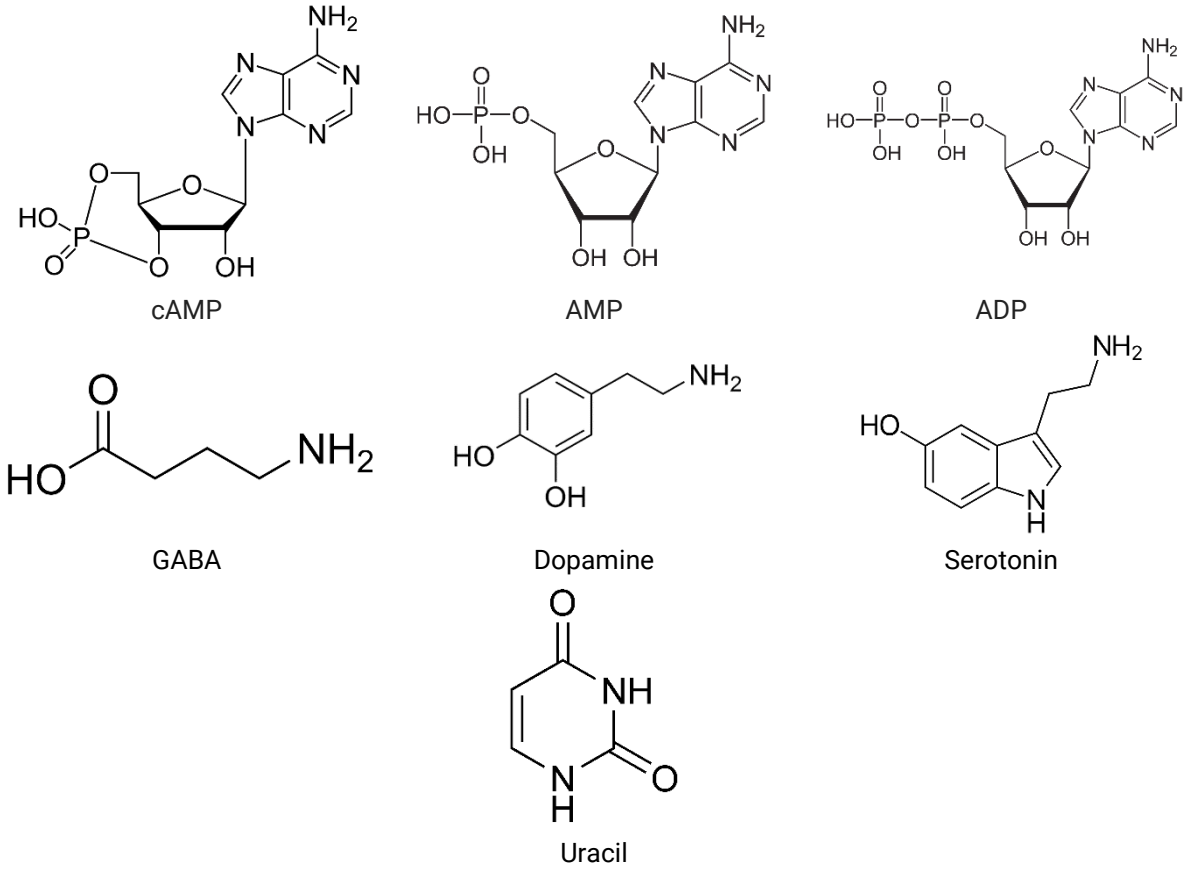

Figure 18 Structures of the compounds investigated. Row 1: cyclic adenosine monophosphate (cAMP), adenosine monophosphate (AMP) and adenosine diphosphate (ADP). Row 2: γ-aminobutyric acid (GABA), dopamine and serotonin. Row 3: uracil.

4.3.1 UiO-66

Chromatography of polar compounds

For the investigation of the chromatography of polar compounds on UiO-66, aqueous MP compositions were chosen. UiO-66 as a separation material is potentially interesting as a complementary SP to C18 on silica support, and, long term, in tandem with MS detection. In this regard, it was desirable to investigate the chromatography of polar compounds on UiO-66 using MPs compatible with both C18 on silica support and MS detection. ACN was chosen as the organic modifier in the MP, as Mrša in his work observed less consistent chromatography using MeOH than ACN as organic modifier[93].

The retention times for the different solutes are presented in **Figure 19** for 0% B, 15% B and 30% B (corresponding to 0%, 13.5% and 27% ACN respectively). Several of the solutes were found to have similar retention times and their retention times are shown more clearly in the

zoomed-in parts of the same figure. The intent of investigating the retention time of uracil in addition to the other solutes was to establish a t_M value to calculate the retention factor of the different solutes. However, uracil appeared to not be a reliable t_M marker. It was not possible to detect a minor disturbance that could indicate t_M in most of the chromatograms either. Due to time constraints, other possible t_M markers were not investigated. For these reasons, retention times rather than retention factors were used to compare the retention of the different compounds.

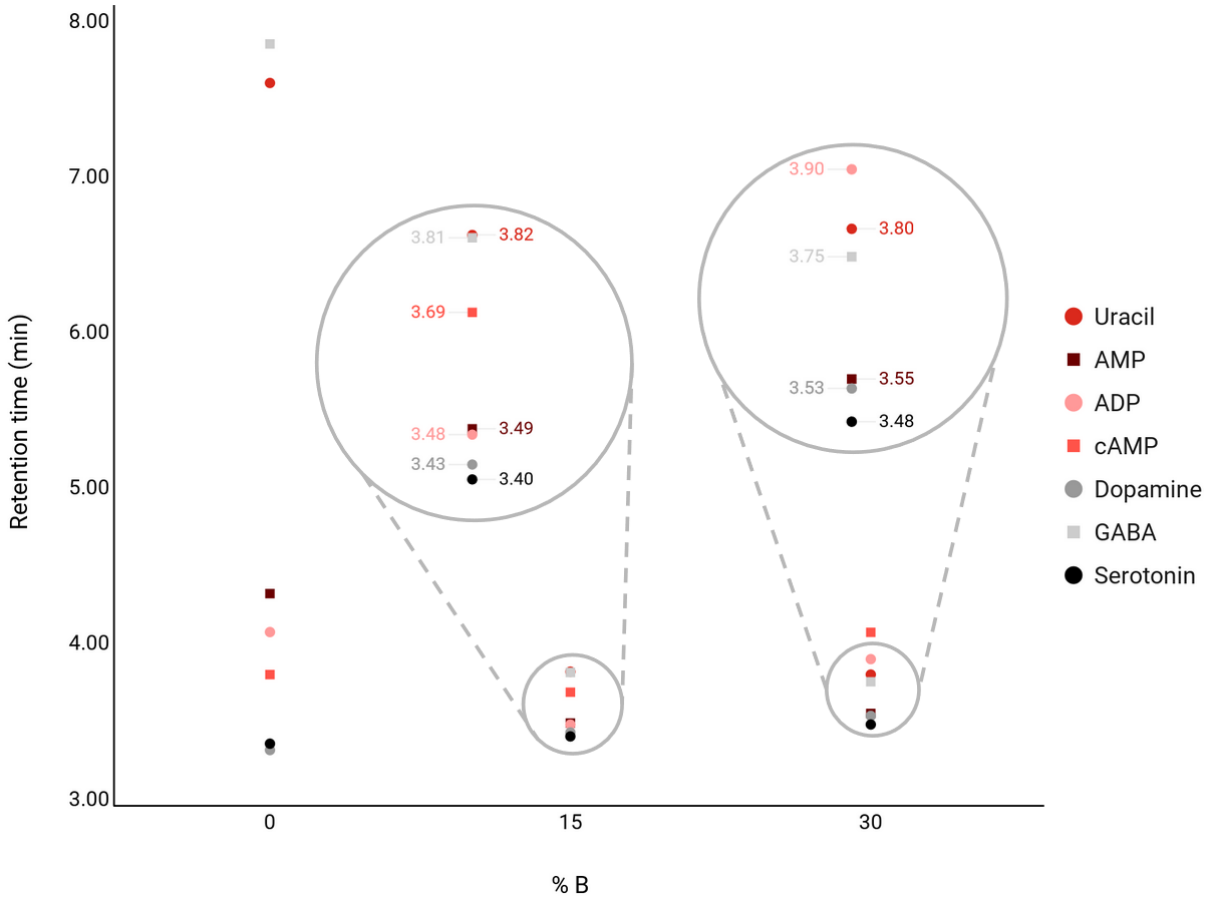

Figure 19 Retention times of uracil (n=3, 4, 3), AMP (n=2, 2, 3), ADP (n=2, 2, 3), cAMP (n=2, 2, 3), dopamine (3, 3, 3), GABA (n=3, 3, 2) and serotonin (n=3, 3, 3) for three different MP compositions (0, 15, 30% B). Mobile phase reservoir A contained 0.1% FA, mobile phase reservoir B contained 90%/0.1% ACN/FA v/v. Chromatography was performed on a 100 µm ID x 95 mm UiO-66-column in LC setup II at a 0.55 µL/min flow rate. Injection volume was 50 nL. UV detection was performed at 270 nm.

GABA and uracil, the smallest molecules of the selected compounds (**Figure 18**), were the most retained across the MP composition range investigated. GABA and uracil are expected to be small enough to enter the pores of UiO-66. GABA can participate in hydrogen bond

interactions with the hydroxy groups of the Zr-cluster in UiO-66 both using its carboxylic acid functionality and its amino functionality.

Uracil is among the most retained compounds. This was unexpected given the assumption that UiO-66 would display a predominately reversed-phase selectivity when used with a highly aqueous MP. However, uracil was most strongly retained, especially when the water content of the MP was the highest. The structure of uracil indicates it can participate in hydrogen bond interactions with the hydroxy groups of the Zr-cluster both as a hydrogen bond donor because of the hydrogens attached to nitrogen atoms in the ring, and as a hydrogen bond acceptor because of the ketone functionalities. It also has several double bonds which enables it to participate in π-π interactions. The ability to participate in both π-π interactions and hydrogen bond interactions could explain the observed retention pattern with varying MP composition.

The larger molecules showed little retention. Dopamine and serotonin showed the least retention across the MP composition range investigated, and little change in retention time as MP composition changed. This raised the question of whether the two compounds are small enough to access the pores, and it was concluded that dopamine and serotonin are too large to enter the pores of UiO-66. To help inform a conclusion, the retention times of these two compounds individually across all three MP compositions using one-way ANOVA at a 0.05 level of significance (**Table 24**, section **6.2.2** in the Appendix). Dopamine showed significant difference in its retention times, but serotonin did not. The retention times of the two compounds were also compared for all MP compositions investigated, once again using one-way ANOVA (**Table 20**, section **6.2.2** in the Appendix). These three comparisons found the retention times of dopamine and serotonin to be significantly different at 30% B, but not at 0% B and 15% B. The lack of statistically significant difference for three of the five comparisons supported the suspicion that serotonin and dopamine could not enter the pores, but the tests were not unequivocal in their outcomes. To establish a better understanding of what size molecules could enter the pores of UiO-66, the pore volume accessibility investigation in **4.5** was conducted.

The adenosine phosphates are even larger in molecular size than dopamine and serotonin, and they were observed to be more strongly retained than the two neurotransmitters. When the adenosine phosphates were injected, unstable baseline upon injections close in time was observed, together with significant tailing of the peaks, as can be seen in **Figure 20**. Both the

tailing and the increased retention, when compared to dopamine and serotonin, could be explained by the affinity of phosphate for zirconium, which is present in the ion cluster nodes of UiO-66, discussed later in this section. The different adenosine phosphates elute in a different order at all three different MP compositions.

The adenosine phosphates also showed to elute with a peak on the shoulder of the largest peak, as can be seen in **Figure 20**. Why this occurred is unknown. The maximum of the largest peak was always used as the retention time for the adenosine phosphates.

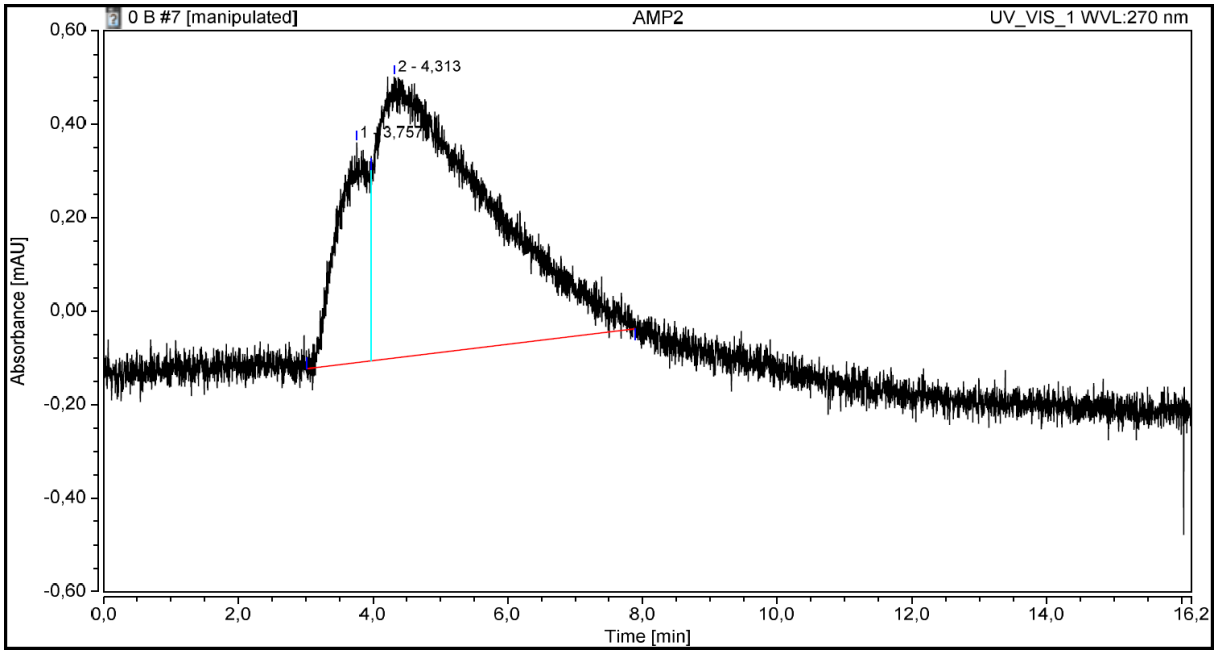

Figure 20 Chromatogram of AMP (1 and 2) at 0% B. Chromatographic conditions were as described in **Figure 19**.

It should be noted that the number of useable replicates for several of the solutes at given % B for UiO-66 is sparse. This is true for the adenosine phosphates and GABA, as the unstable baseline for the adenosine phosphates and low molar absorbtivity for GABA sometimes caused chromatograms where the retention time of the solute could not be determined. Ideally, more injection replicates ought to be performed as soon as the insufficiency of some of the injection replicates was discovered, however, time did not allow for this.

In summary, very small organic compounds with polar functionalities showed retention on UiO-66. Retention was increasing with increasing water content for the small polar molecules, which is consistent with previous observations of UiO-66 displaying reversed-phase selectivity[66,70,77]*. The neurotransmitters serotonin and dopamine were suspected of not being able to enter the pores. The adenosine phosphates did not display consistent trends in retention times.*

Chromatography of alkylbenzenes

While investigating the effect of temperature on retention (see section 4.4), the alkylbenzenes toluene, ethylbenzene and butylbenzene were used. In the process, observations regarding the retention of alkylbenzenes were made.

The retention of alkylbenzenes was investigated using only one MP composition, 75/25 MeOH/0.1% FA, v/v. This MP composition was chosen to match the already prepared standard solutions.

Butylbenzene had the shortest retention time, and the retention time increased inversely with the alkyl chain as shown in **Figure 21**. Thus, with a mobile phase composition of MeOH/0.1% FA (75/25, v/v), molecules with a larger hydrophobic surface are less retained. If UiO-66 had shown reversed-phase selectivity for these conditions, the opposite would have been expected, i.e. the retention would increase with increasing alkyl chain length.

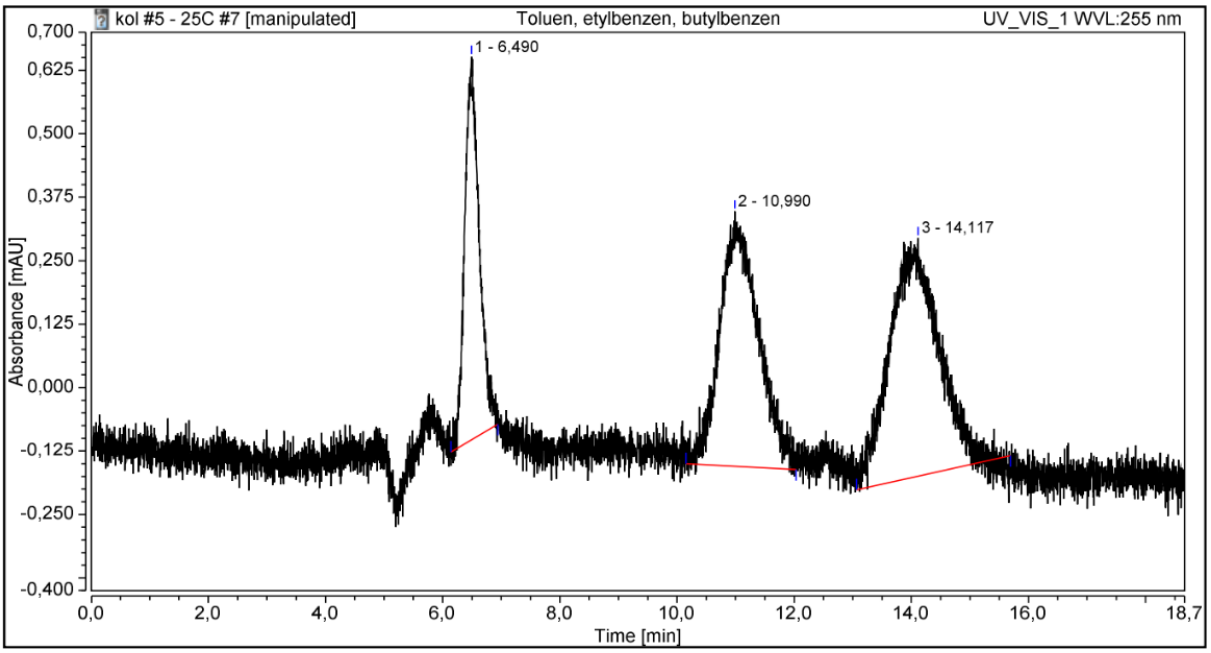

Figure 21 Chromatogram of butylbenzene (1), ethylbenzene (2) and toluene (3). All solutes were present at 0.25 mg/mL concentration. Chromatography performed at 25°C with a 100 µm ID x 95 mm UiO-66-column in system III, MP MeOH/0.1% FA (75/25, v/v) at 0.55 µL/min flow rate. Injection volume was 50 nL, UV detection was performed at 255 nm.

It was deemed unlikely that the observed selectivity was caused by SEC. The retention of alkylbenzenes using 100% MeOH as the MP was investigated as discussed in section **4.5** where the same column was used. The retention times found for the three compounds for that part of the study had smaller differences between them than what is displayed in **Figure 21**. This clearly indicates that the retention times observed in **Figure 21** were affected by the MP used.

Both Zhao et al.[77] and Arrua et al.[70] have performed normal phase chromatography on small substituted benzenes using UiO-66 as a stationary phase. Zhao et al.[77] found the following retention order: ethylbenzene, styrene, o-xylene, m-xylene. Arrua et al.[70] found the following elution order: pentylbenzene, biphenyl, ethylbenzene, styrene, m-xylene, phenylacetylene, naphthalene. In both cases hexane/DCM was used as MP, a commonly used MP in NPLC.

The MP used in the present work is more similar to the MPs commonly used in HILIC than MPs commonly used in NPLC. However, MeOH is considered to have high elution strength in HILIC.

It is difficult to decide from the observations presented here whether the normal phase selectivity is caused by HILIC or NPLC. To investigate, one possibility is to perform the same experiment with ACN as the organic component of the MP. In HILIC, ACN has a weaker elution strength than MeOH, and thus it would be expected to observe longer retention times if ACN was used instead of MeOH. However, due to time restraints, this was not pursued further in this work.

In summary, UiO-66 was found to display normal phase selectivity for alkylbenzenes.

4.3.2 UiO-66-NH_2

For UiO-66-NH_2, the retention of even fewer compounds has been investigated. The amino functionality of the MOF was hypothesised to give a slightly different selectivity than regular UiO-66, both because the pore opening might be smaller and because more possibilities for interactions with solutes are introduced.

The retention times of the different polar solutes on UiO-66-NH_2 are presented in **Figure 22**. Several of the compounds have very similar retention times. For the ones that differed sufficiently to be possible to differentiate in the figure, a zoomed-in view is provided.

Uracil was the most retained compound across all three mobile phase compositions investigated, again suggesting it might not be a suitable t_M marker for the UiO-66 materials. GABA is the second most retained compound, with retention times close to that of uracil for both 15% and 30% B. At 0% B, the retention of GABA is remarkably lower than for 15% B. The highest retention time for GABA is at 15% B. In line with these observations, it was assumed the two compounds both had access to the pores of UiO-66-NH_2.

The possible interactions between uracil or GABA and UiO-66-NH_2 were thought to be similar as those possible for UiO-66, with the addition of hydrogen bond interactions with the amino group of UiO-66-NH_2.

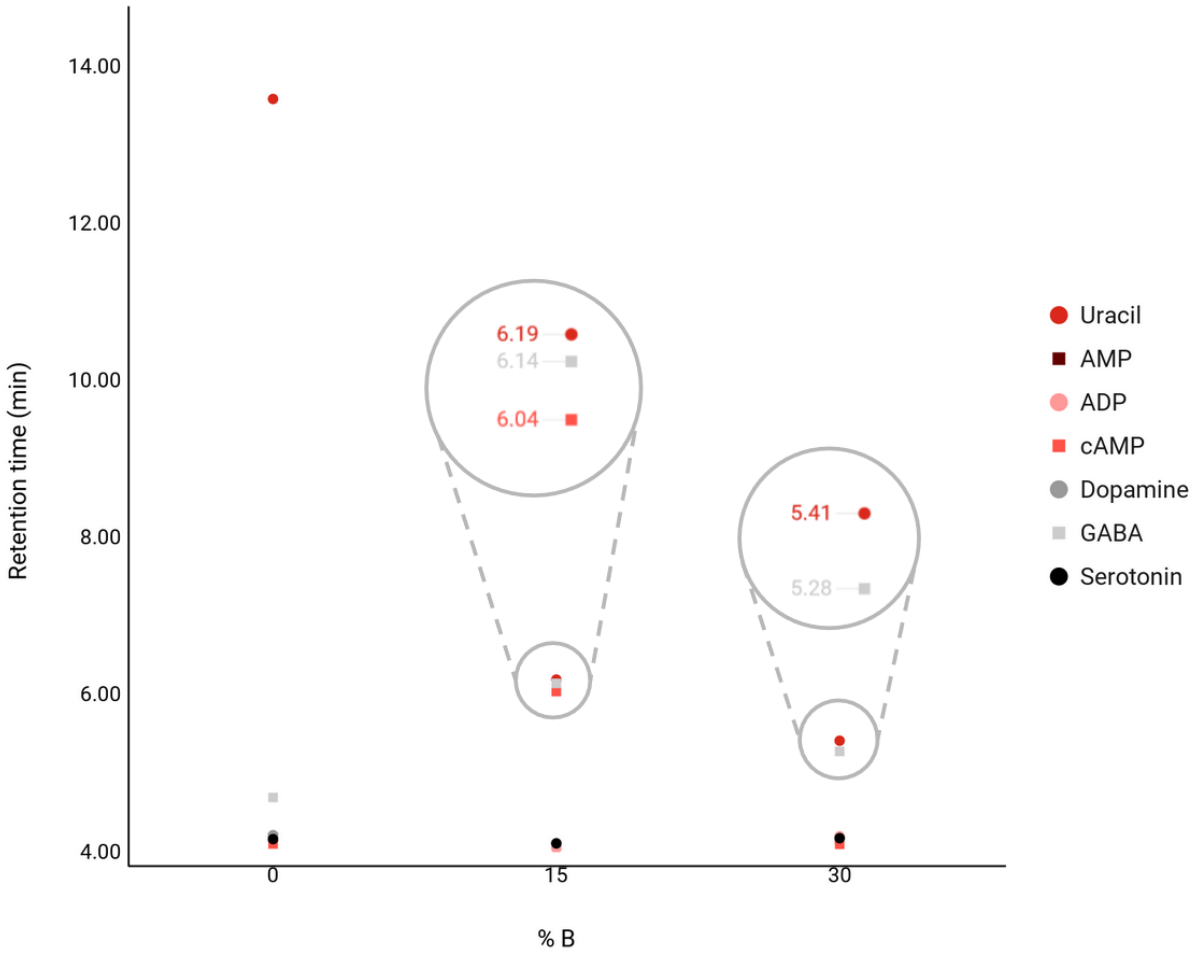

Figure 22 Retention times of uracil (n=6, 5, 3), AMP (n=3, 3, 3), ADP (n=3, 3, 3), cAMP (n=3, 3, 3), dopamine (n=3, 3, 3), GABA (n=2, 3, 3) and serotonin (n=3, 3, 3) for three different MP compositions (0, 15, 30% B). Mobile phase reservoir A contained 0.1% FA, mobile phase reservoir B contained 90%/0.1% ACN/FA v/v. Chromatography was performed on a 100 µm ID x 71 mm UiO-66-NH_2-column in LC setup II at a 0.55 µL/min flow rate. Injection volume was 50 nL. UV detection was performed at 270 nm.

For 15% B, cAMP was also found to have some retention. However, cAMP did not seem to have any retention for the two other MP compositions investigated.

For AMP, ADP, dopamine and serotonin, no retention was observed. ANOVA showed no statistically significant difference between these compounds at any of the MP compositions investigated. For 0% B and 30% B, there was no significant difference between cAMP and the rest of the adenosine phosphates, dopamine and serotonin either.

The lack of significant difference between the different adenosine phosphates and the two neurotransmitters could mean the compounds are too large to enter the pores. The pores of UiO-66-NH_2 are smaller than those of UiO-66 due to the amino group[84]. If the

neurotransmitters could not enter the pores of UiO-66, they would not be able to enter the pores of UiO-66-NH_2 either. The lack of significant difference between the neurotransmitters and the adenosine phosphates indicate that the adenosine phosphates are also too large to enter the pores.

However, this called into question why cAMP showed retention at 15% B. Upon closer inspection of the chromatograms of cAMP at 15% B, a dip before the peak was observed for all chromatograms. However, by the time this was discovered, the LC setup had been changed to accommodate a UiO-66-column, and repeat injections would have to wait until after the column was swapped again. The Covid-19 pandemic unfortunately prevented this from happening.

In summary, the small organic compounds with polar functionalities were retained on UiO-66-NH_2. The larger molecules were for the most part unretained.

Due to extraordinary circumstances (see section **6.3** in the appendix), investigation of retention of alkylbenzenes on UiO-66-NH_2 was not carried out.

4.3.3 Suspected adsorption of adenosine phosphates on UiO-66 and UiO-66-NH_2

The chromatograms following injections of adenosine phosphates on both UiO-66 and UiO-66-NH_2 showed uneven baselines for approximately 20 minutes after adenosine phosphate injections. The chromatograms from the injections of the adenosine phosphates themselves showed pronounced tailing. Based on these observations, it was hypothesised that the affinity of phosphate for zirconium caused the adenosine phosphates to adsorb to the zirconium clusters in the materials. If this was the case, the uneven baseline could be caused by a slow desorption of the adsorbed adenosine phosphates.

A case where an uneven baseline was observed is shown in **Figure 23**. Here, an injection solution of cAMP, AMP and ADP was injected only 9 minutes after the previous injection. Similar chromatograms were observed if the injections were performed too close in time to injections of solutions containing adenosine phosphates.

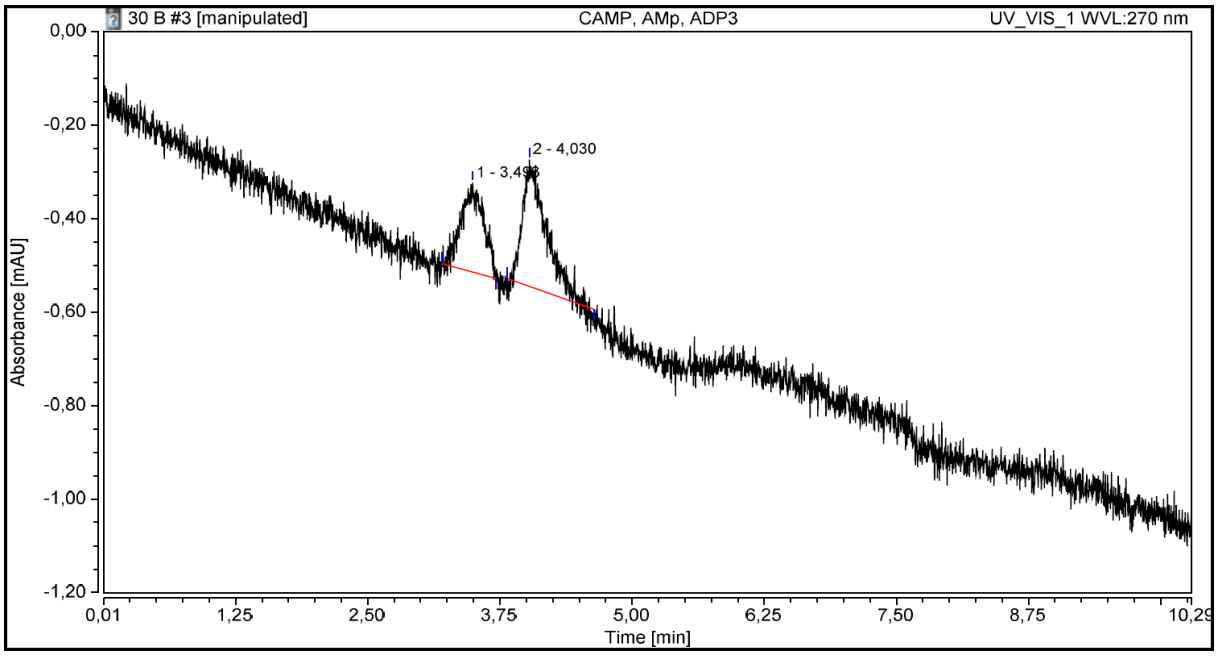

Figure 23 Chromatogram of cAMP, AMP and ADP (0.25 mg/mL each) at 30% B on a 100 µm ID x 95 mm UiO-66-column. Chromatographic conditions were as described in **Figure 19**.

In order to investigate whether any adsorbed adenosine phosphates remained on the SP of columns after use in an LC setup for chromatography of adenosine phosphates, the SPs of one UiO-66-column and one UiO-66-NH_2-column were examined by EDXS in a SEM. No phosphorus was detected as can be seen in **Figure 24** and **Figure 25**, and it was concluded that the adenosine phosphates were completely desorbed while the columns were still attached to the LC setup.

In summary, adenosine phosphates were hypothesised to adsorb to the zirconium clusters of the UiO materials studied in this thesis. No residual phosphate was detected on used SP by EDXS.

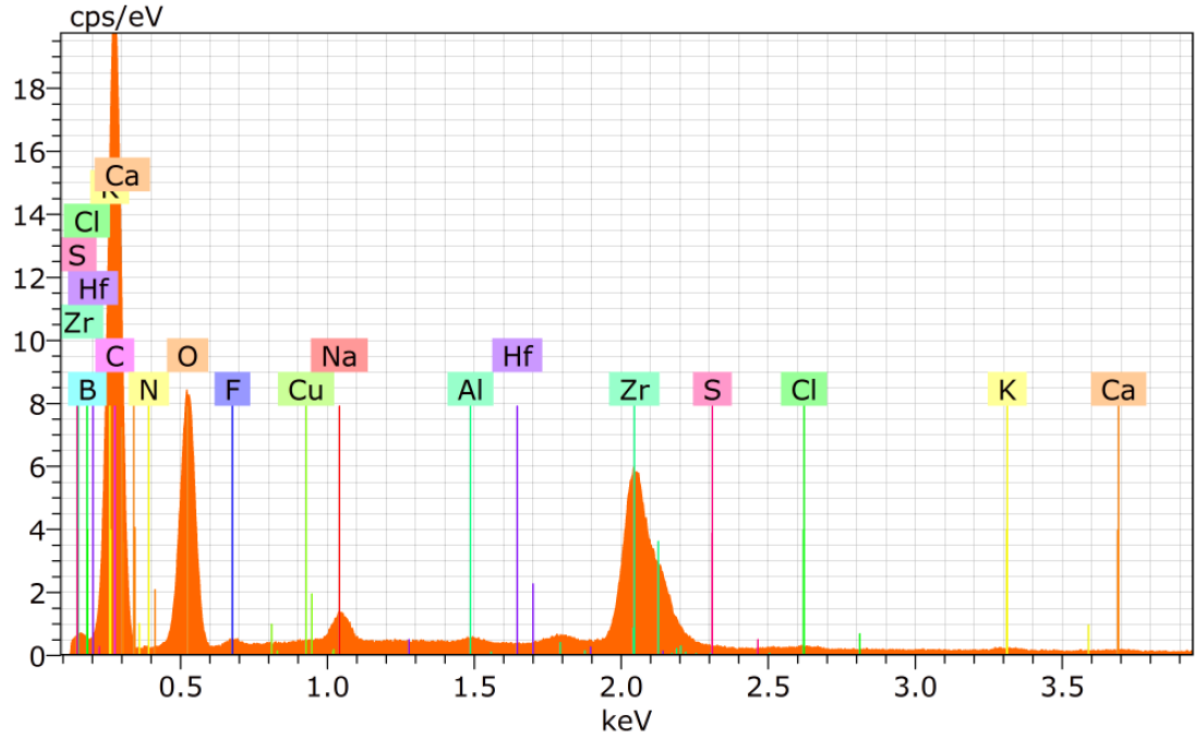

Figure 24 Energy dispersive X-ray spectrum from UiO-66, where counts per second (cps) are measured as a function of energy. No phosphorus was detected. EDXS was performed by Prof. Lillerud.

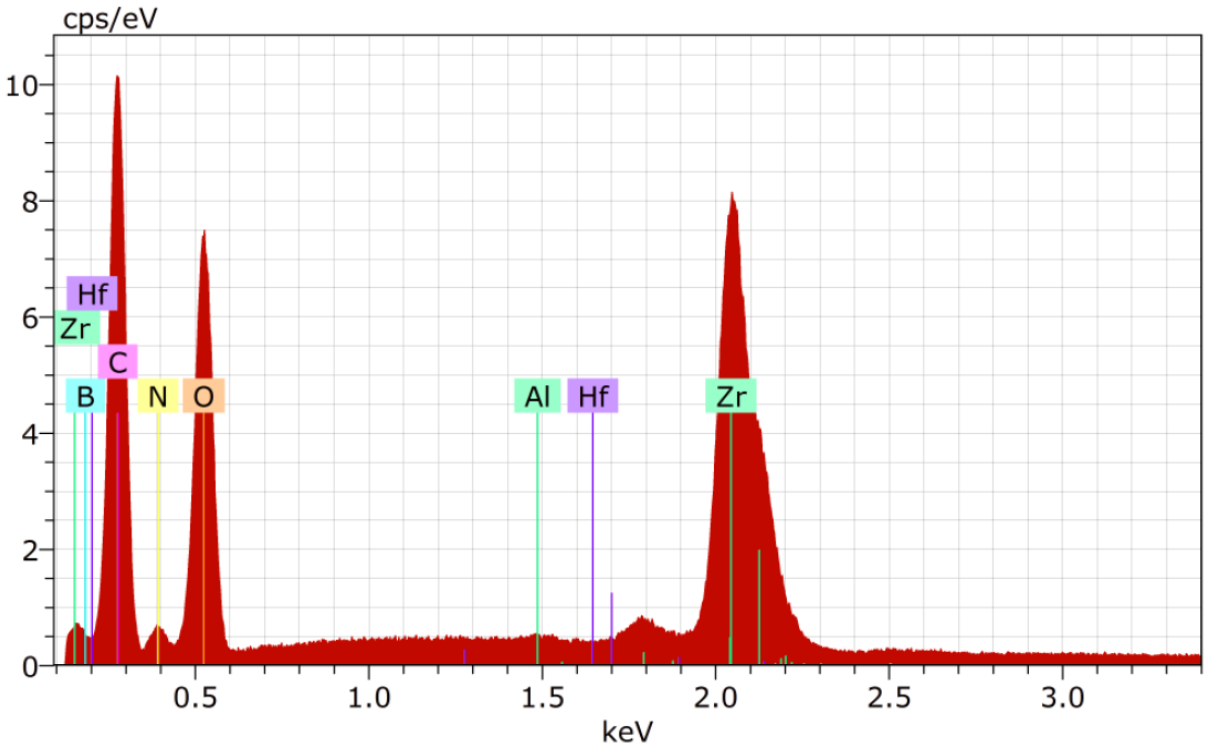

Figure 25 Energy dispersive X-ray spectrum from UiO-66-NH_2, where counts per second (cps) are measured as a function of energy. No phosphorus was detected. EDXS was performed by Prof. Lillerud.

4.4 Van't Hoff experiments

In order to investigate the effect of temperature on retention, a series of experiments designed to result in a Van't Hoff plot for UiO-66 was carried out. In addition to the effect on retention, the effect of temperature on efficiency was of interest, as the efficiency study carried out at room temperature showed mediocre plate heights.

Temperatures from 25 to 55°C at 10°C increments were investigated. The starting temperature was chosen as the column oven used was not found to have a cooling function. Investigation of higher temperatures was planned, but could not be carried out due to extraordinary circumstances further expanded on in section **6.3** in the appendix.

Toluene, ethylbenzene and butylbenzene were chosen as model compounds for this part of the study, as stock solutions for these compounds were already prepared and all three compounds were suspected to be small enough to enter the pores of UiO-66. An injection solution containing all three solutes was prepared for this investigation.

A series of aromatic compounds (benzene, naphthalene and phenanthrene) was also planned included, but due to heavy carry-over when injected at the lowest temperature, requiring time-consuming washing to eliminate, no further injections of aromatic hydrocarbons were performed. The observations leading to this decision are briefly discussed in this section.

Standard solutions of the solutes were injected to enable the identification of the different solutes according to their retention time.

The low molar absorptivity of the alkylbenzenes and suboptimal efficiency of the system resulted in small peaks which could be difficult to identify even though detection was performed at 255 nm. This wavelength was chosen as it was listed as a maximum in the UV absorbance spectrum of benzene. In hindsight, the UV absorbance should have been determined for the solutes in the MP used.

Butylbenzene had little or no retention with 75/25 MeOH/0.1% FA v/v as the MP, and eluted where the solvent disturbances of the baseline occurred. Due to the dips caused by the solvent and low molar absorptivity of butylbenzene, it was not possible to identify which of the peaks around the t_M originated from butylbenzene for the majority of the chromatograms. This is illustrated in **Figure 26**, where butylbenzene is hypothesised to elute in the same time

window as the dips from the solvent appear. As shown previously in **Figure 21**, a peak was visible between the two dips early in the chromatogram for 25°C. Toluene and ethylbenzene eluted well after the solvent baseline disturbances, but due to the low molar absorptivity and poor efficiency, their peaks were not always possible to reliably integrate.

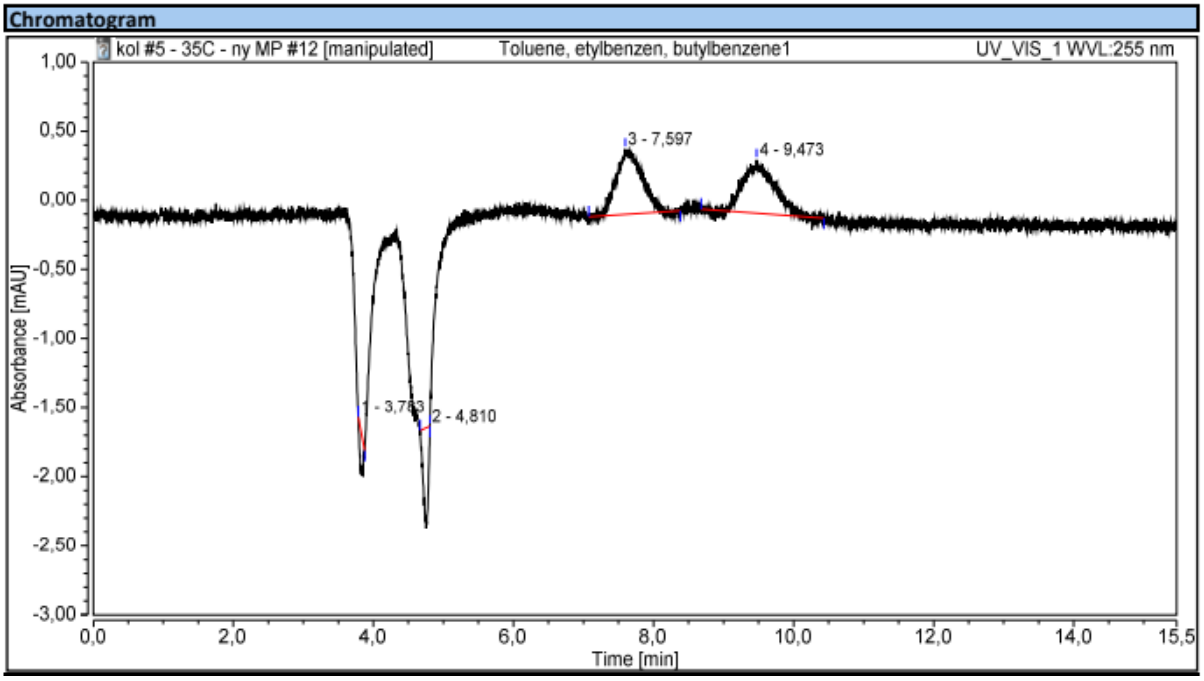

Figure 26 Chromatogram of butylbenzene (peak not visible), ethylbenzene (3) and toluene (4) at 0.25 mg/mL concentrations at 35°C. Chromatography performed with a 100 µm ID x 95 mm UiO-66-column in LC system III, pre-mixed mobile phase MeOH/0.1% FA (75/25, v/v) at 0.55 µL/min flow rate. Injection volume was 50 nL, UV detection was performed at 255 nm.

For benzene, naphthalene and phenanthrene, the molar absorptivity is considerably higher, however, the efficiency was not adequate to separate the compounds as seen in **Figure 27**. There was also severe carry-over from the PAH injections. Although the injection loop and column were washed with both 100% ACN, 100% MeOH and T1 water several times, a stable baseline was not obtained until after the system had been left in "inject" position overnight with a flow rate of 0.55 µL/min. The carry-over issue was not observed for the alkylbenzenes, suggesting that the interactions between UiO-66 and the larger PAHs are quite strong in comparison.

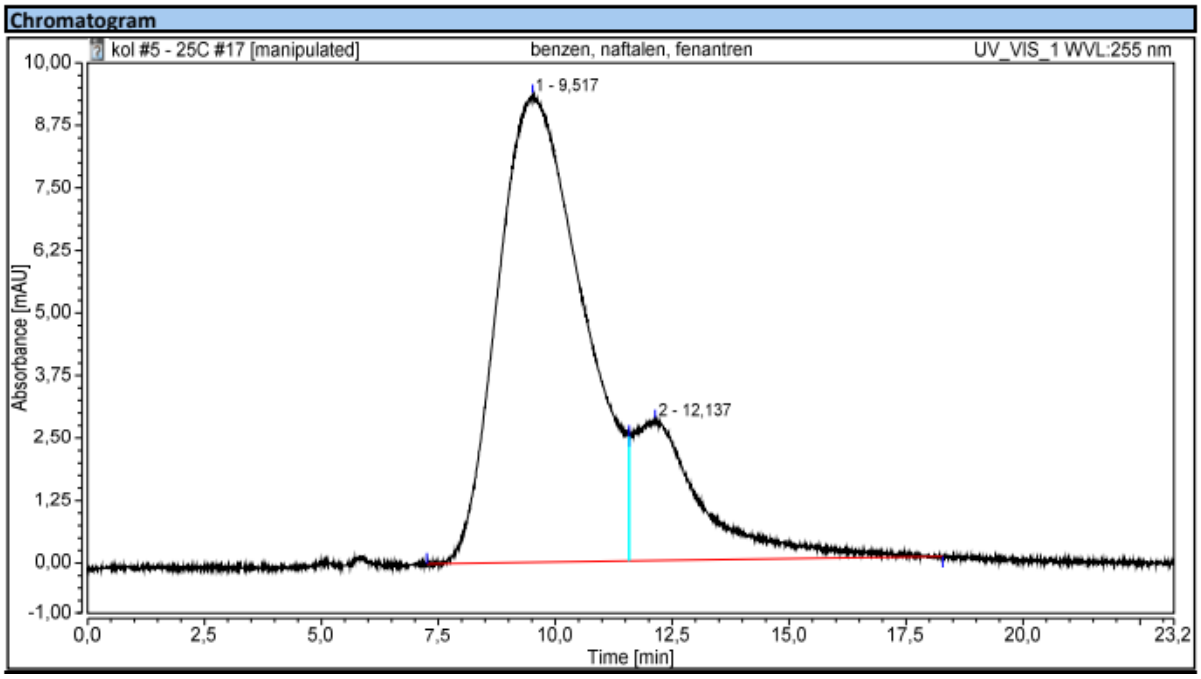

Figure 27 Chromatogram of benzene, naphthalene and phenanthrene (coeluting, 1 and 2) at 25°C. Chromatographic conditions were otherwise as described in **Figure 26**.

Due to circumstances described in section **6.3**, only four temperatures in the range 25–55°C have been investigated, and the Van't Hoff plot shown in **Figure 28**. The average elution time of T1 water and ACN at each temperature was used as t_M for the calculation of the retention factor.

The compounds investigated seemed to display a linear trend, but the data collected at 35°C gave lower values for ln k than expected. The investigation of more temperatures and more replicates at 35°C could help bring clarity to whether linear trends are present or not.

In 2014, Zhao et al.[77] conducted a study where they compared the chromatography of *o*-, *m*- and *p*-xylene, styrene and ethylbenzene at temperatures 20 to 60°C at 10°C increments, both using hexane/DCM as the MP and using MeOH/water. They found decreased retention with increasing temperatures for all compounds with all investigated MPs, suggesting that the interactions that cause retention are in net exothermic.

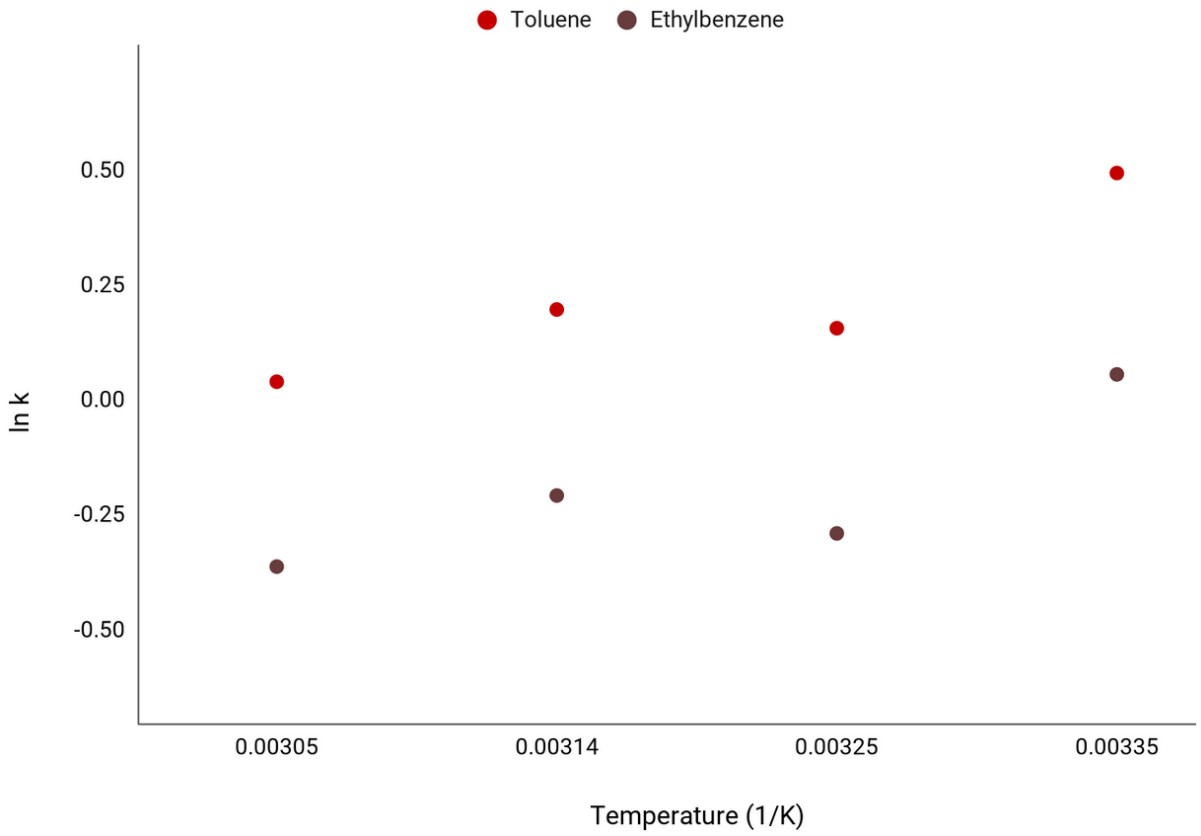

Figure 28 Van't Hoff plot for the compounds toluene and ethylbenzene, both at 0.25 mg/mL concentrations. n=3 for both compounds at all temperatures. Temperatures left to right corresponds to 55°C, 45°C, 35°C and 25°C. Chromatographic conditions were otherwise as described in **Figure 26**.

The same trend was found for UiO-66 in this study using 75% MeOH as the MP. This strengthened the assumption that the interactions that occur between the UiO-66-material and the alkylbenzenes are exothermic. However, while Zhao et al. achieved good correlation with linear regression lines in their work (R^2 ranging from 0.973 to 0.991), linear regression on the data in the present study yields correlation coefficients of 0.779 and 0.687 for toluene and ethylbenzene, respectively.

The need for a column oven for temperature regulation also meant the amount of connective tubing was significantly increased compared to what was used during the other parts of this study. In total, two unions (150 µm bore) and 137.3 cm of 20 µm ID tubing were added. The column volume was only 29% of the total volume, as is shown in **Table 5** in section **3.4**. This additional extra-column volume is likely to have caused more extra-column band broadening, which would increase the observed plate height.

Calculating the plate height from the chromatograms from this part of the study proved to be challenging, as the peaks in the chromatograms were broad and the signal intensity low. As elaborated upon in section **6.3** in the Appendix, there was limited time to perform manual integration, and the automated integration was found to be lacking in quality upon data analysis. Due to this, the peak width measurements might be inaccurate. The reader is advised to regard the plate heights presented in **Table 9** with these remarks in mind.

Table 9 Plate heights calculated at the different temperatures investigated. n=3 for both compounds at all temperatures. Chromatographic conditions were as described in **Figure 28**.
* Only 2 of 3 replicates yielded chromatograms where peak width was discernable.
** Only 1 of 3 replicates yielded chromatograms where peal width was discernable.

Temperature (°C)	Toluene *H* (µm)	Ethylbenzene *H* (µm)
25	25	39
35	27	41
45	17**	13*
55	16	18

The lowest plate height found during the efficiency as a function of linear velocity in section 4.2 was 18 µm. The efficiency study was carried out at room temperature, but is despite this closest to the plate heights found at 45°C and 55°C during the data collection for the Van't Hoff plot. This is thought to be due to the added extra-column volume necessary for this part of the study. Nevertheless, a trend of plate height decreasing with increasing temperature could be observed.

In summary, the hypothesis that the interaction between UiO-66 and small substituted benzenes are exothermic was strengthened. While the plate heights found in this part of the study are thought to be higher due to the extra tubing needed, they show decreasing plate heights with increasing temperature, making increasing the temperature a possible strategy for improving the efficiency of UiO-66-columns.

4.5 Pore volume accessibility

The small and very similar retention factors observed for adenosine phosphates, GABA, serotonin, and dopamine on UiO-66 raised the question of whether or not some or all of them were able to enter the pores of the MOFs. As the diameters of these molecules in common

solvents are not easily available through databases such as SciFinder[95] or ChemSpider[96], an investigation of when molecular size is too large for the molecule to enter the pores of UiO-66 was conducted.

For SEC, the transition between molecular size small enough to enter the pores and molecular size too large to enter is observed by the retention times being smaller than t_M. For this to be true, chromatographic conditions should be so no retention by other interactions than access to pore volume are present. By injecting a series of 1-alkylbenzenes and a series of aromatic compounds, the expected outcome was that the compounds that had no access to the pores would elute before t_M. This could provide an estimate of how large a molecule could be while still small enough to enter the pores of UiO-66.

The MP was chosen to minimise the effect of other interactions between the solutes and the SP. However, as there are several modes of interactions between UiO-66 and solutes available due to the structure of UiO-66, it was suspected that it would be difficult to find a suitable MP to accomplish this goal. Therefore, 100% MeOH was chosen, as this hopefully would cause there to be little hydrophobic interaction causing retention while also be able to solvated the 1-alkylbenzenes. Using a solvent that is commonly used as the organic modifier in MPs for RPLC was thought to give a better impression of what molecular size compounds might be able to enter the pores of UiO-66 when solvated in an MP containing MeOH.

Alkylbenzenes were chosen for the ease of stepwise increase in the size of the molecules. The aromatic compound series of benzene, naphthalene, phenanthrene and chrysene was chosen to get an idea of which sizes of planar molecules might be able to enter the pores. The kinetic diameter of chrysene was reported to be 8.16 Å by Zhao et al.[77], which is larger than the assumed 6 Å pore openings of UiO-66. As such, chrysene should be too large to access the pores, and could serve as a control of whether or not the experimental setup was suited to investigate pore access for different size molecules. The structures of the three PAHs are shown in **Figure 29**.

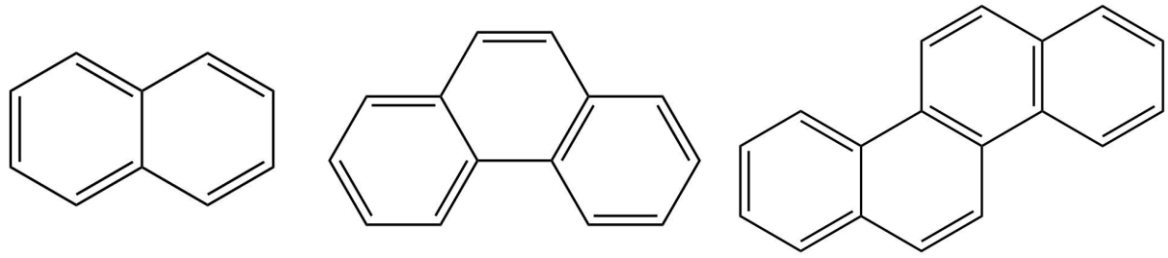

Naphthalene Phenanthrene Chrysene

Figure 29 Structures of naphthalene, phenanthrene and chrysene.

T1 water and ACN were injected to identify t_M. This was done because the well-defined size of the pores of UiO-66 should imply that the regular discouragement[8] of the use of mobile phase hold-up volume as elution volume (related to t_M by the linear velocity of the MP) could be disregarded. For conventional SEC materials, it is argued that the MP molecules are small enough to access every pore of the material, while even the most retained solutes will not be able to access the same volume[8].

The retention times of the alkylbenzene series are presented in **Figure 30**. The injections of benzene, toluene and ethylbenzene showed two peaks in the chromatogram, as shown in **Figure 31**. This was an unexpected outcome. The retention times of the second peak of the three smallest alkylbenzenes are indicated in light red in **Figure 30**.

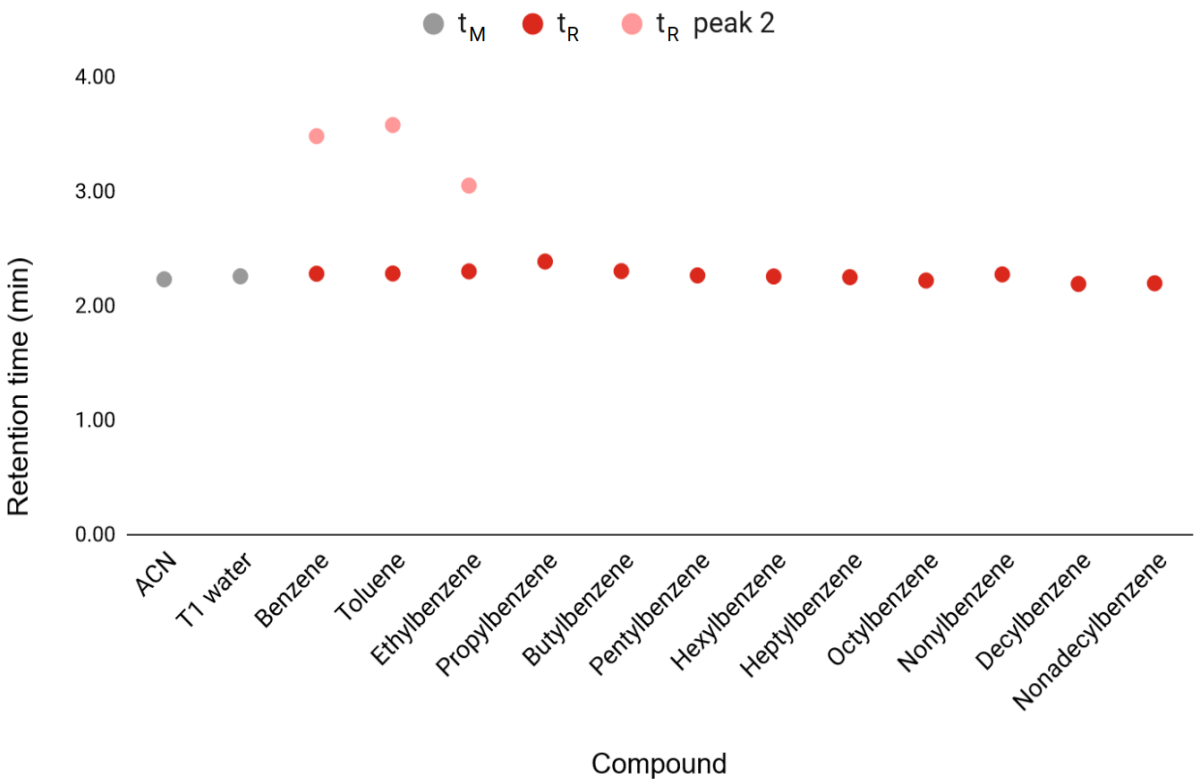

Figure 30 Retention times of the alkylbenzene series on UiO-66. n=5 for ACN, n=5 for T1 water, n=9 for benzene, toluene and ethylbenzene, n=6 for propylbenzene, and n=3 for butylbenzene throughout nonadecylbenzene. Chromatography performed with a 100 µm ID x 95 mm UiO-66-column in LC setup II, mobile phase 100% MeOH at a 0.55 µL/min flow rate. Injection volume was 50 nL, UV detection was performed at 255 nm.

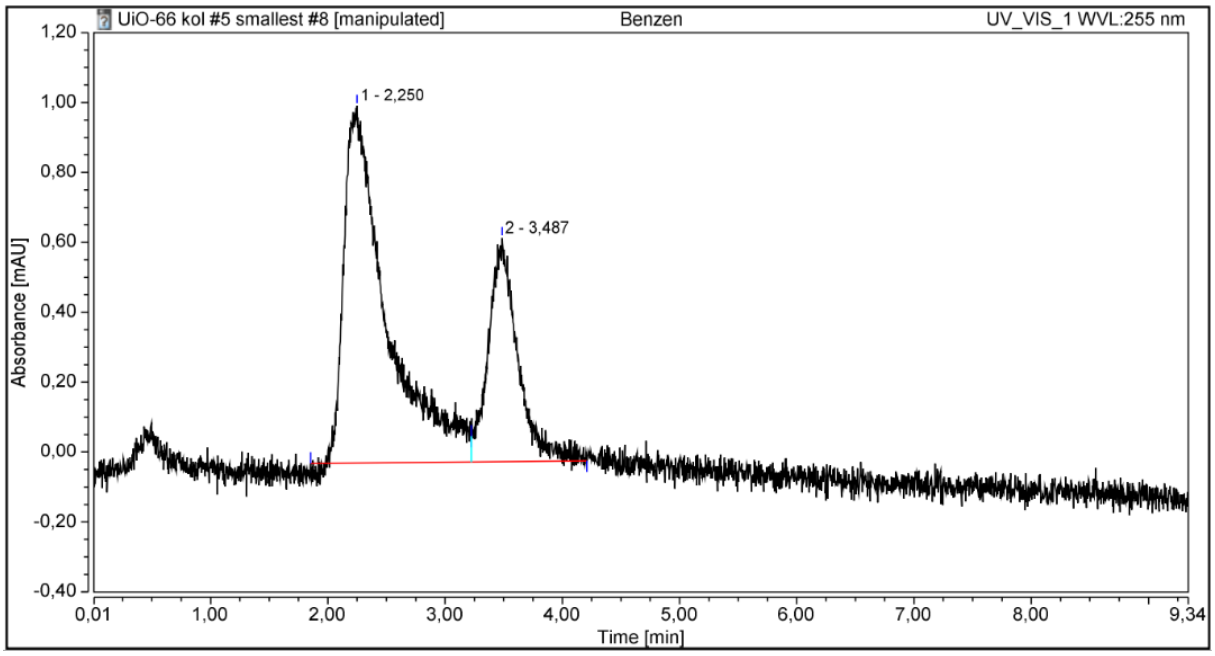

Figure 31 Chromatogram of benzene (0.25 mg/mL). Chromatographic conditions were as described in **Figure 30**.

It is unknown why two peaks appeared for the three smallest solutes. It is deemed highly unlikely that it is a solvent peak, as the solvent used in all injection solutions for this part of the study was 100% MeOH, and the MP was 100% MeOH. A possible explanation is that only some of the solute molecules had access to the UiO-66 pores. However, it is difficult to explain why this might be the case, as there ought to be no difference between for example toluene molecules that justifies the separation of one toluene band into two distinct bands. If the column was overloaded in the sense that all accessible pores were occupied, causing the surplus molecules to move further along the column while not being included into the pores of the particles, it stands to reason this would only cause the band to broaden, as these molecules would have access to unoccupied cavities as they moved further along the column. When calculating the resolution of the two peaks, it ranged between 0.79 and 1.04. This confirmed the impression from visual examination of the chromatograms that the solute band has separated into two bands, or that more than one solute band was present.

Following the observation of the second peak, three more injections of propylbenzene were performed, making for a total of six injections of the propylbenzene solution. Only one peak was observed for the three most recent injections, as was the case for the three previous injections of propylbenzene. Thus the only solutes observed displaying the two-peak pattern were benzene, toluene and ethylbenzene.

The two-peak pattern of the three smallest solutes investigated was suspected to be caused by carry-over. To investigate this, two new series of injections of these three solutes were performed. In one series (n=3 for each solute) the loop was washed several times with both T1 water, MeOH and ACN between all injections, and in the other (n=3 for each solute) the loop was not washed at all between injections of the same solution. If the two-peak pattern was caused by carry-over, it was expected that the amount of carry-over would not be the same for the two injection series. Analysis of peak areas showed no significant difference between the injection series, and it was concluded that carry-over from the injection loop was not the cause of the two peaks.

The retention times from the aromatic compound series are presented in **Figure 32**.

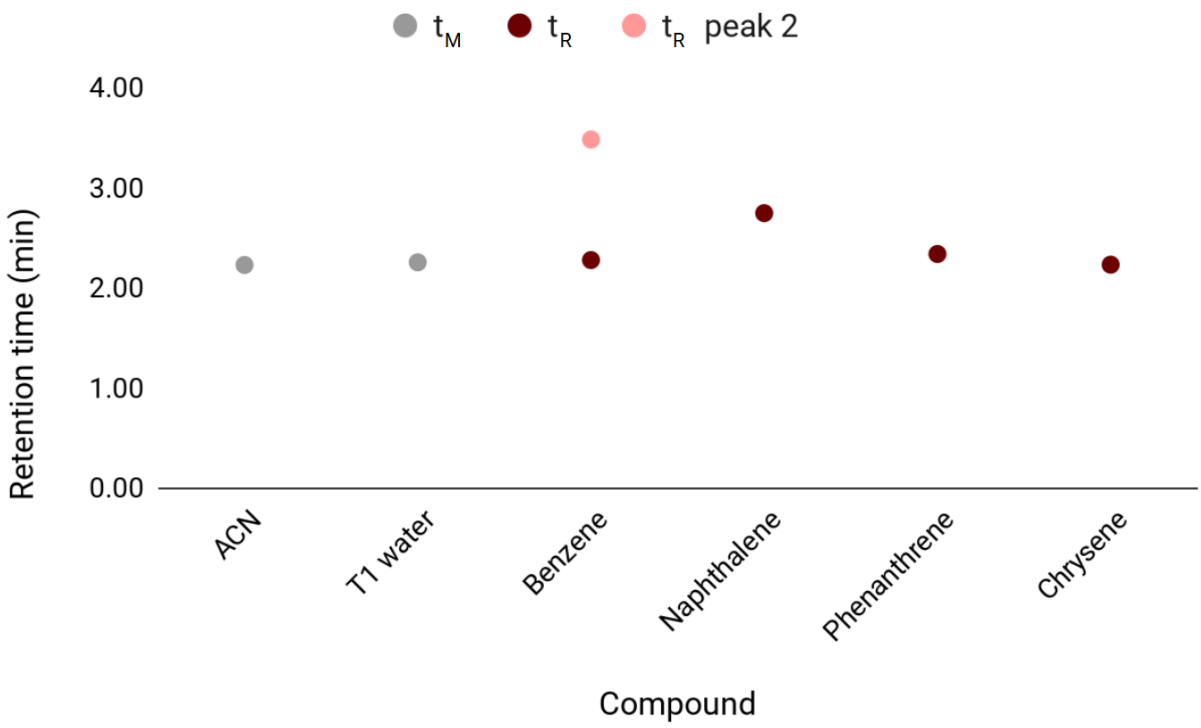

Figure 32 Retention times of the series of aromatic compounds on UiO-66. n=5 for ACN, n=5 for T1 water, n=9 for benzene, and n=3 for naphthalene, phenanthrene and chrysene. Chromatographic conditions were as described in **Figure 30**.

In order to determine whether the retention times for the different alkylbenzenes and aromatics were significantly different, t-tests were used. Because chrysene has been reported to be larger than the pore opening[77], the retention times were tested against the retention time of chrysene. Two-tailed unpaired t-tests were performed, with F-tests used to determine whether a pool standard deviation could be used or not. A 0.05 level of significance was used for these tests.

According to the tests conducted on the t_R of propylbenzene, butylbenzene, naphthalene and phenanthrene, t_R *were* significantly different from that of chrysene. For benzene, toluene and ethylbenzene, the retention times of the second peaks *were* significantly different from that of chrysene, while the retention times of the first peaks were *not*. The remainder of the tested compounds (pentylbenzene–decylbenzene and nonadecylbenzene) did not have retention times statistically significantly different from chrysene.

The compounds that had retention times that differed significantly from that of chrysene were hypothesised to *have* access to the pores, as chrysene was hypothesised to *not* have access to the pores.

Initially, t-tests comparing the t_R of the different solutes to the t_M values resulting from ACN and T1 water injection was intended. However, upon comparing the t_R of chrysene to the t_M values, it was discovered that the three populations were not statistically different at a 0.05 level of significance. This called into question the assumptions that ACN and T1 water had access to the pores, as well as the assumption that chrysene did not have access to the pores. The latter was deemed less likely to be false based on the reported kinetic diameter of the molecule being larger than the pore opening[77], and chrysene was chosen as the basis of comparison for further testing. It was also thought to be highly unlikely that T1 water and ACN did not have access to the pores. A more reasonable explanation could be that the variances between the retention and elution time values found was too large for a significant difference between the retention times. As shown in **Table 28**, T1 water had a large relative standard deviation (29%). While ACN and chrysene had more moderate relative standard deviations (2.7% and 1.8%, respectively), the average detection time for the two was the same (2.24 min).

The lack of statistically significant differences between ACN, T1 water and chrysene could be because the packed column volume was relatively small compared to extra-column volumes. For LC setup II as used for this part of the study, 39% of the total volume between injector and detector was packed column volume, and the remaining 61% was extra-column volume. Because of this, extra-column band broadening could make it more difficult to quantify the difference in elution time for the different compounds.

The method chosen for establishing an estimate of the maximum size of molecules that can enter the pores of UiO-66 has room for improvement. As described above, the testing LC system could be better suited for detecting differences in retention times by having smaller extra-column volume compared to the length of the packed column. The choice of 1-alkylbenzenes as test molecules was made to make a gradual increase in the molecular size possible. In theory, the alkyl chain could be sterically oriented in a multitude of ways. Depending on the length of the alkyl chain, it could trail next to the phenyl ring, coil up on itself, coil up on the phenyl ring, or a combination of these, to name a few options. The orientation of the alkyl chain would affect the diameter of the molecule. However, the author

was unsuccessful in finding the diameter of the 1-alkylbenzenes in different solvents in the literature. The aromatic compounds are rigid molecules and thus have a more well-defined diameter, and should as such be better suited to estimate the maximum size of molecules that has access to the pores of UiO-66. The aromatic compounds might also be easier to compare in size to other molecules with planar geometries. However, it is important to keep in mind that the size of the molecule when in solution is the deciding factor of whether or not the molecule can enter the pores.

In summary, the investigation of pore volume accessibility yielded two unexpected observations: two peaks appeared in the benzene, toluene and ethylbenzene chromatograms, and the lack of significant difference between the t_R value of chrysene and the t_M values of T1 water and ACN. Hypothesis testing suggested benzene and alkylbenzenes up to and including butylbenzene had access to the pores of UiO-66, and that the PAHs naphthalene and phenanthrene did as well.

5 Conclusions

In this thesis, the aim was to gain more knowledge about the UiO-66 materials for use in LC separations. Both reversed-phase selectivity and normal-phase selectivity were observed for UiO-66 with aqueous MPs, whereas normal phase selectivity has previously only been observed with hexane/DCM MPs. However, the efficiencies found for UiO-66 were not up to par with current separation materials. The testing systems used were not optimal in this regard, as the extra-column volume was large relative to column volume.

Small organic compounds with polar functional groups were the most retained when the LC system was operated in RPLC mode. This was found for both UiO-66 and UiO-66-NH_2. The retention was strongest for low percentages of organic modifier. The observed retention of small polar molecules is promising, as there is a potential application area for UiO-66 materials as a complementary SP to C18 and C8 on silica support.

Adenosine phosphates were found to adsorb onto the zirconium clusters of the materials, resulting in pronounced tailing and unstable baselines for the injection following. This suggests phosphate-containing compounds might not be suited for chromatography on UiO-66 materials.

The interactions between solute and UiO-66 were found to be exothermic, and efficiencies were improved with elevated temperatures.

The findings in this study suggested only very small molecules could enter the pores of UiO-66 and UiO-66-NH_2. While it was concluded that 1-alkylbenzenes larger than butylbenzene and PAHs larger than phenanthrene were excluded from the pores, the lack of statistically significant difference between the elution times of T1 water and ACN and that of chrysene suggests the testing system might not have been optimal for determining the difference in retention times.

Even though this thesis has contributed to the knowledge of the properties of the MOF materials UiO-66 and UiO-66-NH_2, especially the former, more research is needed to fully characterize their properties. A more solid understanding of the chromatographic properties of these materials will be a benefit when continuing the exploration of UiO-66 materials as chromatographic separation materials for various types of compounds and applications.

5.1 Further work

In the author's opinion, the following should be investigated to gain more knowledge of the properties of UiO-66 and similar materials and their potential for use in separation science.

The potential application of UiO-66 as an SP for the separation of small polar molecules should be further investigated to determine if small polar analytes with little retention on C_{18} or C_8 materials might be suitable for separation on UiO-66 materials. An investigation of the chromatography of amino acids and dipeptides on UiO-66 could be a beneficial starting point. Similar investigations should also be conducted on UiO-67, which has larger pores and thus can accommodate larger analytes.

The observed change in retention factor with flow rate for UiO-66 is so far unexplained and should be further investigated to better understand the material as an SP. The investigation of the impact of flow rate on retention factor and chromatographic efficiency on UiO-66-NH_2 as well as UiO-67 was not prioritised in this thesis, but should nevertheless be investigated.

To better be able to conclude on the pore volume access investigations, improvements to the method used could be attempted. Other MPs which might give fewer and weaker interactions between the solvents and the SP should be explored. Injection solutions of varying concentrations should be investigated for benzene, toluene and ethylbenzene, in order to verify if the two peaks observed for these solutes appear consistently.

An important issue to be resolved for UiO-66 materials is the inferior efficiency when compared to conventional SPs. A testing system with smaller extra-column volume would make it more clear which efficiencies might be possible to achieve with UiO-66 materials. An optimalisation of packing procedure to maximise column efficiency and optimalisation of chromatographic conditions to enhance efficiency is needed to get a better understanding of the limitations of the materials in terms of efficiency.

In order to better understand the interactions between solute and UiO-66, molecular simulations might be useful. However, these would likely be very demanding, as UiO-66 is a large and complex chemical system even without solutes present. Simulations would still provide more data to support or undermine current hypotheses of which interactions might cause solute retention on UiO-66 materials.

References

1. Knox, J. H., Kaur, B. & Millward, G. R. Structure and performance of porous graphitic carbon in liquid chromatography. *Journal of Chromatography A* **352**, 3–25 (1986).

2. Pereira, L. Porous Graphitic Carbon as a Stationary Phase in HPLC: Theory and Applications. *Journal of Liquid Chromatography & Related Technologies* **31**, 1687–1731 (2008).

3. Alpert, A. J. Hydrophilic-interaction chromatography for the separation of peptides, nucleic acids and other polar compounds. *Journal of Chromatography A* **499**, 177–196 (1990).

4. Buszewski, B. & Noga, S. Hydrophilic interaction liquid chromatography (HILIC)-a powerful separation technique. *Analytical and Bioanalytical Chemistry* **402**, 231–247 (2012).

5. Lundanes, E., Reubsaet, L. & Greibrokk, T. *Chromatography : basic principles, sample preparations and related methods*. (Wiley-VCH, 2014).

6. Dinh, N. P., Jonsson, T. & Irgum, K. Probing the interaction mode in hydrophilic interaction chromatography. *Journal of Chromatography A* **1218**, 5880–5891 (2011).

7. Jandera, P. Stationary and mobile phases in hydrophilic interaction chromatography: A review. *Analytica Chimica Acta* **692**, 1–25 (2011).

8. Ettre, L. Nomenclature for chromatography (IUPAC Recommendations 1993). *Pure and Applied Chemistry* **65**, 819–872 (1993).

9. Gritti, F. & Guiochon, G. Mass transfer kinetics, band broadening and column efficiency. *Journal of Chromatography A* **1221**, 2–40 (2012).

10. Harris, D. C. *Quantitative chemical analysis*. (Freeman, 2010).

11. Grinias, J. P. Characterization and Control of Band Broadening in Ultra-High Pressure Liquid Chromatography Columns. in (2014).

12. Rimmer, C. A., Simmons, C. R. & Dorsey, J. G. The measurement and meaning of void volumes in reversed-phase liquid chromatography. *Journal of Chromatography A* **965**, 219–232 (2002).

13. McNair, H. M. & Kazakevich, Y. V. Thermodynamic definition of hplc dead volume. *Journal of Chromatographic Science* **31**, 317–322 (1993).

14. Kazakevich, Y. V. & McNair, H. M. Low-energy interactions in high-performance liquid chromatography. *Journal of Chromatography A* **872**, 49–59 (2000).

15. Kazakevich, Y. V., LoBrutto, R., Chan, F. & Patel, T. Interpretation of the excess adsorption isotherms of organic eluent components on the surface of reversed-phase adsorbents: Effect on the analyte retention. *Journal of Chromatography A* **913**, 75–87 (2001).

16. Chester, T. L. & Coym, J. W. Effect of phase ratio on van't Hoff analysis in reversed-phase liquid chromatography, and phase-ratio-independent estimation of transfer enthalpy. *Journal of Chromatography A* **1003**, 101–111 (2003).

17. Batten, S. R. *et al.* Terminology of metal–organic frameworks and coordination polymers (IUPAC Recommendations 2013). *Pure and Applied Chemistry* **85**, (2013).

18. Hoskins, B. F. & Robson, R. Infinite Polymeric Frameworks Consisting of Three Dimensionally Linked Rod-like Segments. *Journal of the American Chemical Society* **111**, 5962–5964 (1989).

19. Hoskins, B. F. & Robson, R. Design and Construction of a New Class of Scaffolding-like Materials Comprising Infinite Polymeric Frameworks of 3D-Linked Molecular Rods. A Reappraisal of the $Zn(CN)_2$ and $Cd(CN)_2$ Structures and the Synthesis and Structure of the Diamond-Related Framework. *Journal of the American Chemical Society* **112**, 1546–1554 (1990).

20. Yaghi, O. M., Li, G. & Li, H. Selective binding and removal of guests in a microporous metal–organic framework. *Nature* **378**, 703–706 (1995).

21. Rosi, N. L. *et al.* Hydrogen Storage in Microporous Metal-Organic Frameworks. *Science* **300**, 1127–1129 (2003).

22. Senkovska, I. *et al.* New highly porous aluminium based metal-organic frameworks: Al(OH)(ndc) (ndc = 2,6-naphthalene dicarboxylate) and Al(OH)(bpdc) (bpdc = 4,4′-biphenyl dicarboxylate). *Microporous and Mesoporous Materials* **122**, 93–98 (2009).

23. Yang, S. *et al.* A partially interpenetrated metal–organic framework for selective hysteretic sorption of carbon dioxide. *Nature Materials* **11**, 710 (2012).

24. Millange, F., Serre, C. & Férey, G. Synthesis, structure determination and properties of MIL-53as and MIL-53ht: the first Cr^{III} hybrid inorganic–organic microporous solids: $Cr^{III}(OH)\cdot\{O_2C–C_6H_4–CO_2\}\cdot\{HO_2C–C_6H_4–CO_2H\}_x$. *Chemical Communications* **2**, 822–823 (2002).

25. Cavka, J. H. *et al.* A New Zirconium Inorganic Building Brick Forming Metal Organic Frameworks with Exceptional Stability. *Journal of the American Chemical Society* **130**, 13850–13851 (2008).

26. Chui, S. S. A Chemically Functionalizable Nanoporous Material [Cu3(TMA)2(H2O)3]n. *Science* **283**, 1148–1150 (1999).

27. Férey, G. Hybrid porous solids: Past, present, future. *Chemical Society Reviews* **37**, 191–214 (2008).

28. Devic, T. & Serre, C. High valence 3p and transition metal based MOFs. *Chemical Society Reviews* **43**, 6097–6115 (2014).

29. Roy, P., Schaate, A., Behrens, P. & Godt, A. Post-synthetic modification of Zr-metal-organic frameworks through cycloaddition reactions. *Chemistry - A European Journal* **18**, 6979–6985 (2012).

30. Long, J. *et al.* Amine-functionalized zirconium metal–organic framework as efficient visible-light photocatalyst for aerobic organic transformations. *Chemical Communications* **48**, 11656–11658 (2012).

31. Lee, J. *et al.* Metal-organic framework materials as catalysts. *Chemical Society Reviews* **38**, 1450–1459 (2009).

32. Ma, L., Abney, C. & Lin, W. Enantioselective catalysis with homochiral metal-organic frameworks. *Chemical Society Reviews* **38**, 1248–1256 (2009).

33. Abid, H. R. *et al.* Nanosize Zr-metal organic framework (UiO-66) for hydrogen and carbon dioxide storage. *Chemical Engineering Journal* **187**, 415–420 (2012).

34. Suh, M. P., Park, H. J., Prasad, T. K. & Lim, D. W. Hydrogen storage in metal-organic frameworks. *Chemical Reviews* **112**, 782–835 (2012).

35. Murray, L. J., Dinc, M. & Long, J. R. Hydrogen storage in metal-organic frameworks. *Chemical Society Reviews* **38**, 1294–1314 (2009).

36. Kato, S. *et al.* Zirconium-Based Metal-Organic Frameworks for the Removal of Protein-Bound Uremic Toxin from Human Serum Albumin. *Journal of the American Chemical Society* **141**, 2568–2576 (2019).

37. Zhang, W. *et al.* Metal-organic framework UiO-66 modified magnetite@silica core-shell magnetic microspheres for magnetic solid-phase extraction of domoic acid from shellfish samples. *Journal of Chromatography A* **1400**, 10–18 (2015).

38. Yao, W., Fan, Z. & Zhang, S. Preparation of metal-organic framework UiO-66-incorporated polymer monolith for the extraction of trace levels of fungicides in environmental water and soil samples. *Journal of Separation Science* **42**, 2679–2686 (2019).

39. Gu, Z.-Y., Jiang, J.-Q. & Yan, X.-P. Fabrication of Isoreticular Metal–Organic Framework Coated Capillary Columns for High-Resolution Gas Chromatographic Separation of Persistent Organic Pollutants. *Analytical Chemistry* **83**, 5093–5100 (2011).

40. Chen, C. *et al.* Adsorption Behaviors of Organic Micropollutants on Zirconium Metal-Organic Framework UiO-66: Analysis of Surface Interactions. *ACS Applied Materials and Interfaces* **9**, 41043–41054 (2017).

41. Valenzano, L. *et al.* Disclosing the complex structure of UiO-66 metal organic framework: A synergic combination of experiment and theory. *Chemistry of Materials* **23**, 1700–1718 (2011).

42. Shearer, G. C. *et al.* In situ infrared spectroscopic and gravimetric characterisation of the solvent removal and dehydroxylation of the metal organic frameworks UiO-66 and UiO-67. in *Topics in Catalysis* **56**, 770–782 (2013).

43. Ghosh, P., Colón, Y. J. & Snurr, R. Q. Water adsorption in UiO-66: The importance of defects. *Chemical Communications* **50**, 11329–11331 (2014).

44. Wu, H. *et al.* Unusual and highly tunable missing-linker defects in zirconium metal-organic framework UiO-66 and their important effects on gas adsorption. *Journal of the American Chemical Society* **135**, 10525–10532 (2013).

45. Su, Z., Miao, Y. R., Zhang, G., Miller, J. T. & Suslick, K. S. Bond breakage under pressure in a metal organic framework. *Chemical Science* **8**, 8004–8011 (2017).

46. Wu, H., Yildirim, T. & Zhou, W. Exceptional mechanical stability of highly porous zirconium metal-organic framework UiO-66 and its important implications. *Journal of Physical Chemistry Letters* **4**, 925–930 (2013).

47. Greeves, N. UiO-66 ChemTube3D structure. Available at: http://www.chemtube3d.com/solidstate/MOF-UiO66.html. (Accessed: 12th April 2018)

48. Garibay, S. J. & Cohen, S. M. Isoreticular synthesis and modification of frameworks with the UiO-66 topology. *Chemical Communications* **46**, 7700–7702 (2010).

49. Katz, M. J. *et al.* A facile synthesis of UiO-66, UiO-67 and their derivatives. *Chemical Communications* **49**, 9449–9451 (2013).

50. ProfMOF. Discover our MOF products. Available at: https://profmof.com/discover-our-mof-products/. (Accessed: 31st May 2020)

51. Chavan, S. M. *et al.* Synthesis and characterization of amine-functionalized mixed-ligand metal-organic frameworks of UiO-66 topology. *Inorganic Chemistry* **53**, 9509–9515 (2014).

52. Kandiah, M. *et al.* Post-synthetic modification of the metal-organic framework compound UiO-66. *Journal of Materials Chemistry* **20**, 9848–9851 (2010).

53. Chang, Z. *et al.* Selective and efficient adsorption of Au (III) in aqueous solution by Zr-based metal-organic frameworks (MOFs): An unconventional way for gold recycling. *Journal of Hazardous Materials* **391**, (2020).

54. Katz, M. J. *et al.* Exploiting parameter space in MOFs: A 20-fold enhancement of phosphate-ester hydrolysis with UiO-66-NH_2. *Chemical Science* **6**, 2286–2291 (2015).

55. Gu, Z. & Yan, X. Metal–Organic Framework MIL-101 for High-Resolution Gas-Chromatographic Separation of Xylene Isomers and Ethylbenzene. *Angewandte Chemie International Edition* **49**, 1477–1480 (2010).

56. Chang, N. & Yan, X.-P. Exploring reverse shape selectivity and molecular sieving effect of metal-organic framework UIO-66 coated capillary column for gas chromatographic separation. *Journal of Chromatography A* **1257**, 116–124 (2012).

57. Duerinck, T. *et al.* Understanding Hydrocarbon Adsorption in the UiO-66 Metal-Organic Framework: Separation of (Un)saturated Linear, Branched, Cyclic Adsorbates, Including Stereoisomers. *Journal of Physical Chemistry C* **117**, 12567–12578 (2013).

58. Bozbiyik, B. *et al.* Adsorption and separation of n-hexane and cyclohexane on the UiO-66 metal-organic framework. *Microporous and Mesoporous Materials* **183**, 143–149 (2014).

59. Yang, C.-X. & Yan, X.-P. Metal–Organic Framework MIL-101(Cr) for High-Performance Liquid Chromatographic Separation of Substituted Aromatics. *Analytical Chemistry* **83**, 7144–7150 (2011).

60. Liu, S.-S., Yang, C.-X., Wang, S.-W. & Yan, X.-P. Metal-organic frameworks for reverse-phase high-performance liquid chromatography. *Analyst* **137**, 816–818 (2012).

61. Yusuf, K., Badjah-Hadj-Ahmed, A. Y., Aqel, A. & ALOthman, Z. A. Monolithic metal-organic framework MIL-53(Al)-polymethacrylate composite column for the reversed-phase capillary liquid chromatography separation of small aromatics. *Journal of Separation Science* **39**, 880–888 (2016).

62. Liu, X., Wang, C., Wu, Q. & Wang, Z. Porous carbon derived from a metal-organic framework as an efficient adsorbent for the solid-phase extraction of phthalate esters. *Journal of Separation Science* **38**, 3928–3935 (2015).

63. Li, W., Wang, R. & Chen, Z. Zr-based metal-organic framework-modified cotton for solid phase micro-extraction of non-steroidal anti-inflammatory drugs. *Journal of Chromatography A* **1576**, 19–25 (2018).

64. Gao, G. *et al.* A combination of computational−experimental study on metal-organic frameworks MIL-53(Al) as sorbent for simultaneous determination of estrogens and glucocorticoids in water and urine samples by dispersive micro-solid-phase extraction

coupled to UPLC-MS/MS. *Talanta* **180**, 358–367 (2018).

65. González-Rodríguez, G. *et al.* Mixed functionalization of organic ligands in UiO-66: A tool to design metal-organic frameworks for tailored microextraction. *Molecules* **24**, (2019).

66. Van Der Perre, S. *et al.* Chromatographic separation through confinement in nanocages. *Microporous and Mesoporous Materials* **189**, 216–221 (2014).

67. Ameloot, R. *et al.* Silica-MOF composites as a stationary phase in liquid chromatography. *European Journal of Inorganic Chemistry* 3735–3738 (2010). doi:10.1002/ejic.201000494

68. Peristyy, A. *et al.* Flow-dependent separation selectivity for organic molecules on metal-organic frameworks containing adsorbents. *Chemical Communications* **52**, 5301–5304 (2016).

69. Zhang, X., Han, Q. & Ding, M. One-pot synthesis of UiO-66@SiO_2 shell-core microspheres as stationary phase for high performance liquid chromatography. *RSC Advances* **5**, 1043–1050 (2015).

70. Arrua, R. D. *et al.* UiO-66@ SiO_2 core-shell microparticles as stationary phases for the separation of small organic molecules. *Analyst* **142**, 517–524 (2017).

71. Fu, Y. Y., Yang, C. X. & Yan, X. P. Fabrication of ZIF-8@SiO_2 core-shell microspheres as the stationary phase for high-performance liquid chromatography. *Chemistry - A European Journal* **19**, 13484–13491 (2013).

72. Yan, Z. *et al.* Preparation and evaluation of silica-UIO-66 composite as liquid chromatographic stationary phase for fast and efficient separation. *Journal of Chromatography A* **1366**, 45–53 (2014).

73. Yang, S., Ye, F., Zhang, C., Shen, S. & Zhao, S. In situ synthesis of metal-organic frameworks in a porous polymer monolith as the stationary phase for capillary liquid chromatography. *Analyst* **140**, 2755–2761 (2015).

74. Yang, S. *et al.* Incorporation of metal-organic framework HKUST-1 into porous polymer monolithic capillary columns to enhance the chromatographic separation of small molecules. *Journal of Chromatography A* **1360**, 143–149 (2014).

75. Fu, Y.-Y., Yang, C.-X. & Yan, X.-P. Incorporation of metal-organic framework UiO-66 into porous polymer monoliths to enhance the liquid chromatographic separation of small molecules. *Chemical Communications* **49**, 7162–7164 (2013).

76. Svec, F. Quest for organic polymer-based monolithic columns affording enhanced efficiency in high performance liquid chromatography separations of small molecules

in isocratic mode. *Journal of Chromatography A* **1228**, 250–262 (2012).

77. Zhao, W. W. *et al.* Separations of substituted benzenes and polycyclic aromatic hydrocarbons using normal- and reverse-phase high performance liquid chromatography with UiO-66 as the stationary phase. *Journal of Chromatography A* **1370**, 121–128 (2014).

78. Gao, B. *et al.* Hybridization of metal–organic framework and monodisperse spherical silica for chromatographic separation of xylene isomers. *Chinese Journal of Chemical Engineering* **27**, 818–826 (2019).

79. Bárcia, P. S. *et al.* Reverse shape selectivity in the adsorption of hexane and xylene isomers in MOF UiO-66. *Microporous and Mesoporous Materials* **139**, 67–73 (2011).

80. Lin, S., Gan, N., Cao, Y., Chen, Y. & Jiang, Q. Selective dispersive solid phase extraction-chromatography tandem mass spectrometry based on aptamer-functionalized UiO-66-NH2 for determination of polychlorinated biphenyls. *Journal of Chromatography A* **1446**, 34–40 (2016).

81. Xia, L. *et al.* Determination of chlorophenoxy acid herbicides by using a zirconium-based metal-organic framework as special sorbent for dispersive micro-solid-phase extraction and high-performance liquid chromatography. *New Journal of Chemistry* **41**, 2241–2248 (2017).

82. Hatamluyi, B., Hashemzadeh, A. & Darroudi, M. A novel molecularly imprinted polymer decorated by CQDs@HBNNS nanocomposite and UiO-66-NH_2 for ultra-selective electrochemical sensing of Oxaliplatin in biological samples. *Sensors and Actuators B: Chemical* **307**, 127614 (2020).

83. Ning, C. *et al.* HPLC using capillary monolithic column molecularly imprinted with composite metal organic frame for enrichment and detection of Ponceau 4R in Carthami flos. *Nan fang yi ke da xue xue bao = Journal of Southern Medical University* **40**, 203–210 (2020).

84. Zhao, W. *et al.* Preparation, characterization, and performance evaluation of UiO-66 analogues as stationary phase in HPLC for the separation of substituted benzenes and polycyclic aromatic hydrocarbons. *PLoS ONE* **12**, (2017).

85. Chen, K., Zhang, L. & Zhang, W. Preparation and evaluation of open-tubular capillary column combining a metal–organic framework and a brush-shaped polymer for liquid chromatography. *Journal of Separation Science* **41**, 2347–2353 (2018).

86. Johnsen, E., Leknes, S., Wilson, S. R. & Lundanes, E. Liquid chromatography-mass spectrometry platform for both small neurotransmitters and neuropeptides in blood, with automatic and robust solid phase extraction. *Scientific Reports* **5**, 9308 (2015).

87. Berg, H. S. *et al.* Self-packed core shell nano liquid chromatography columns and silica-based monolithic trap columns for targeted proteomics. *Journal of Chromatography A* **1498**, 111–119 (2017).

88. Vissers, J. P. C., Hoeben, M. A., Laven, J., Claessens, H. A. & Cramers, C. A. Hydrodynamic aspects of slurry packing processes in microcolumn liquid chromatography. *Journal of Chromatography A* **883**, 11–25 (2000).

89. Shelly, D. C., Antonucci, V. L., Edkins, T. J. & Dalton, T. J. Insights into the slurry packing and bed structure of capillary liquid chromatographic columns. *Journal of Chromatography A* **458**, 267–279 (1988).

90. Fekete, S., Schappler, J., Veuthey, J.-L. & Guillarme, D. Current and future trends in UHPLC. *Trends in Analytical Chemistry* **63**, 2–13 (2014).

91. Wilson, S. R., Vehus, T., Berg, H. S. & Lundanes, E. Nano-LC in proteomics: recent advances and approaches. *Bioanalysis* **7**, 1799–1815 (2015).

92. Hodoroaba, V.-D., Motzkus, C., Macé, T. & Vaslin-Reimann, S. Performance of High-Resolution SEM/EDX Systems Equipped with Transmission Mode (TSEM) for Imaging and Measurement of Size and Size Distribution of Spherical Nanoparticles. *Microscopy and microanalysis* **20**, 602–612 (2014).

93. Mrša, A. Investigation of in-house packed UiO-66 particle-based nano liquid chromatography columns. (University of Oslo, 2017).

94. Gika, H. G., Theodoridis, G. A., Plumb, R. S. & Wilson, I. D. Current practice of liquid chromatography–mass spectrometry in metabolomics and metabonomics. *Journal of Pharmaceutical and Biomedical Analysis* **87**, 12–25 (2014).

95. CAS. SciFinder. Available at: https://scifinder.cas.org. (Accessed: 7th June 2020)

96. Royal Society of Chemistry. ChemSpider. Available at: http://www.chemspider.com/. (Accessed: 7th June 2020)

97. Brodusch, N., Demers, H. & Gauvin, R. *Field Emission Scanning Electron Microscopy: New Perspectives for Materials Characterization*. (Springer, 2017).

98. Surface and thin film analysis : a compendium of principles, instrumentation, and applicaitons. (2011).

99. Det kongelige kunnskapsdepartement. Informasjon i forbindelse med koronavirus og Covid-19-pandemien. (2020). Available at: https://www.regjeringen.no/contentassets/5d55fe8ddb1141d38482ffc3de0fbdee/informasjom-om-regelverk-for-universitets--og-hoyskolesektoren-ifm.-covid-19.pdf. (Accessed: 16th March 2020)

6 Appendix

6.1 Supplementary theoretical background

In this section, theoretical background deemed not central enough to the thesis to be included in the main text is provided. The subsections are kept brief for this very reason.

6.1.1 Scanning electron microscopy

SEM is a technique that allows the surface of a solid to be examined in resolutions in the nm scale[97]. An image is created by scanning a focused high energy electron beam over the surface of the specimen examined. The electrons in the beam will interact with the specimen through elastic and inelastic collisions with the atoms of the specimen. These interactions give rise to lower energy electrons, which are emitted by the atoms on the surface due to inelastic interactions with the beam electrons, and beam electrons which are backscattered through elastic interactions with the nuclei of the sample atoms and have higher energy. Electron detectors and x-ray detectors detect both the secondary electrons (low energy) and the backscattered electrons.

6.1.2 Energy-dispersive X-ray spectroscopy

EDXS is a spectroscopic technique which allows for element analysis of the surface of a sample. If the sample is thin enough, a comprehensive analysis is possible. EDXS is commonly combined with SEM, as an energy dispersive x-ray spectrometer is often integrated in electron microscopes[98]. When the electrons in the beam cause atoms in the sample to be ionized due to an atom electron being ejected, an electron from a higher energy orbital will transition to fill the vacancy. This transition causes an x-ray with a characteristic energy to be emitted, which in turn can be detected. The different transitions that are detected can be used to determine which elements are present in the sample, and quantification is also possible down to concentrations of 1–0.01% of the atoms present[98]. Detection and quantification of elements heavier than sodium can be performed with most instruments, but elements between boron and sodium require specialized equipment due to the lower energy of the x-rays emitted from these elements. Quantification of lighter elements is unreliable, as the

electrons involved in transitions which cause x-ray emission are valence electrons, and thus their energy is strongly influenced by their chemical environment.

6.1.3 Hypothesis testing

In order to help determine whether differences between observations are due to different populations being observed or due to coincidence, several methods of comparing sets of observations have been developed. These methods are commonly referred to as hypothesis testing methods. In this study, both F-tests, unpaired t-tests and ANOVA are used to compare means and variances.

In all hypothesis testing, the establishing of a null hypothesis (H_0) and an alternative hypothesis (H_a) is the first step. A general formulation of the two hypotheses is shown below:

> H_0: *There is no statistically significant difference between the populations which are compared*.
>
> H_a: *There is a statistically significant difference between the populations which are compared*.

From here, the test is conducted and a decision to keep or reject H_0 is made. The decision is made based on a quotient resulting from the test, which is compared to the desired confidence level.

The value used is one where the quotient (for example t-value, in the case of a t-test being conducted) is compared to the threshold value (critical value) for the quotient for a given level of confidence and degrees of freedom as found in a table (for example a t-value table). Most spreadsheet software has inbuilt functions for hypothesis testing. These commonly yield a P-value, which can be directly compared to the desired level of confidence

When using hypothesis tests, it is important to keep in mind that the tests are only a statistical tool which can inform the researcher of whether an observed difference is likely to be random or due to there actually being a difference present. A failure to reject H_0 does not unequivocally mean the populations compared are the same, but rather means it cannot be ruled out at the chosen level of confidence, and vice versa.

6.2 Supplementary information

This section contains supplementary information. The subsections are categorised first by the same subsections found in section **4**, and each subsection contains tables summarising finds, selected chromatograms, and calculations associated with hypothesis testing. No supplementary information on packing properties is provided in this appendix.

In the subsections for column efficiency and investigation of retention of compounds, the reader will also find results and discussion of work not included in the main text.

6.2.1 Column efficiency

In this section, a brief summary of early column efficiency investigations are given, and supplementary information to the column efficiency investigation discussed in the main text is given.

Early column efficiency investigation

The results from this part of the thesis are not included in the main text as they are deemed to be unreliable due to a leak discovered in the pump shortly after the investigation was conducted.

The van Deemter plot constructed from the initial column efficiency investigation can be seen in **Figure 33**. As can clearly be seen, the column did not display the expected behaviour where low linear velocities give large plate heights which decrease with increasing linear velocity until a minimum in the graph is found. **Figure 34** shows the logged backpressure corresponding to the different linear velocities investigated. It is noteworthy that the flow rates where plate height that deviate the most from the expected van Deemter curve also deviate from the expected in regards of backpressure: these linear velocities have higher plate number than expected, and lower backpressure than expected.

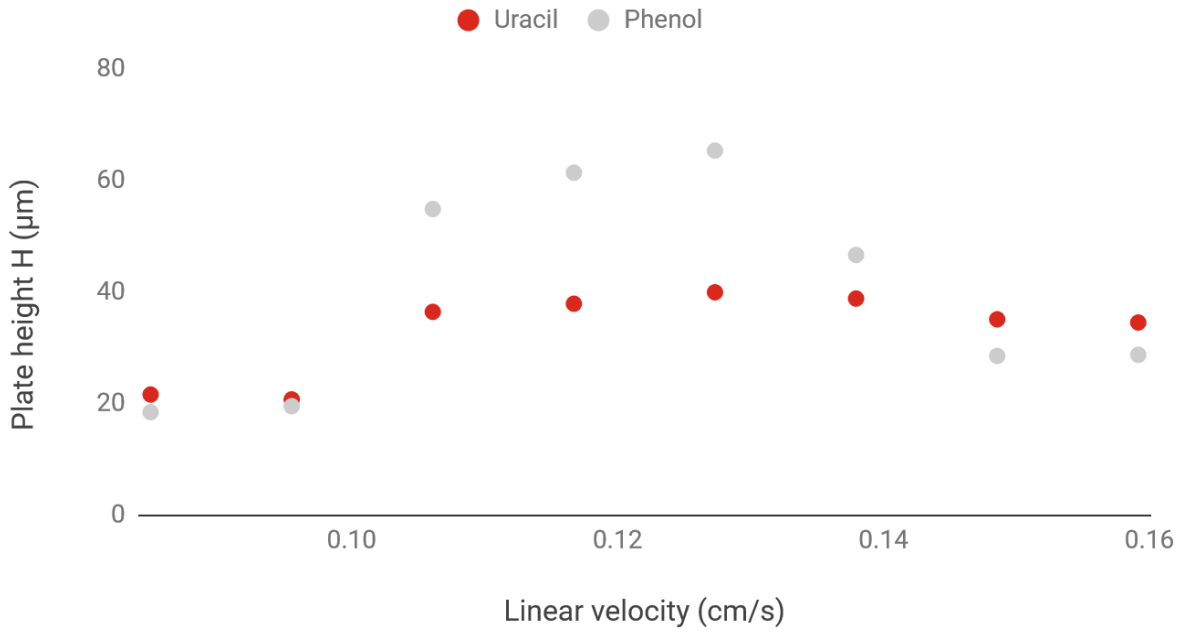

Figure 33 Van Deemter plot for UiO-66-column (100 µm ID x 5.0 cm) for uracil and phenol (0.25 mg/mL each). The mobile phase was ACN/0.1% formic acid (13.5/86.5, v/v). The injection volume was 50 nL and UV detection was performed at 270 nm on LC setup I. Points are the average from n=3 injections for all flow rates.

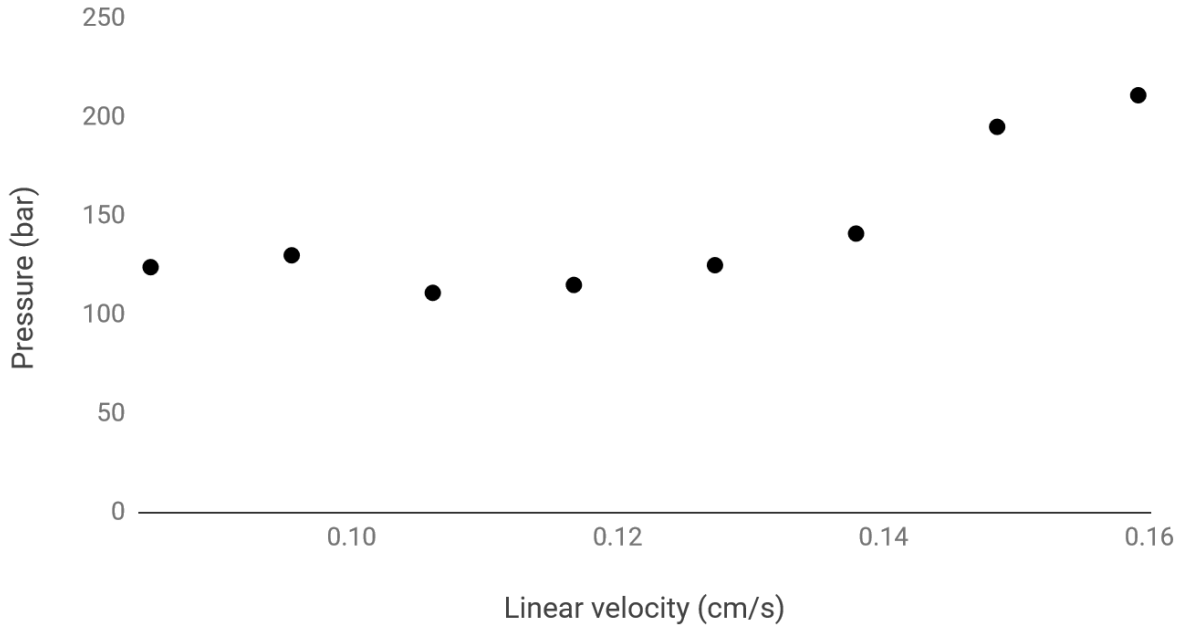

Figure 34 Average backpressure observed at linear velocities corresponding to flow rates 0.40–0.75 µL/min at 0.05 µL/min increments. Chromatographic conditions as described in **Figure 33**.

Upon inspection of the chromatograms, it became evident that more unexpected features were present. Phenol was observed to elute closer to uracil for each injection, as can be seen in **Figure 35**. Uracil also shows slightly shorter retention time for each consecutive injection.

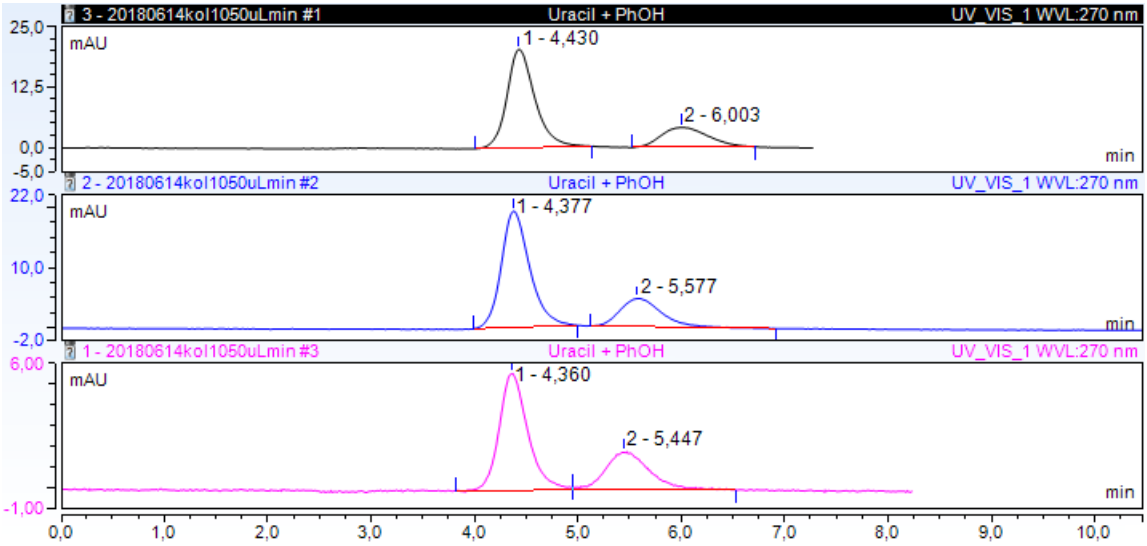

Figure 35 Chromatograms demonstrating the gradual decrease in retention time for uracil (1) and phenol (2) for three consecutive injection replicates (top–bottom) for the same flow rate. Flow rate was 0.50 µL/min, other chromatographic conditions were as described in **Figure 33**.

The observations described in the previous paragraphs were difficult to find possible explanations for until the pump leak was discovered. When the leak was discovered, LC setup II was used to repeat the efficiency investigation. Because the backpressure was observed to increase with increasing flow rates, and no gradual decrease in retention time for neither phenol nor uracil was observed, these observations from the first investigation were attributed to the pump leak.

An overview of the retention times and peak widths found for uracil and phenol during the early efficiency investigations are found in **Table 12**. The corresponding flow rates to the different linear velocities are found in **Table 10**.

In summary, the early investigations of column efficiency yielded unreliable data due to a leak in the pump. Unexpected outcomes were observed, but these were in all likelihood caused by the leak. The investigation was repeated on a different pump.

Supplementary information to later investigation

In **Table 10**, the corresponding linear velocities for the different flow rates used are presented. In **Table 13**, the average values and standard deviations from the column efficiency investigation described in the main text can be found.

The hypothesis tests conducted that lead to the data collected at timepoint 3 being discarded is presented in **Table 11**. The tests were two-tailed, and a 0.05 level of confidence was used.

Chromatograms of uracil and phenol at 0.55 µL/min and 0.45 µL/min are shown in **Figure 36** and **Figure 37**, respectively. Note that there is no baseline separation between the two solutes in the chromatogram in **Figure 37**, which was recorded at timepoint 3 (**Table 7**).

Table 10 The corresponding linear velocities for the different flow rates investigated.

Flow rate (µL/min)	Linear velociy (cm/s)
0.40	0.08
0.45	0.10
0.50	0.11
0.55	0.12
0.60	0.13
0.65	0.14
0.70	0.15
0.75	0.16

Table 11 Hypothesis testing comparing retention times for uracil and phenol collected at 0.40 µL/min and 0.45 µL/min at timepoints 2 and 3.

	0.40 µL/min				**0.45 µL/min**			
	Uracil		**Phenol**		**Uracil**		**Phenol**	
	Timepoint 2	**Timepoint 3**	**Timepoint 2**	**Timepoint 3**	**Timepoint 2**	**Timepoint 3**	**Timepoint 2**	**Timepoint 3**
$\bar{x}$	5.73	5.27	10.45	7.20	5.022	4.667	9.04	6.24
s	0.01	0.03	0.06	0.06	0.007	0.004	0.02	0.04
n	3	3	3	3	3	3	3	3
	P-value	**H0 rejected?**	**P-value**	**H0 rejected?**	**P-value**	**H0 rejected?**	**P-value**	**H0 rejected?**
F-test	0.35	No	0.98	No	0.42	No	0.51	No
t-test	0.0000218	Yes	0.0000003	Yes	0.0000001	Yes	0.00000003	Yes

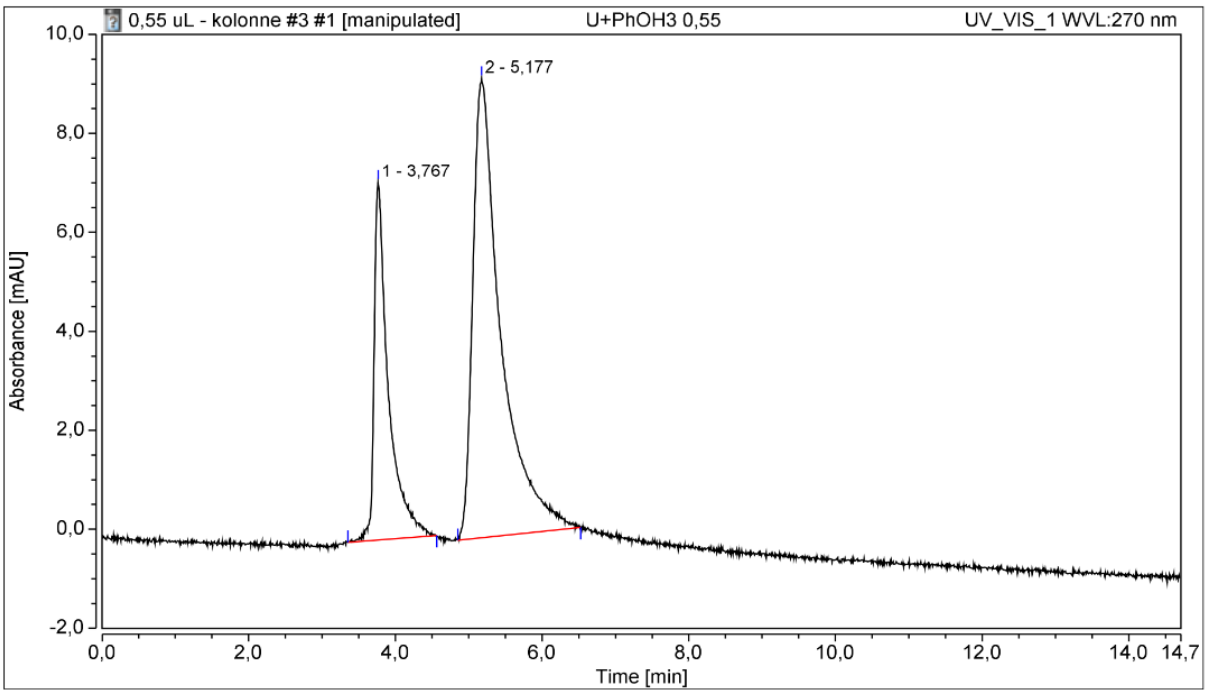

Figure 36 Chromatogram of uracil (1) and phenol (2) at 0.55 µL/min flow rate. The chromatogram was recorded at timepoint 1 as described in **Table 7**. The mobile phase was ACN/0.1 % formic acid (13.5/86.5, v/v). The injection volume was 50 nL and UV detection was performed at 270 nm. LC setup II was used with a 52 mm long 100 µm ID UiO-66-column.

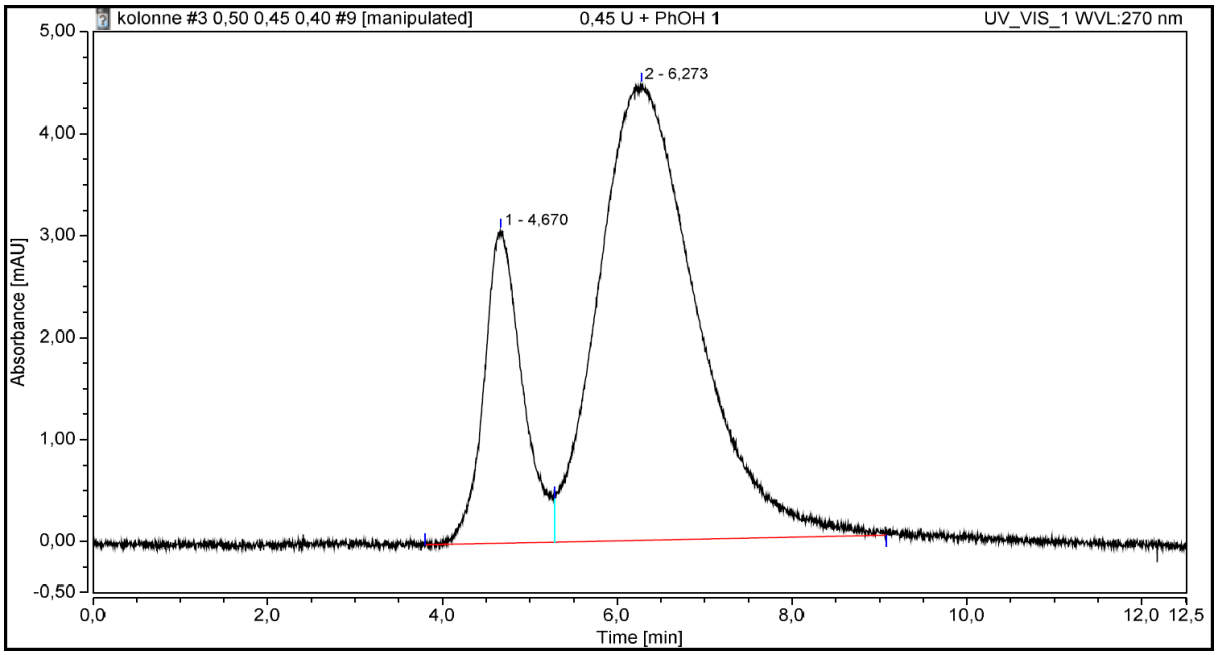

Figure 37 Chromatogram of uracil (1) and phenol (2) at 0.45 µL/min flow rate. The chromatogram was recorded at timepoint 3 as described in **Table 7**. Chromatographic conditions were as described in **Figure 36**.

Table 12 Overview of average values and standard deviations from the early efficiency investigation. Chromatographic conditions were as described in **Figure 33**. Corresponding flow rates to linear velocities are found in **Table 10**. The column header symbols denote: P – backpressure; n – number of replicates; t_R – retention time; N – plate number; H – plate height; s – standard deviation; $s_{\%}$ - relative standard deviation.

Linear velociy (cm/s)	P (bar)	n	t_R (min)		w_{50} (min)		N		H (µm)		$s\ t_R$ (min)		$s\ w_{50}$(min)		$s\ N$		$s\ H$ (µm)	
			Uracil	Phenol	Uracil	Phenol	Uracil	Phenol	Uracil	Phenol	Uracil	Phenol	Uracil	Phenol	Uracil	Phenol	Uracil	Phenol
0.08	124	5	5.7	7.7	0.28	0.35	2315	2712	22	18	0.1	0.9	0.01	0.04	176	188	2	1
0.10	130	5	5.0	7	0.24	0.33	2412	2563	21	20	0.2	1	0.01	0.06	303	152	3	1
0.11	111	5	4.39	5.6	0.279	0.44	1373	911	36	55	0.03	0.2	0.004	0.04	54	89	1	6
0.12	115	3	4.00	5.14	0.26	0.42	1320	815	38	61	0.04	0.09	0.01	0.02	104	100	3	8
0.13	125	5	3.7	5.0	0.246	0.43	1252	765	40	65	0.1	0.7	0.004	0.07	87	59	3	5
0.14	141	5	3.5	4.6	0.23	0.33	1288	1072	39	47	0.1	0.4	0.01	0.07	217	467	7	17
0.15	195	7	3.3	4.2	0.206	0.236	1425	1753	35	29	0.1	0.1	0.005	0.007	125	125	3	2
0.16	211	5	3.54	4.46	0.219	0.251	1449	1741	35	28.7	0.03	0.04	0.004	0.005	53	54	1	0.9

Table 13 Overview of average values and standard deviations resulting from the column efficiency investigation described in the main text. A UiO-66-column was used (100 µm ID x 5.1 cm) and the injection solution contained phenol and uracil at 0.25 mg/mL concentration. The mobile phase was ACN/0.1% formic acid (13.5/86.5, v/v). The injection volume was 50 nL and UV detection was performed at 270 nm on LC setup II. Symbol explanation is as in **Table 12**.

Linear velocity (cm/s)	P (bar)	n	t_R (min)		w_{50} (min)		N		H (µm)		$s\ t_R$ (min)		$s\ w_{50}$(min)		$s\ N$		$s\ H$ (µm)	
			Uracil	Phenol	Uracil	Phenol	Uracil	Phenol	Uracil	Phenol	Uracil	Phenol	Uracil	Phenol	Uracil	Phenol	Uracil	Phenol
0.08	51	3	5.73	10.45	0.42	1.64	1025	225	51	231	0.01	0.06	0.02	0.02	91	7	5	7
0.10	50	3	5.022	9.04	0.374	1.45	1001	216	52	241	0.007	0.02	0.004	0.04	20	11	1	13
0.12	70	3	3.764	5.180	0.167	0.351	2804	1207	19	43	0.002	0.009	0.003	0.002	103	16	0.7	0.6
0.13	85	3	3.431	4.71	0.18	0.33	1954	1116	27	47	0.003	0.02	0.04	0.03	798	173	13	8
0.14	97	3	3.15	4.30	0.20	0.34	1394	865	37	60	0.01	0.01	0.04	0.04	698	241	14	14
0.15	107	3	2.919	3.99	0.19	0.35	1272	729	41	71	0.009	0.02	0.04	0.04	625	195	15	17

6.2.2 Investigation of retention of compounds

In this section, a brief description of an early investigation of the retention of adenosine phosphates is given, followed by supplementary information on the investigations of the retention of compounds presented in the main text.

Early investigations of retention of compounds

The results from this part of the thesis are not included in the main texts as the frit of the column came loose during the last parts of the investigation. This caused the final column length to be unknown. As the data set was incomplete and column length was unknown, it was decided that the experiments would have to be repeated with a new column. The retention times found can be viewed in **Table 14**.

The UV detector showed no change in operation after the frit and packed material was flushed through the detector.

Table 14 Retention times found during the early investigation of retention times of solutes. The column header symbols denote: t_R – retention time; s – standard deviation; $s_{\%}$ - relative standard deviation. Chromatography was performed on a 100 µm ID x 52 mm UiO-66-column in LC system II at a 0.55 µL/min flow rate. Mobile phase reservoir A contained 0.1% FA, mobile phase reservoir B contained 90%/0.1% ACN/FA v/v. Injection volume was 50 nL, UV detection was performed at 270 nm.

Solute	% B	% ACN	n	t_R (min)	t_R s	t_R $s_{\%}$
ADP	5.0	4.5%	3	2.2	0.4	19%
	10.0	9.0%	3	2.24	0.01	0.6%
	15.0	13.5%	3	2.41	0.07	3%
AMP	5.0	4.5%	3	2.30	0.02	1%
	10.0	9.0%	3	2.23	0.02	0.8%
	15.0	13.5%	3	2.49	0.08	3%
cAMP	5.0	4.5%	3	2.25	0.02	1%
	10.0	9.0%	3	2.25	0.02	1%
	15.0	13.5%	3	2.0	0.5	27%

Supplementary information to later investigations

An overview of the average values from injections performed on UiO-66 is shown in **Table 15**, and an overview of the average values from injections performed on UiO-66-NH_2 is shown in **Table 16**.

Retention factors were calculated using the retention time of uracil at the same MP composition as t_M. As discussed previously, it was strongly suspected that uracil was not a good t_M marker. It was still used, as the solvent signal was not pronounced enough for t_M to be consistently determined from it.

Table 17 shows a comparison between the retention time per column length, in an effort to compare the retention times of the different solutes on the two different SP materials. In this comparison, the time it would take for the MP to travel through the extra-column volume is subtracted. A comparison shows most of the compounds had longer retention on UiO-66 compared to UiO-66-NH_2.

Table 15 Overview of average values from injections performed on UiO-66. The column header symbols denote: n – number of replicates; P – backpressure; t_R – retention time; k – retention factor; N – plate number; H – plate height; s – standard deviation; $s_{\%}$ - relative standard deviation. N/A denotes not applicable. Chromatographic conditions were as described in **Figure 19**.
* Only 2 of 3 replicates yielded chromatograms where efficiency could be determined.
** Only 1 of 2 replicates yielded chromatograms where efficiency could be determined.
***None of the replicates yielded chromatograms where efficiency could be determined.

Solute	n	% B	P (bar)	t_R (min)	$t_R\ s$ (min)	$t_R\ s_{\%}$	k	N	H (µm)	$N\ s$	$N\ s_{\%}$
ADP	2**	0	84	4.1	0.6	14.93%	-0.5	55	942	N/A	N/A
	2***	15	81	3.48	0.2	4.82%	-0.1	N/A	N/A	N/A	N/A
	3*	30	83	3.9	0.3	7.82%	0.0	6774	8	N/A	N/A
AMP	2***	0	84	4.32	0.01	0.23%	-0.43	N/A	N/A	N/A	N/A
	2	15	81	3.49	0.02	0.47%	-0.09	153	340	24	16%
	3	30	83	3.550	0.009	0.25%	-0.066	501	104	12	2%
cAMP	2***	0	84	3.8	0.1	3.72%	-0.5	N/A	N/A	N/A	N/A
	2**	15	81	3.69	0.05	1.29%	-0.03	141	370	N/A	N/A
	3*	30	83	4.07	0.03	0.76%	0.07	1524	34	N/A	N/A
Dopamine	3	0	29	3.31	0.03	0.91%	-0.56	305	170	35	11%
	3	15	32	3.43	0.02	0.48%	-0.10	364	143	16	4%
	3	30	28	3.53	0.03	0.79%	-0.07	392	133	27	7%
GABA	3***	0	29	7.9	0.4	5.40%	0.0	N/A	N/A	N/A	N/A
	3	15	32	3.81	0.08	2.04%	0.00	893	58	90	10%
	2	30	29	3.754	0.005	0.13%	-0.012	408	128	3	0.7%
Serotonin	3	0	29	3.36	0.01	0.29%	-0.56	331	157	17	5%
	3	15	32	3.402	0.004	0.12%	-0.109	433	120	18	4%
	3	30	28	3.479	0.003	0.10%	-0.084	451	115	16	3%
Uracil	3	0	29	7.6	0.06	0.84%	N/A	63	832	1	2%
	4	15	61	3.82	0.1	2.82%	N/A	1179	44	1259	107%
	3	30	28	3.8	0.009	0.23%	N/A	478	109	2	0.4%

Table 16 Overview of average values from injections performed on UiO-66-NH_2. Symbol explanation is as in **Table 15**. Chromatographic conditions were as described in **Figure 22**.
* Only 1 of 3 replicates yielded chromatograms where efficiency could be determined.
** Only 2 of 3 replicates yielded chromatograms where efficiency could be determined.

Solute	n	% B	P (bar)	t_R (min)	$t_R\ s$ (min)	$t_R\ s_{\%}$	k	N	H (µm)	$N\ s$	$N\ s_{\%}$
ADP	3	0	50.3	4.17	0.02	0.004	-1.39	218	326	9	4%
	3	15	85.0	4.05	0.04	0.01	-0.69	426	167	61	14%
	3	30	50.0	4.20	0.04	0.01	-0.45	66	1068	218	328%
AMP	3	0	51.3	4.18	0.02	0.01	-1.38	210	338	58	28%
	3	15	85.0	4.08	0.03	0.01	-0.68	331	214	66	20%
	3	30	50.0	4.17	0.01	0.002	-0.46	447	159	5	1%
cAMP	3*	0	50.3	4.1	0.1	0.03	-1.4	1455	49	N/A	N/A
	3	15	85.0	6.04	0.05	0.01	-0.05	333	213	31	9%
	3**	30	50.0	4.10	0.02	0.004	-0.49	336	211	N/A	N/A
Dopamine	3	0	50.7	4.21	0.02	0.01	-1.38	251	283	80	32%
	3	15	93.0	4.11	0.04	0.01	-0.67	319	222	25	8%
	3	30	50.0	4.18	0.02	0.004	-0.46	521	136	15	3%
GABA	2	0	51.0	4.69	0.02	0.005	-1.31	851	83	150	18%
	3	15	93.0	6.14	0.07	0.01	-0.02	565	126	123	22%
	3	30	48.3	5.3	0.2	0.03	-0.1	565	126	114	20%
Serotonin	3	0	52.0	4.16	0.02	0.004	-1.39	216	328	6	3%
	3	15	93.0	4.11	0.03	0.01	-0.67	363	196	35	10%
	3	30	49.7	4.17	0.05	0.01	-0.46	574	124	52	9%
Uracil	6	0	51.2	13.6	0.2	0.01	0	118	600	78	66%
	5	15	91.4	6.19	0.03	0.01	0	356	199	138	39%
	3	30	47.3	5.41	0.02	0.004	0	302	235	8	3%

Table 17 Comparison of retention time per column length for one UiO-66-column and one UiO-66-NH_2-column. Chromatographic conditions were as described in **Figure 19** and **Figure 22**, respectively.

Solute	% B	UiO-66 t_R/L (min/mm)	UiO-66-NH_2 t_R/L (min/mm)
ADP	0	5	2.27
	15	3.9	2.09
	30	4.7	2.30
AMP	0	5.52	2.28
	15	3.93	2.14
	30	4.04	2.26
cAMP	0	4.5	2.2
	15	4.31	4.90
	30	5.05	2.16
Dopamine	0	3.59	2.33
	15	3.81	2.18
	30	4.01	2.27
GABA	0	12.3	3.00
	15	4.5	5.0
	30	4.43	3.8
Serotonin	0	3.67	2.25
	15	3.76	2.18
	30	3.91	2.27
Uracil	0	11.8	15.5
	15	4.6	5.11
	30	4.52	4.02

Chromatograms

Below, a selection of chromatograms is shown to give an impression of the visual appearance of the chromatography of the different solutes investigated using UiO-66 and UiO-66-NH_2 as SPs. As can be seen in several of the following chromatograms, the solutes take quite a while to elute, with some peaks spanning over several minutes.

Figure 38–**Figure 42** show chromatograms from when UiO-66 was used as the SP, while **Figure 43** l–**Figure 46** show chromatograms from when UiO-66-NH_2 was used as the SP. The intervals of figures are separated by subheaders to make the distinction easier for the reader.

UiO-66

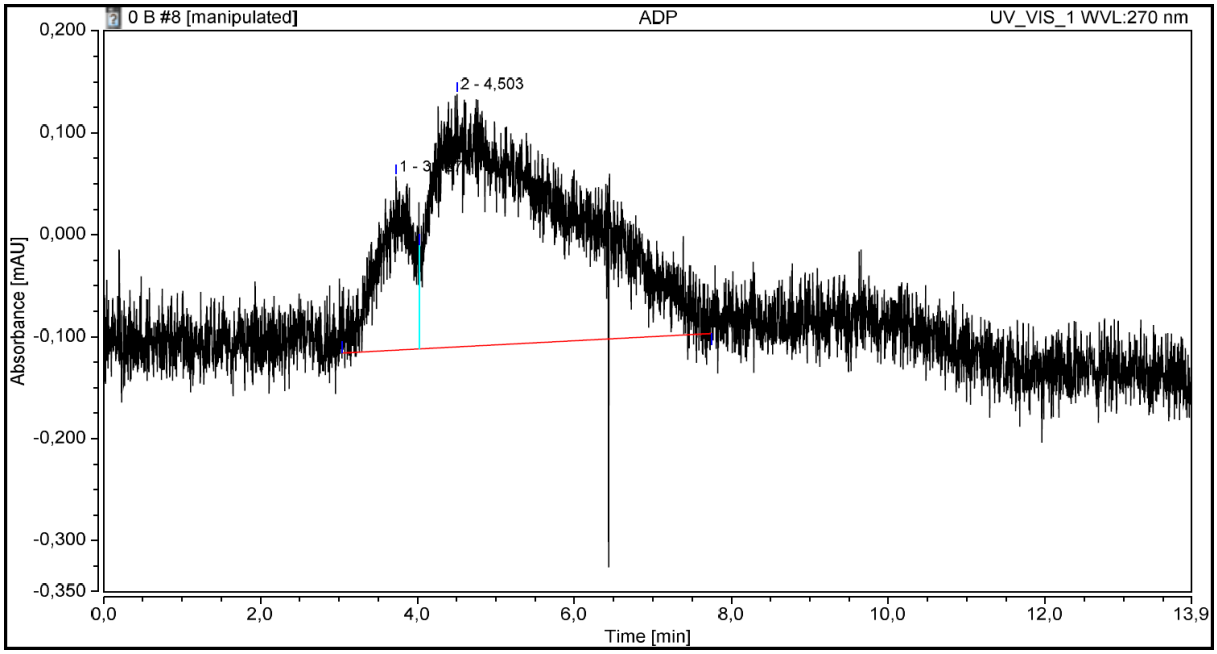

Figure 38 Chromatogram of ADP at 0% B using UiO-66 as the SP. Chromatographic conditions as described in **Figure 19**.

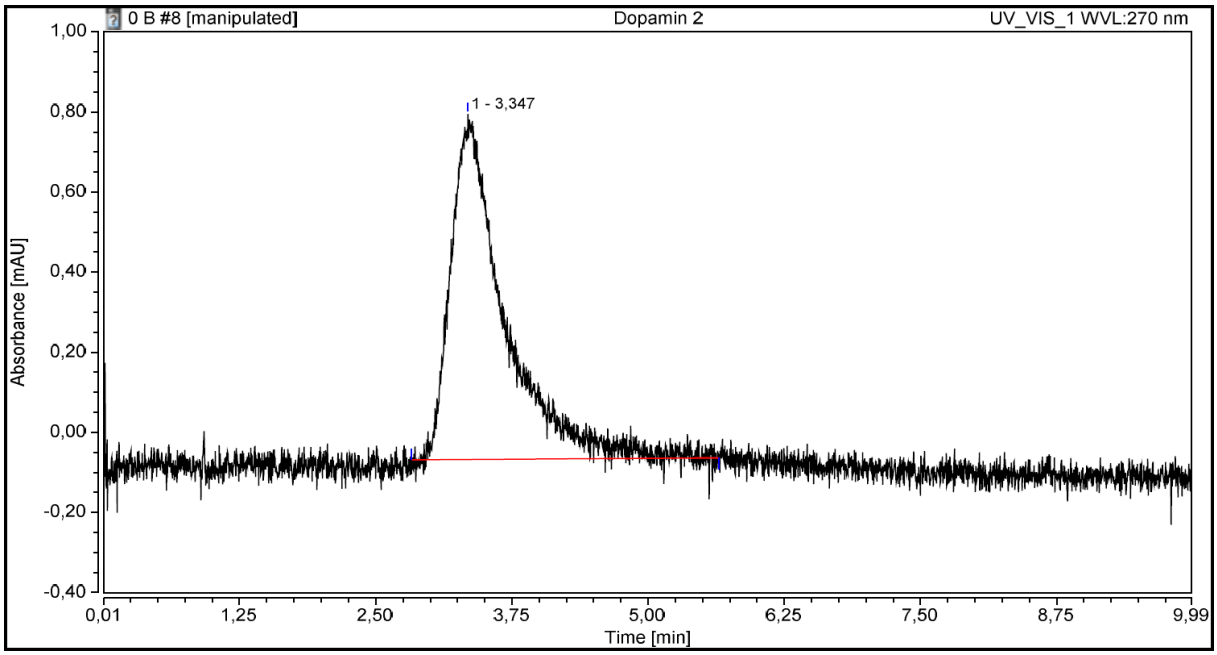

Figure 39 Chromatogram of dopamine at 0% B using UiO-66 as the SP. Chromatographic conditions as described in **Figure 19**.

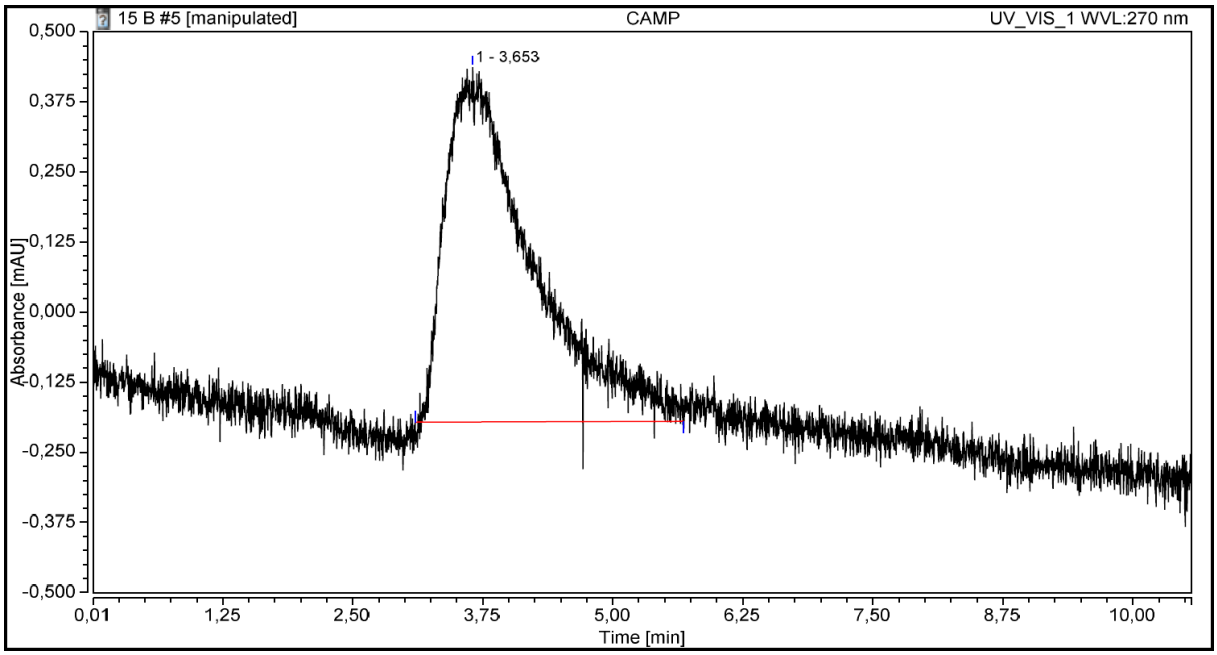

Figure 40 Chromatogram of cAMP at 15% B using UiO-66 as the SP. Chromatographic conditions as described in **Figure 19**.

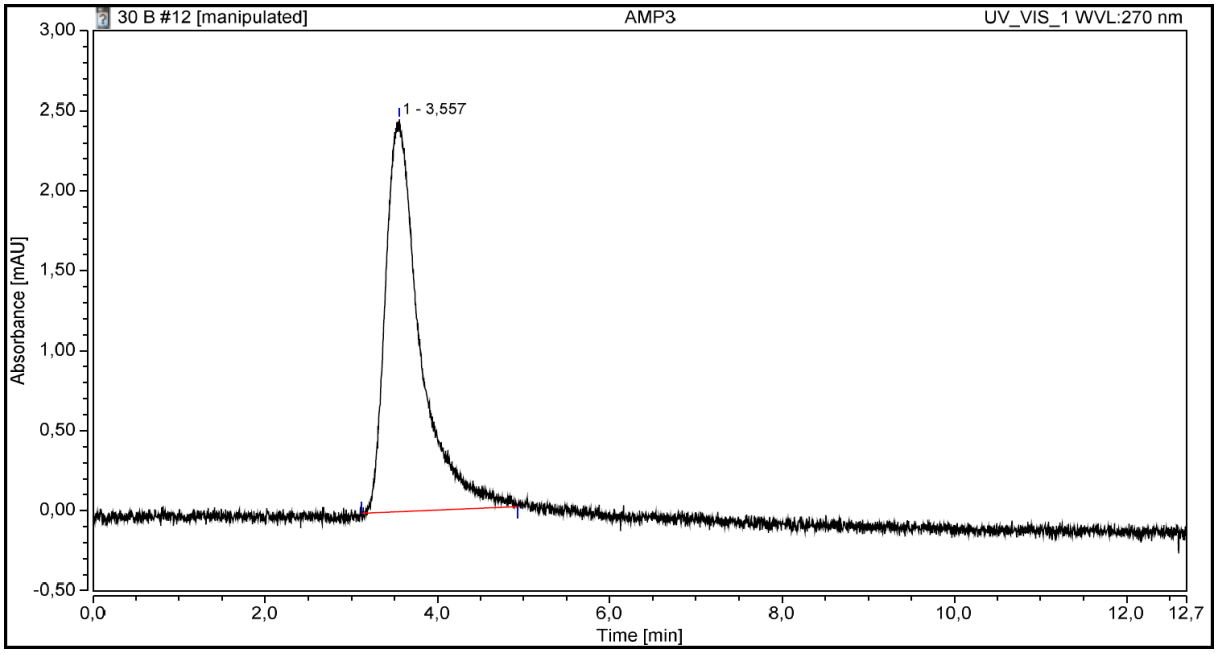

Figure 41 Chromatogram of AMP at 30% B using UiO-66 as the SP. Chromatographic conditions as described in **Figure 19**.

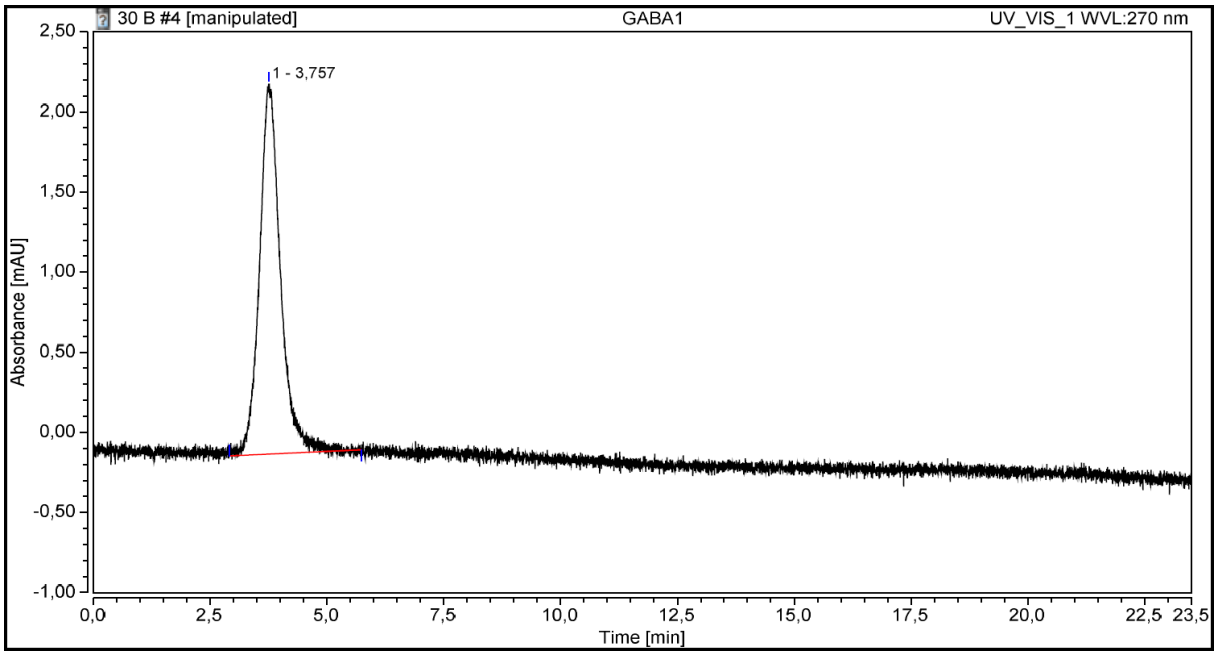

Figure 42 Chromatogram of GABA at 30% B using UiO-66 as the SP. Chromatographic conditions as described in **Figure 19**.

UiO-66-NH$_2$

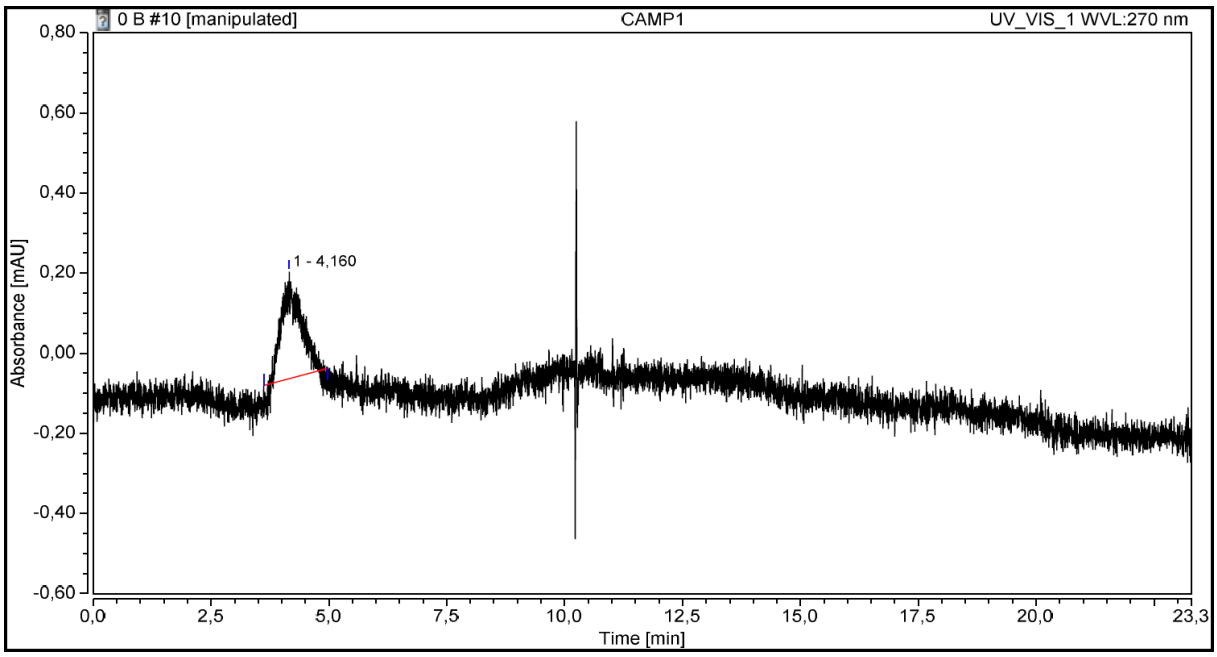

Figure 43 Chromatogram of cAMP at 0% B using UiO-66-NH$_2$ as the SP. Chromatographic conditions as described in **Figure 22**.

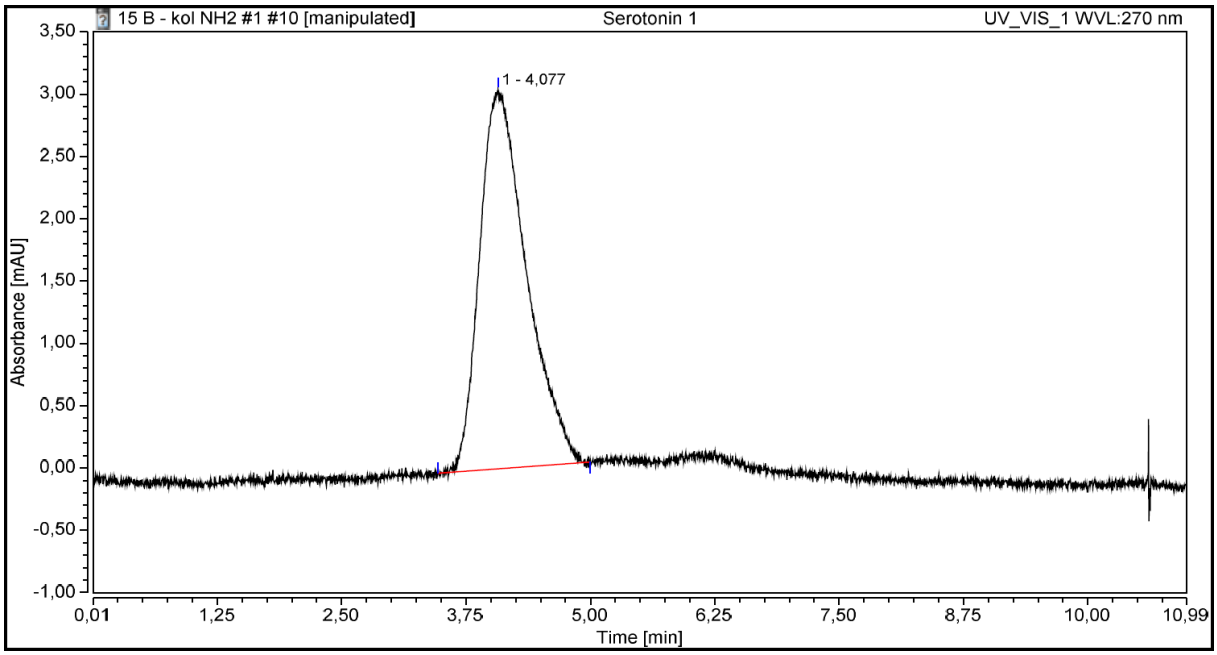

Figure 44 Chromatogram of serotonin at 15% B using UiO-66-NH_2 as the SP. Chromatographic conditions as described in **Figure 22**.

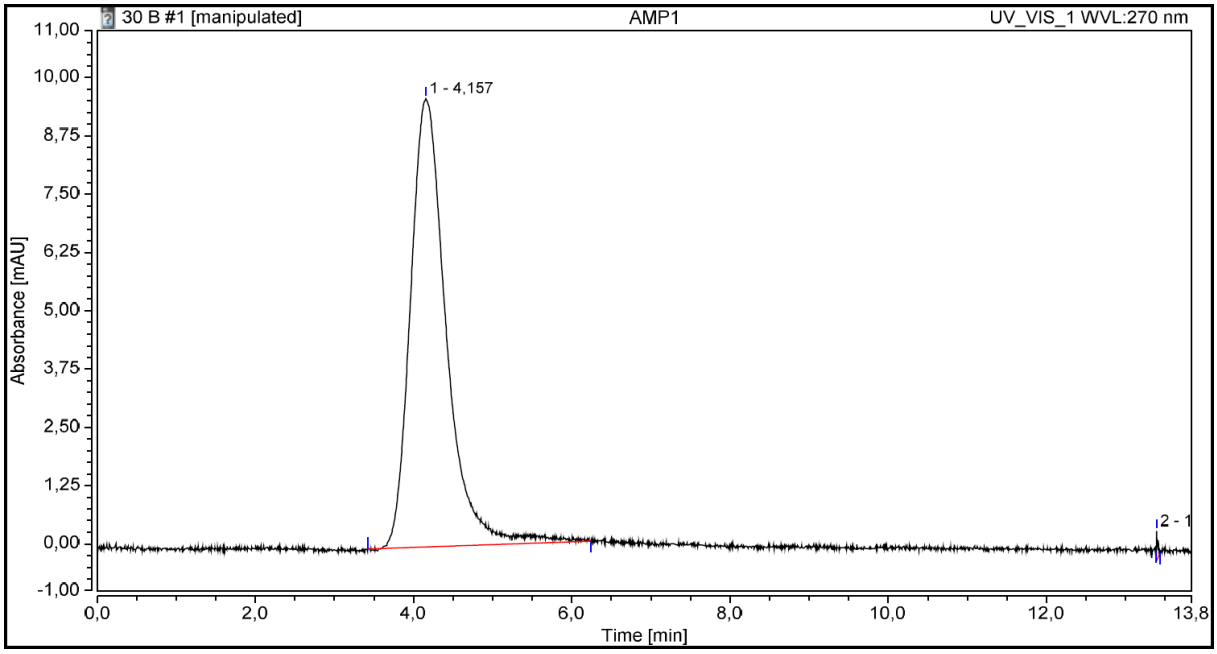

Figure 45 Chromatogram of AMP at 30% B using UiO-66-NH_2 as the SP. Chromatographic conditions as described in **Figure 22**.

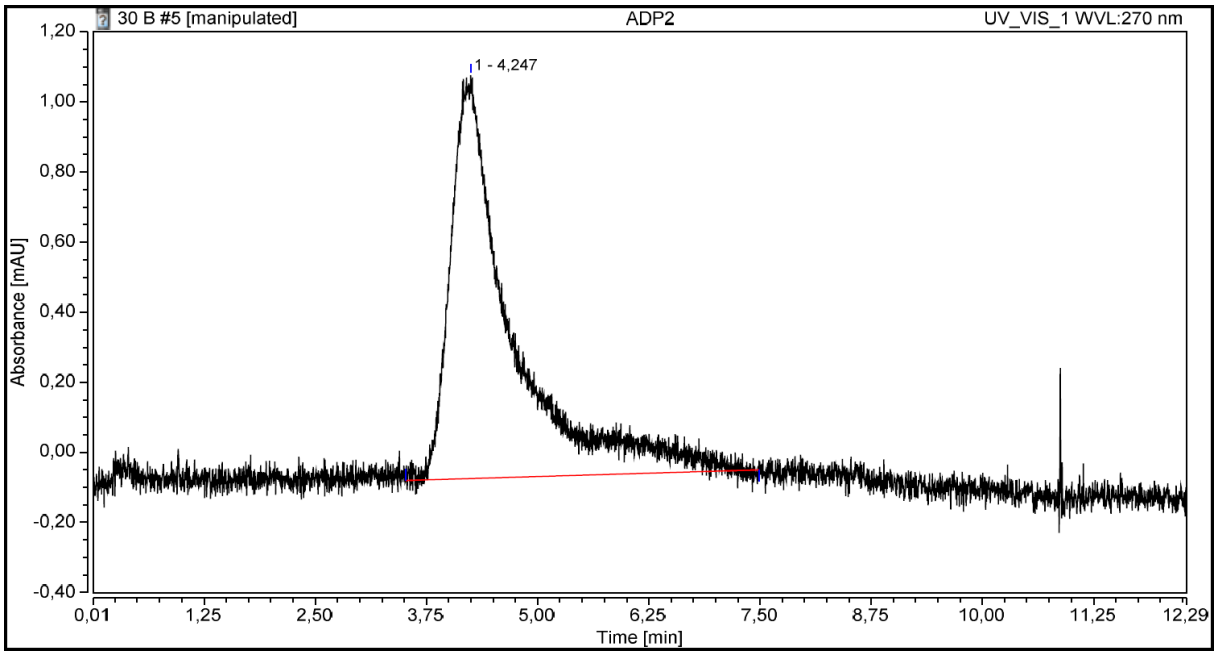

Figure 46 Chromatogram of ADP at 30% B using UiO-66-NH_2 as the SP. Chromatographic conditions as described in **Figure 22**.

Calculations

Due to the close retention times of several compounds, the compounds with very similar retention times were checked for statistically significant difference between retention times by the use of one-way ANOVA. A significance level of 0.05 was chosen.

For UiO-66, the different solutes compared at the same MP compositions are presented in **Table 18**. The calculations can be found in **Table 20**, **Table 21**, **Table 22** and **Table 23**. Because dopamine and serotonin showed little difference in retention time regardless of MP composition, they were compared as well, as can be seen in **Table 24**.

For UiO-66-NH_2, the different solutes compared are presented in **Table 19**. The calculations are found in **Table 25** and **Table 26**.

The reader is advised to note that the viable injection replicates for particularly the adenosine phosphates are few, meaning the degrees of freedom are small numbers. The critical F-values for the F-distributions with few degrees of freedom are large. It is unknown whether the lack of significant difference was due to the variation from the system. However, the statistical tests would be more reliable if more injection replicates for each compound were made.

Table 18 The data sets from the investigation of compound retention in UiO-66 evaluated by ANOVA.

% B	Solutes compared	Calculations	Statistically significant difference found?
0	Dopamine, serotonin	**Table 20**	No
	AMP, ADP, cAMP	**Table 21**	No
	Uracil, GABA	**Table 22**	Yes
15	Dopamine, serotonin	**Table 20**	No
	AMP, ADP, cAMP	**Table 21**	No
	Dopamine, Serotonin, AMP, ADP	**Table 23**	No
	Uracil, GABA	**Table 22**	No
30	Dopamine, serotonin	**Table 20**	Yes
	AMP, ADP, cAMP	**Table 21**	No
	Dopamine, Serotonin, AMP	**Table 23**	Yes
	Uracil, GABA	**Table 22**	Yes

Table 19 The three data sets from the investigation of compound retention on UiO-66-NH_2 evaluated by ANOVA.

% B	Solutes compared	Calculations	Statistically significant difference found?
0	ADP, AMP, cAMP, dopamine, serotonin	**Table 25**	No
15	ADP, AMP, dopamine, serotonin	**Table 25**	No
	cAMP, GABA, uracil	**Table 26**	Yes
30	ADP, AMP, cAMP, dopamine, serotonin	**Table 25**	No

Table 20 ANOVA of the retention times of dopamine and serotonin on UiO-66 for all MP compositions.

0% B				**15 % B**				**30 % B**			
Solute	$\bar{x}_{t_R}$ **(min)**	n		**Solute**	$\bar{x}_{t_R}$ **(min)**	n		**Solute**	$\bar{x}_{t_R}$ **(min)**	n	
Dopamine	3.315	3		Dopamine	3.428	3		Dopamine	3.534	3	
Serotonin	3.356	3		Serotonin	3.402	3		Serotonin	3.479	3	
Grand mean	3.335			**Grand mean**	3.415			**Grand mean**	3.507		
SSB	0.00252	k_B	1	**SSB**	0.00096	k_B	1	**SSW**	0.00230	k_B	1
SSW	0.00203	k_W	4	**SSW**	0.00059	k_W	4	**SSB**	0.00027	k_W	4
$F(k_B, k_W)$	4.98			$F(k_B, k_W)$	6.58			$F(k_B, k_W)$	11.52		
$F(k_B, k_W)_{crit}$	7.71			$F(k_B, k_W)_{crit}$	7.71			$F(k_B, k_W)_{crit}$	7.71		
H₀ rejected?	No			**H₀ rejected?**	No			**H₀ rejected?**	Yes		

Table 21 ANOVA of the retention times of AMP, ADP and cAMP on UiO-66 for all MP compositions.

0% B				**15% B**				**30% B**			
Solute	$\bar{x}_{t_R}$ **(min)**	n		**Solute**	$\bar{x}_{t_R}$ **(min)**	n		**Solute**	$\bar{x}_{t_R}$ **(min)**	n	
AMP	4.320	2		AMP	3.500	1		AMP	3.5485	2	
ADP	4.073	2		ADP	3.479	2		ADP	4.075	2	
cAMP	3.800	2		cAMP	3.687	2		cAMP	4.067	2	
Grand mean	4.064			**Grand mean**	3.583			**Grand mean**	4.071		
SSB	0.27063	k_B	2	**SSB**	0.05007	k_B	2	**SSB**	0.54608	k_B	2
SSW	0.38990	k_W	3	**SSW**	0.03033	k_W	2	**SSW**	0.28080	k_W	3
$F(k_B, k_W)$	1.04			$F(k_B, k_W)$	1.65			$F(k_B, k_W)$	2.92		
$F(k_B, k_W)_{crit}$	9.55			$F(k_B, k_W)_{crit}$	19.00			$F(k_B, k_W)_{crit}$	9.55		
H₀ rejected?	No			**H₀ rejected?**	No			**H₀ rejected?**	No		

Table 22 ANOVA of the retention times of uracil and GABA on UiO-66 for all MP compositions.

0% B				**15% B**				**30% B**			
Solute	$\bar{x}_{t_R}$ **(min)**	n		**Solute**	$\bar{x}_{t_R}$ **(min)**	n		**Solute**	$\bar{x}_{t_R}$ **(min)**	n	
Uracil	7.602	3		Uracil	3.764	4		Uracil	3.800	3	
GABA	7.853	2		GABA	3.813	3		GABA	3.750	1	
Grand mean	7.702			**Grand mean**	3.789			**Grand mean**	3.788		
SSB	0.07560	k_B	1	**SSB**	0.00420	k_B	1	**SSB**	0.001875	k_B	1
SSW	0.18822	k_W	3	**SSW**	0.05859	k_W	5	**SSW**	0.000158	k_W	2
$F(k_B, k_W)$	1.20			$F(k_B, k_W)$	0.36			$F(k_B, k_W)$	23.73		
$F(k_B, k_W)_{crit}$	10.13			$F(k_B, k_W)_{crit}$	6.61			$F(k_B, k_W)_{crit}$	18.51		
H₀ rejected?	No			**H₀ rejected?**	No			**H₀ rejected?**	Yes		

Table 23 ANOVA of the retention times on UiO-66 of dopamine, serotonin, AMP and ADP at 15% B, and dopamine, serotonin and AMP at 30% B.

15% B				**30% B**			
Solute	$\bar{x}_{t_R}$ **(min)**	n		**Solute**	$\bar{x}_{t_R}$ **(min)**	n	
Dopamine	3.428	3		Dopamine	3.534	3	
Serotonin	3.402	3		Serotonin	3.479	3	
AMP	3.500	1		AMP	3.550	3	
ADP	3.479	2					
Grand mean	3.439			**Grand mean**	3.521		
SSB	0.01126	k_B	3	**SSB**	0.00835	k_B	2
SSW	0.02867	k_W	5	**SSW**	0.00175	k_W	6
$F(k_B, k_W)$	0.6544851958			$F(k_B, k_W)$	14.28946367		
$F(k_B, k_W)_{crit}$	5.41			$F(k_B, k_W)_{crit}$	5.14		
H₀ rejected?	No			**H₀ rejected?**	Yes		

Table 24 ANOVA analysis comparing retention times at the different MP compositions on UiO-66 for dopamine and serotonin.

Dopamine				**Serotonin**			
% B	$\bar{x}_{t_R}$ **(min)**	n		**% B**	$\bar{x}_{t_R}$ **(min)**	n	
0	3.315	3		0	3.356	3	
15	3.428	3		15	3.402	3	
30	3.534	3		30	3.479	3	
Grand mean	3.426			**Grand mean**	3.412		
SSB	0.03690	k_B	2	**SSB**	0.03690	k_B	2
SSW	0.00396	k_W	6	**SSW**	0.00396	k_W	6
$F(k_B, k_W)$	27.98			$F(k_B, k_W)$	1.82		
$F(k_B, k_W)_{crit}$	5.14			$F(k_B, k_W)_{crit}$	5.14		
H₀ rejected?	Yes			**H₀ rejected?**	No		

Table 25 ANOVA of the retention times on UiO-66-NH_2 of AMP, ADP, cAMP, dopamine and serotonin at 0% B, AMP, ADP, dopamine and serotonin at 15% B, and AMP, ADP, cAMP, dopamine and serotonin at 30% B.

0% B				**15% B**				**30% B**			
Solute	$\bar{x}_{t_R}$ **(min)**	n		**Solute**	$\bar{x}_{t_R}$ **(min)**	n		**Solute**	$\bar{x}_{t_R}$ **(min)**	n	
AMP	4.182	3		AMP	4.078	3		AMP	4.182	3	
ADP	4.173	3		ADP	4.047	3		ADP	4.173	3	
cAMP	4.100	3		Dopamine	4.109	3		cAMP	4.1	3	
Dopamine	4.212	3		Serotonin	4.107	3		Dopamine	4.212	3	
Serotonin	4.162	3						Serotonin	4.162	3	
Grand mean	4.166			**Grand mean**	4.085			**Grand mean**	4.166		
SSB	0.02049	k_B	4	**SSB**	0.00770	k_B	3	**SSB**	0.02049	k_B	4
SSW	0.02893	k_W	10	**SSW**	0.00993	k_W	8	**SSW**	0.02893	k_W	10
$F(k_B, k_W)$	1.77			$F(k_B, k_W)$	2.07			$F(k_B, k_W)$	1.77		
$F(k_B, k_W)_{crit}$	3.48			$F(k_B, k_W)_{crit}$	4.07			$F(k_B, k_W)_{crit}$	3.48		
H₀ rejected?	No			**H₀ rejected?**	No			**H₀ rejected?**	No		

Table 26 ANOVA of the retention times of cAMP, GABA and uracil on UiO-66-NH_2 with 15% B.

15% B			
Solute	$\bar{x}_{t_R}$ **(min)**	n	
cAMP	6.040	3	
GABA	6.144	3	
Uracil	6.193	5	
Grand mean	6.138		
SSB	**0.044**	k_B	2
SSW	0.02019	k_W	8
$F(k_B, k_W)$	11.97331678		
$F(k_B, k_W)_{crit}$	4.46		
H_0 rejected?	Yes		

6.2.3 Van't Hoff experiments

In the following section, supplementary data to the van't Hoff experiments discussed in the main text is presented.

Tables

Average values for retention time and efficiency for ethylbenzene and toluene in the van't Hoff experiments can be found in **Table 27**.

Table 27 Overview of retention times and efficiencies found during the van't Hoff experiments. Chromatographic conditions were as described in **Figure 28**. The column header symbols denote: n – number of replicates; t_R – retention time; k – retention factor; N – plate number; H – plate height; s – standard deviation; $s_{\%}$ - relative standard deviation. N/A denotes not applicable.
* Only 2 of 3 replicates yielded chromatograms where efficiency could be determined.
** Only 1 of 3 replicates yielded chromatograms where efficiency could be determined.

Solute	**T (°C)**	**n**	t_R **(min)**	$t_R\ s$ **(min)**	$t_R\ s_{\%}$	N	H **(µm)**	$N\ s$	$N\ s_{\%}$	$H\ s$	$H\ s_{\%}$
Ethylbenzene	25	3	11.0	0.1	0.9%	1660	39	304	18%	6	2%
	35	3	7.55	0.05	0.7%	1575	41	676	43%	16	2%
	45	3*	7.02	0.07	1%	5005	13	N/A	N/A	N/A	N/A
	55	3	6.55	0.08	1%	3518	18	2269	64%	8	0.4%
Toluene	25	3	14.1	0.2	1%	2565	25	6570	256%	21	0.3%
	35	3	9.37	0.09	0.9%	2447	27	517	21%	6	1%
	45	3**	8.6	0.2	2%	22228	17	N/A	N/A	N/A	N/A
	55	3	7.88	0.04	0.5%	3957	16	4470	113%	10	0.2%

Chromatograms

One example chromatogram is shown for 25–55°C each (**Figure 47**–**Figure 50**). As can be seen in **Figure 48**, the butylbenzene peak cannot be detected at 35°C. This is thought to be because butylbenzene might have eluted at the same time as the dip from the solvent occurred.

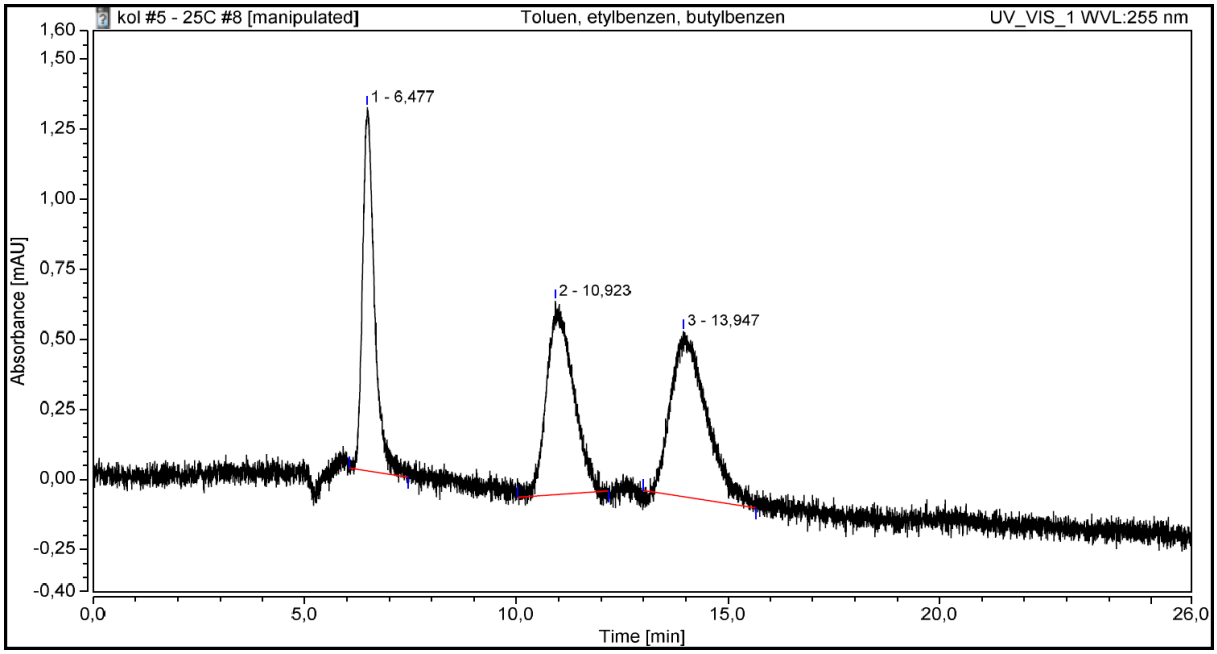

Figure 47 Chromatogram of butylbenzene (1), ethylbenzene (2) and toluene (1) at 25°C. Chromatographic conditions were as described in **Figure 28**.

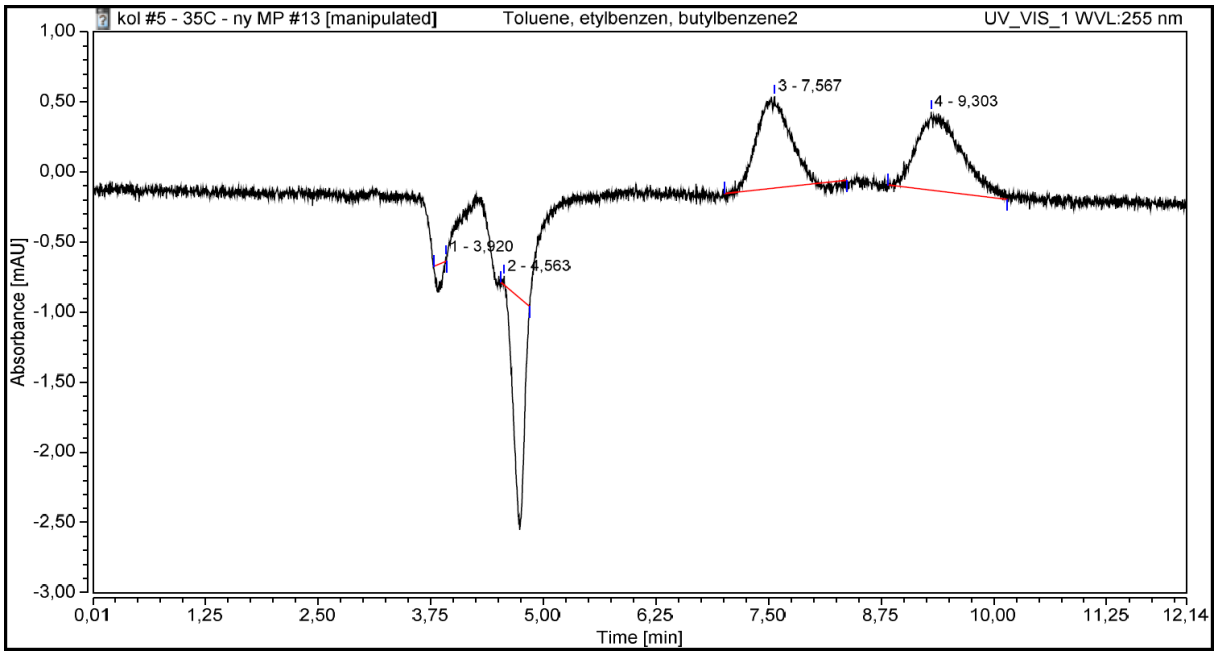

Figure 48 Chromatogram of butylbenzene (no peak detected), ethylbenzene (3) and toluene (4) at 35°C. Chromatographic conditions were as described in **Figure 28**.

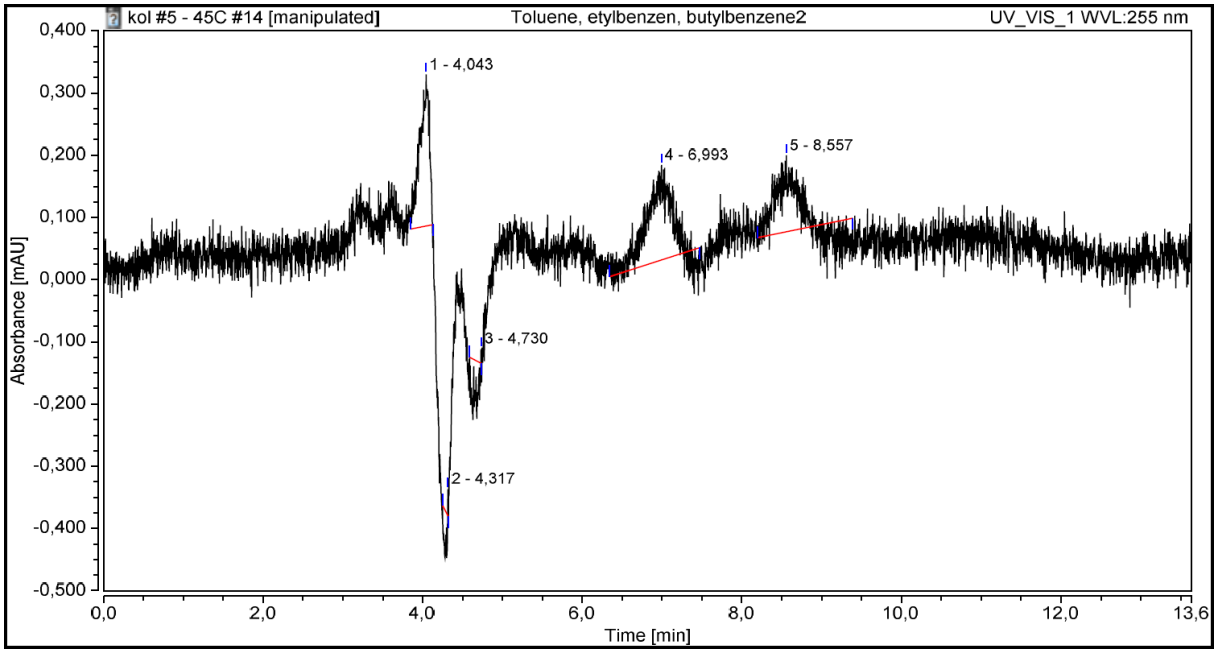

Figure 49 Chromatogram of butylbenzene (1), ethylbenzene (2) and toluene (1) at 45°C. Chromatographic conditions were as described in **Figure 28**.

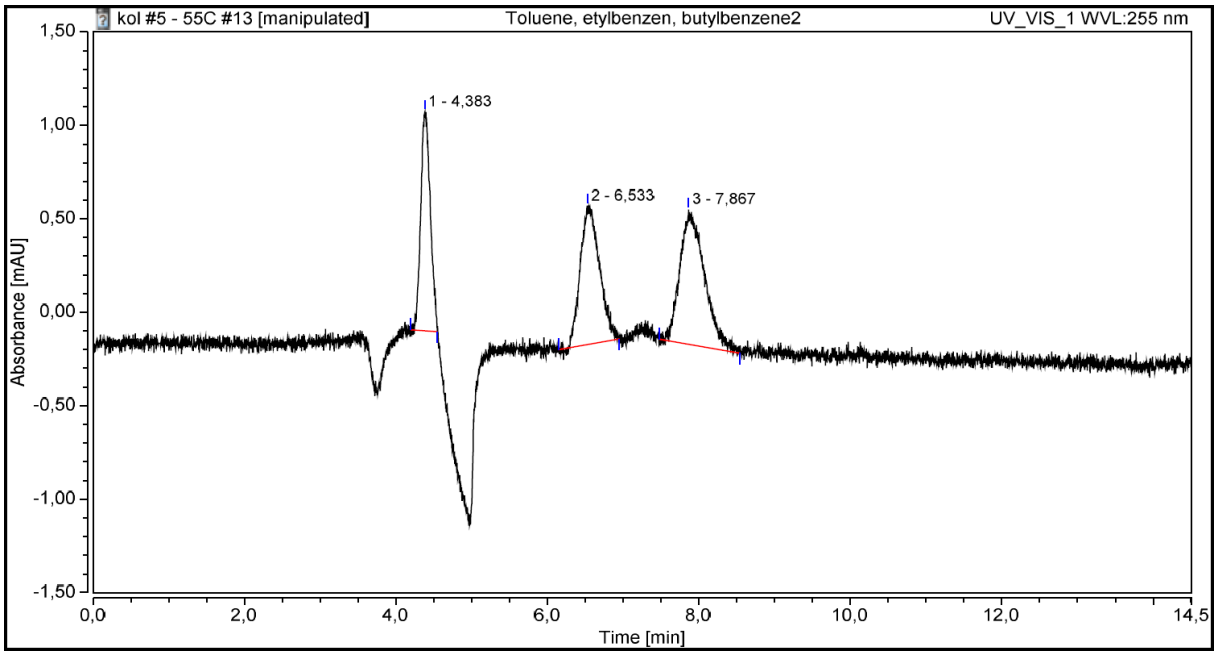

Figure 50 Chromatogram of butylbenzene (1), ethylbenzene (2) and toluene (1) at 55°C. Chromatographic conditions were as described in **Figure 28**.

6.2.4 Pore volume accessibility

In the following section, supplementary data to the pore volume accessibility investigation discussed in the main text can be found. Calculations associated with hypothesis testing is also presented.

Tables

In **Table 28**, an overview of the retention times found during the pore volume accessibility investigation is presented.

Table 28 Overview of retention times found during the pore volume accessibility investigations of UiO-66. Chromatographic conditions were as described in **Figure 30**. The column header symbols denote: n – number of replicates; P – backpressure; t_R – retention time; s – standard deviation; $s_{\%}$ - relative standard deviation.

Solute	n	P (bar)	t_R (min)		t_R s (min)		t_R $s_{\%}$	
			Peak 1	Peak 2	Peak 1	Peak 2	Peak 1	Peak 2
ACN	5	166	2.24		0.06		3%	
T1 water	6	178	2.6		0.8		29%	
Benzene	9	171	2.28	3.49	0.04	0.02	2%	0.6%
Toluene	9	171	2.29	3.59	0.07	0.03	3%	0.8%
Ethylbenzene	9	172	2.31	3.06	0.05	0.01	2%	0.4%
Propylbenzene	6	162	2.39		0.09		4%	
Butylbenzene	3	155	2.308		0.007		0.3%	
Pentylbenzene	3	155	2.27		0.02		0.9%	
Hexylbenzene	3	152	2.261		0.002		0.1%	
Heptylbenzene	3	155	2.25		0.02		1%	
Octylbenzene	3	156	2.23		0.02		0.7%	
Nonylbenzene	3	156	2.28		0.01		0.5%	
Decylbenzene	3	155	2.20		0.07		3%	
Nonadecylbenzene	3	157	2.20		0.02		1%	
Naphthalene	3	159	2.753		0.004		0.1%	
Phenanthrene	3	164	2.35		0.03		1%	
Chrysene	3	165	2.24		0.04		2%	

Chromatograms

Chromatograms for benzene (**Figure 51**), toluene (**Figure 52**) and ethylbenzene (**Figure 53**) are shown to demonstrate the two-peak pattern observed. A chromatogram for propylbenzene (**Figure 54**) is shown to demonstrate that no such pattern was observed for propylbenzene. Two larger 1-alkylbenzenes, nonylbenzene (**Figure 55**) and nonadecylbenzene (**Figure 56**), are shown to illustrate the appearance of the chromatograms of the larger 1-alkylbenzenes. The PAHs naphthalene (**Figure 57**) and chrysene (**Figure 58**) are shown from the aromatics series.

In some of the chromatograms, a small peak is visible in the void space, i.e. the time space between injection and elution time (t_M is at ca. 2.2 min for this system). This small peak is caused by a small fluctuation in the signal due to the injector being turned back from 'inject'- to 'load'-position after the previous injection.

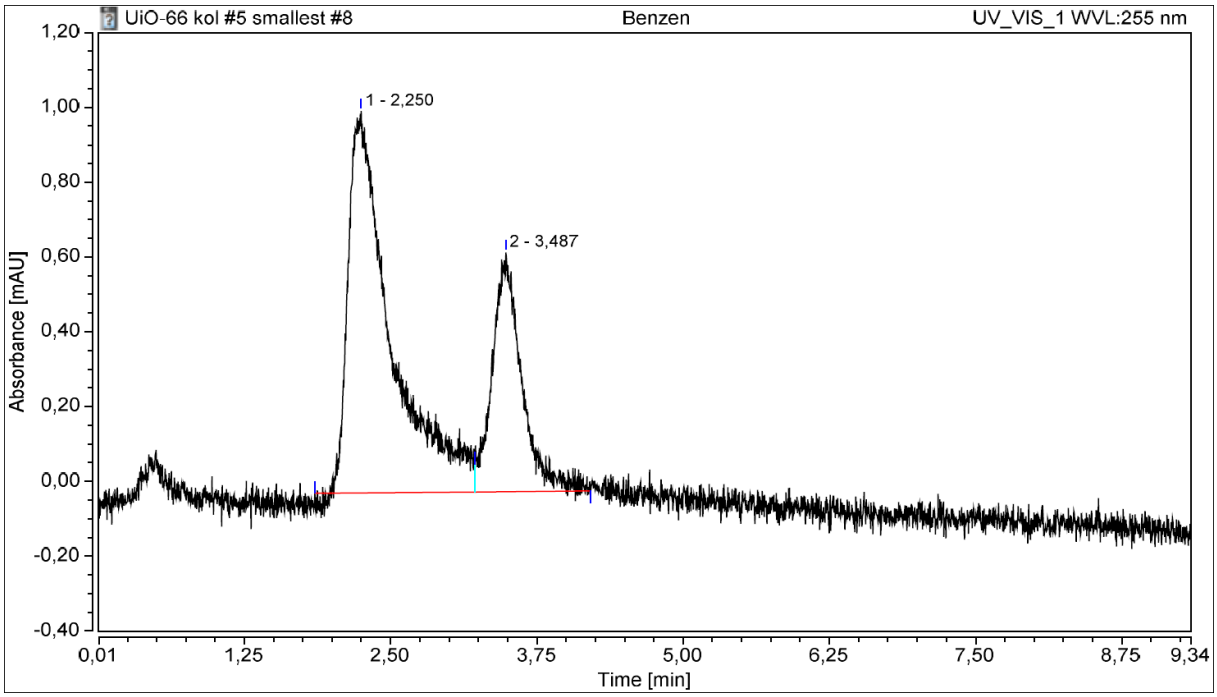

Figure 51 Chromatogram of benzene (1 and 2) on UiO-66. The small peak between 0 min and 0.125 min is caused by the turning of the injector as described in section **6.2.4**. Chromatographic conditions were as described in **Figure 30**.

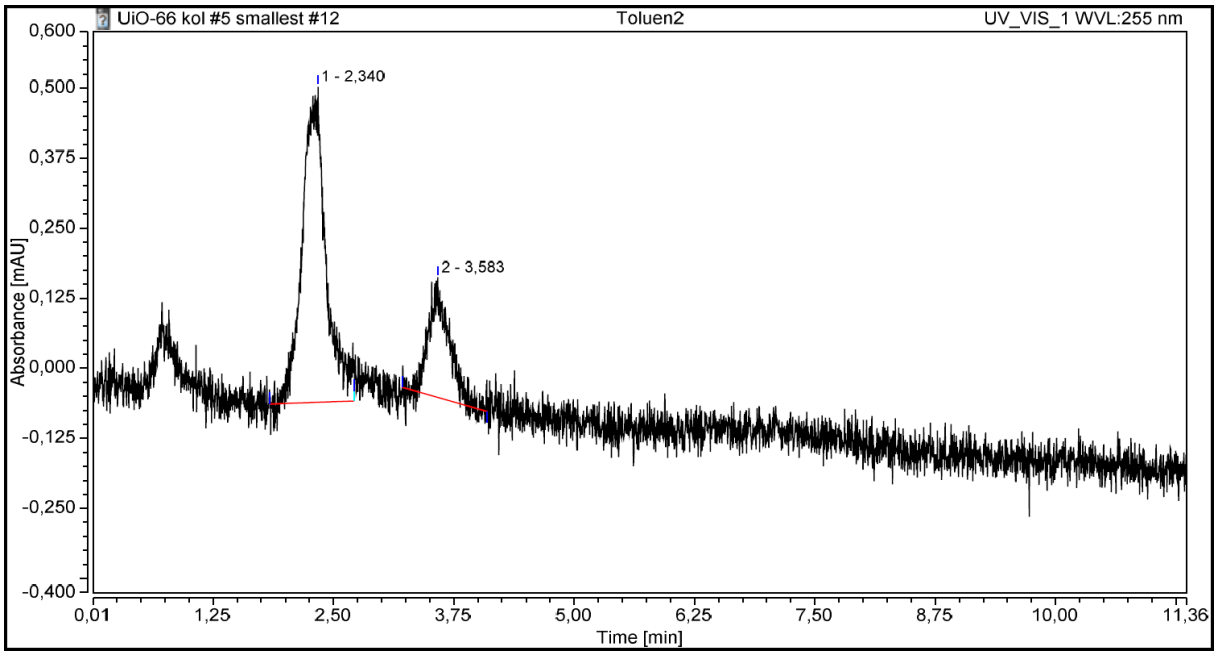

Figure 52 Chromatogram of toluene (1 and 2) on UiO-66. The small peak between 0 min and 0.125 min is caused by the turning of the injector as described in section **6.2.4**. Chromatographic conditions were as described in **Figure 30**.

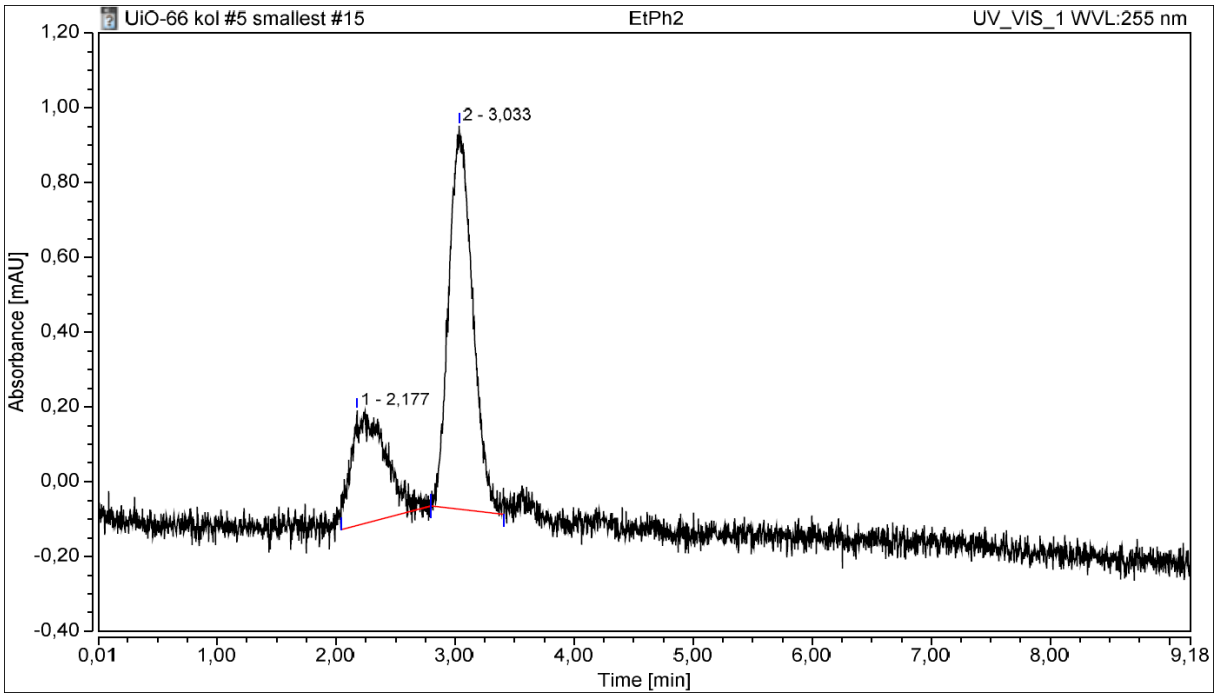

Figure 53 Chromatogram of ethylbenzene (1 and 2) on UiO-66. Chromatographic conditions were as described in **Figure 30**.

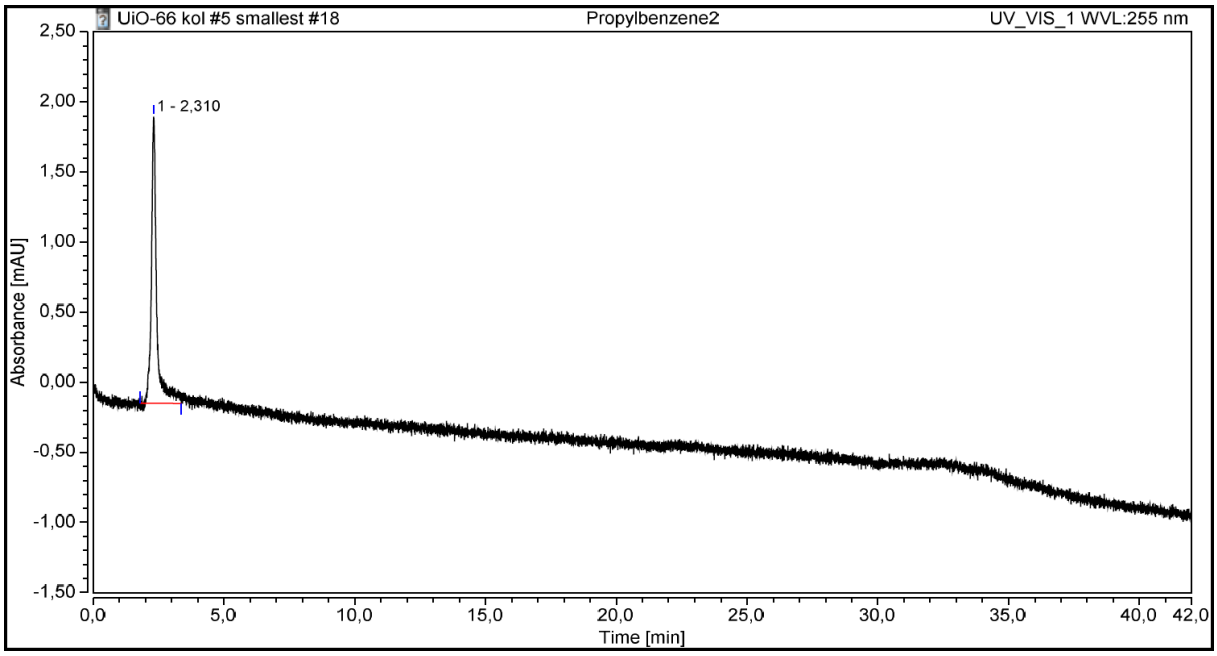

Figure 54 Chromatogram of propylbenzene (1) on UiO-66. Chromatographic conditions were as described in **Figure 30**.

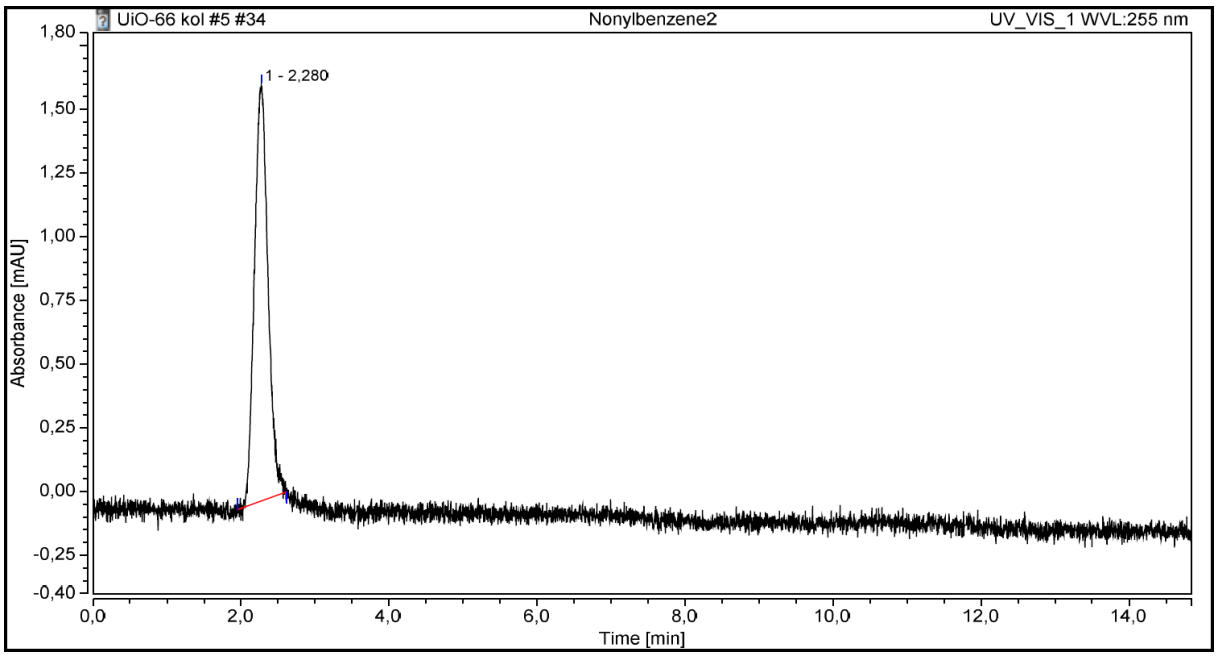

Figure 55 Chromatogram of nonylbenzene (1) on UiO-66. Chromatographic conditions were as described in **Figure 30**.

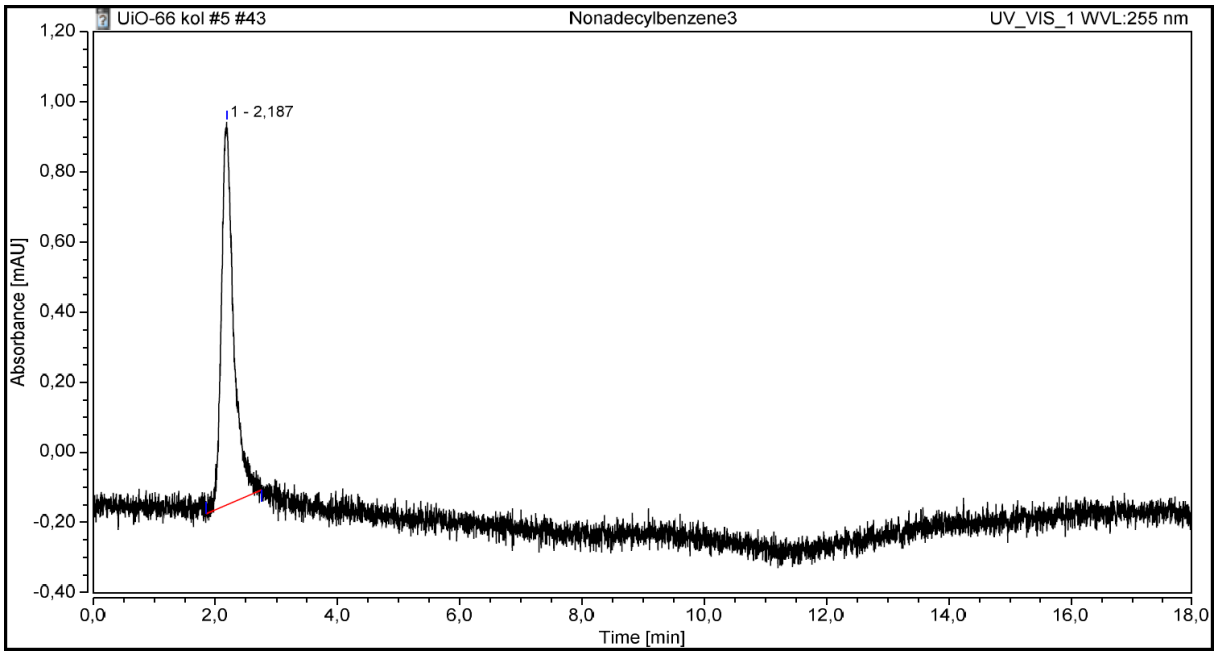

Figure 56 Chromatogram of nonadecylbenzene (1) on UiO-66. Chromatographic conditions were as described in **Figure 30**.

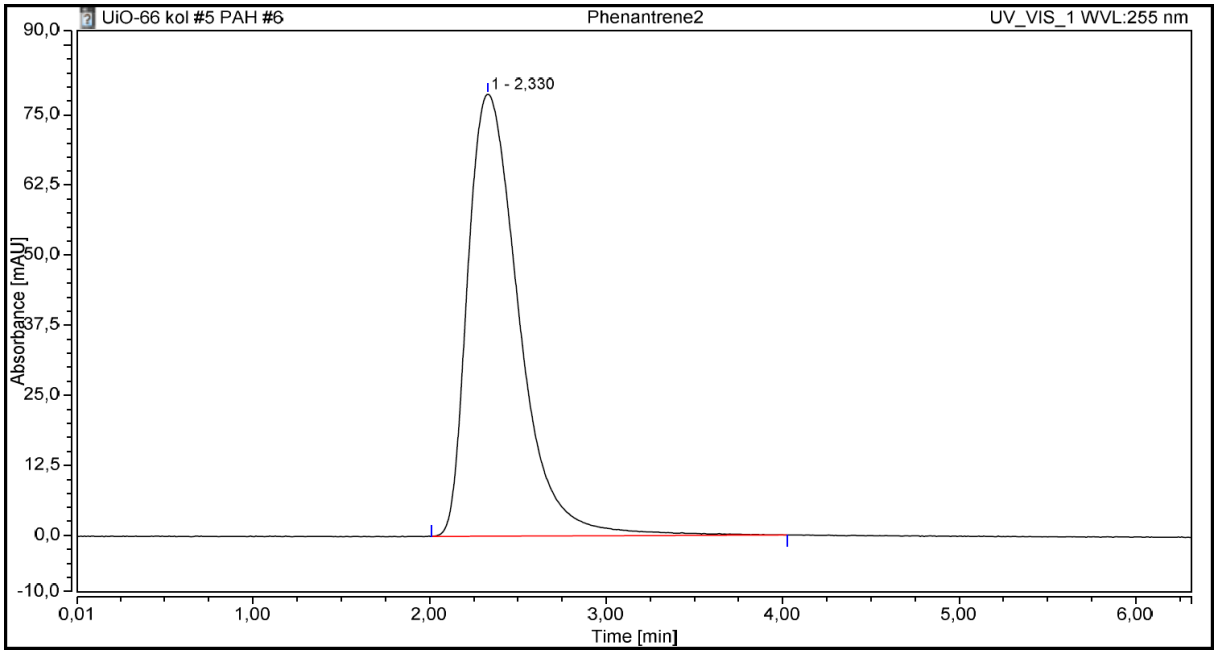

Figure 57 Chromatogram of phenanthrene (1) on UiO-66. Chromatographic conditions were as described in **Figure 30**.

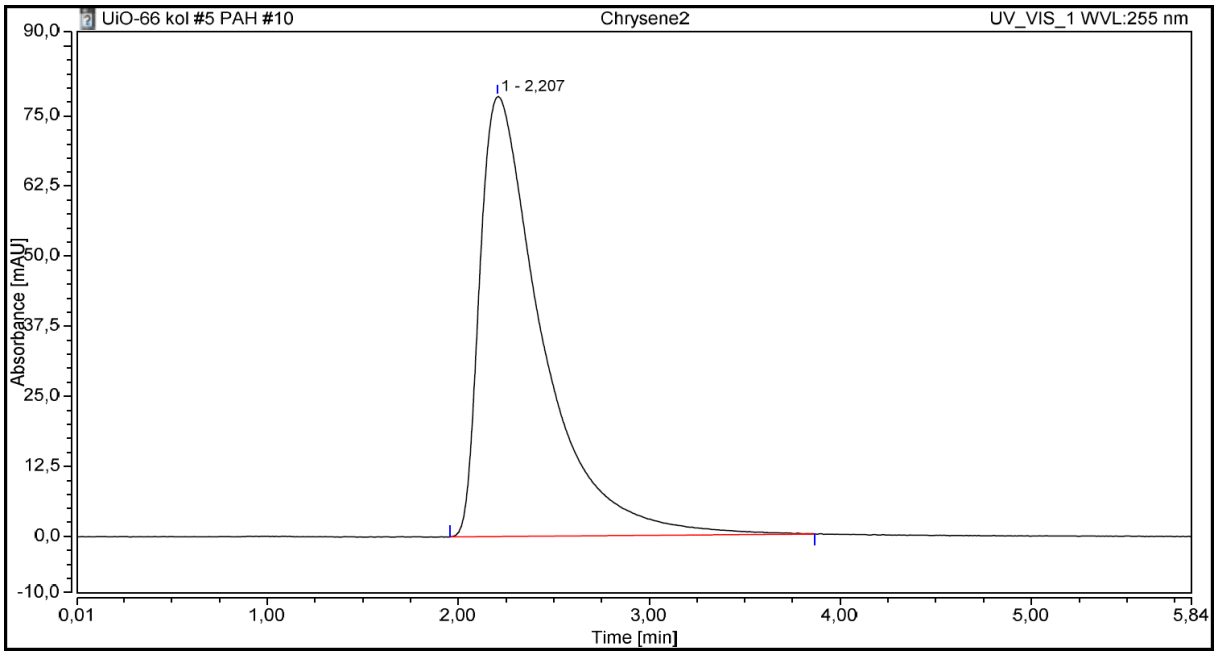

Figure 58 Chromatogram of chrysene (1) on UiO-66. Chromatographic conditions were as described in **Figure 30**.

Calculations

Table 29 shows P-values resulting from the t-tests which were executed to determine whether there was a statistically significant difference between the different retention times of the different solutes and the retention time of chrysene. Chrysene was chosen as a reference to test against because its size has been reported to be too large for it to enter the pores. Two-tailed tests were used, and F-tests were performed prior to the t-tests to determine whether a pooled standard deviation was to be used. A confidence level of 0.05 was used for these tests.

Table 29 P-values from t-tests comparing solute retention times to retention time of chrysene. A 0.05 level of significance was used.

Solute	$\bar{x}$	s	n	F-test	H_0 rejected?	t-test	H_0 rejected?
Benzene	2.28	0.04	9	0.92	No	0.13	Yes
Benzene peak 2	3.49	0.02	9	0.17	Yes	0.00	Yes
Toluene	2.29	0.07	9	0.57	No	0.27	Yes
Toluene peak 2	3.59	0.03	9	0.36	Yes	0.00	Yes
Ethylbenzene	2.31	0.05	9	0.99	No	0.05	Yes
Ethylbenzene peak 2	3.06	0.01	9	0.01	Yes	0.00	Yes
Propylbenzene	2.39	0.09	6	0.36	Yes	0.03	Yes
Butylbenzene	2.308	0.007	3	0.06	Yes	0.04	Yes
Pentylbenzene	2.27	0.02	3	0.41	Yes	0.29	Yes
Hexylbenzene	2.261	0.002	3	0.00	Yes	0.44	Yes
Heptylbenzene	2.25	0.02	3	0.53	No	0.59	No
Octylbenzene	2.23	0.02	3	0.25	Yes	0.61	No
Nonylbenzene	2.28	0.01	3	0.16	Yes	0.17	Yes
Decylbenzene	2.20	0.07	3	0.49	Yes	0.40	Yes
Nonadecylbenzene	2.20	0.02	3	0.57	No	0.23	Yes
Naphthalene	2.753	0.004	3	0.02	Yes	0.00	Yes
Phenanthrene	2.35	0.03	3	0.64	No	0.02	Yes

In order to determine if carry-over might be the cause of the two-peak pattern observed for benzene, toluene and ethylbenzene, two sets of three injections were compared for each compound. For the first set, the loop and injector were washed with MeOH between all injections, and for the second set, the loop and injector were not washed between injections of the same solution. The sum of the areas beneath the two peaks were compared between the two sets of injections.

The areas were chosen for comparison to determine if the two-peak pattern was related to carry-over because hypothetically, the carry-over should be greater if the injector and loop were not washed between injections of the same solution. Therefore, it was expected that the first or second peak would have a greater area if it occurred due to carry-over when washing was not performed between injections.

An f-test was performed to determine if the standard deviations of the different sets should be pooled or not. For all three compounds, the resulting P-value was >0.05. Thus, the standard deviations were deemed to be similar, and pooled standard deviation for the two sets were

used for all three compounds. Two-tailed t-tests were conducted, resulting in P-values >0.05 for all three compounds. In accordance with this, it was concluded there was no statistically significant difference in the peak area rising from whether or not washing was conducted between injections of the same solution at a 0.05 level of significance. Based on this, it was concluded that the two-peak pattern was unlikely to be caused by carry-over.

The basis to the calculations and the resulting P-values can be found in **Table 30**.

Table 30 Overview of the total area for the three compounds benzene, toluene and ethylbenzene, and the hypothesis tests performed. Both F-test and t-test performed at a significance level of 0.05.

	BENZENE		**TOLUENE**		**ETHYLBENZENE**	
	A_{Wash}	**$A_{No\ wash}$**	**A_{Wash}**	**$A_{No\ wash}$**	**A_{Wash}**	**$A_{No\ wash}$**
$\bar{x}$	0.19	0.18	0.22	0.21	0.21	0.29
s	0.05	0.03	0.02	0.04	0.05	0.05
n	3	3	3	3	3	3
	P-value	**H_0 rejected?**	**P-value**	**H_0 rejected?**	**P-value**	**H_0 rejected?**
F-test	0.74	no	0.62	no	0.96	no
t-test	0.92	no	0.58	no	0.11	no

6.3 Extraordinary circumstances due to COVID-19 pandemic

March 12th 2020 the Norwegian government decided that all institutions of higher education in Norway would have their campuses temporarily closed due to the COVID-19 pandemic and its spread in Norway[99]. This caused the laboratory work for this thesis to come to an abrupt halt. When restricted access to university buildings was permitted from April 27th 2020, a decision was made to not prioritise laboratory access for work related to this thesis, as extensive data collection had already taken place.

Originally, the van't Hoff experiments were to be continued for temperatures up to 90°C were to be conducted for both materials. Pore accessibility studies and column efficiency investigations for UiO-66-NH_2 were also to be conducted.

Due to the lockdown, there was no time to perform manual integration on several chromatograms. The automatic integration was for many of these chromatograms found to be poor, but this could regrettably not be remedied without the raw files and access to the software. The computer storing the raw chromatogram files and which had appropriate software installed was offline and on campus. The text clarifies where chromatograms which had been poorly integrated by automatic integration were used.